International Journal of Heat and Mass Transfer 115 (2017) 1174–1205

Contents lists available at ScienceDirect

International Journal of Heat and Mass Transfer

journal homepage: www.elsevier.com/locate/ijhmt

Review of spray cooling – Part 1: Single-phase and nucleate boiling regimes, and critical heat flux

Gangtao Liang [a,b], Issam Mudawar [b,*]

[a] Key Laboratory of Ocean Energy Utilization and Energy Conservation of Ministry of Education, School of Energy and Power Engineering, Dalian University of Technology, Dalian 116024, China
[b] Purdue University Boiling and Two-Phase Flow Laboratory (PU-BTPFL), School of Mechanical Engineering, 585 Purdue Mall, West Lafayette, IN 47907, USA

ARTICLE INFO

Article history:
Received 22 January 2017
Received in revised form 7 June 2017
Accepted 8 June 2017
Available online 26 June 2017

Keywords:
Spray cooling
Nucleate boiling
Critical heat flux (CHF)

ABSTRACT

This study is the first part of a two-part review of spray cooling, which addresses the relatively high-flux, low-temperature mechanisms and predictive tools associated with the single-phase liquid cooling and nucleate boiling regimes, as well as critical heat flux (CHF). The second part will be focused on the relatively high-temperature transition boiling and film boiling regimes, and the Leidenfrost point, which are encountered in quenching of metal alloy parts. In this part, key spray hydrodynamic parameters influencing heat transfer performance are identified, including volumetric flux, mean droplet diameter, and mean droplet velocity. This is followed by detailed identification of dominant mechanisms, data trends, correlations, and predictive models recommended by different research teams. Also discussed are spray cooling enhancement schemes, including micro and macro modifications to the surface itself, additives to the liquid, and use of nanofluids. Overall, contradictory findings point to a need for future experimental work that must be conducted systematically using many fluids with vastly different thermophysical properties, and broad ranges of operating conditions. There is also a need for further research to investigate parameters that influence CHF, including dissolved gas, spray inclination angle, and interaction between neighboring sprays when using multi-nozzle arrays to cool large surfaces.

Contents

* Corresponding author.
E-mail address: mudawar@ecn.purdue.edu (I. Mudawar).
URL: https://engineering.purdue.edu/BTPFL (I. Mudawar).

http://dx.doi.org/10.1016/j.ijheatmasstransfer.2017.06.029
0017-9310/

Nomenclature

A	area defined along heated surface
a	system acceleration
A'	area defined along spherical surface centered at nozzle orifice
A_e	area of impact ellipse
Bo^*	boiling number
C	empirical coefficient
C_q	discharge coefficient
c_p	specific heat at constant pressure
D	surface diameter
d	droplet diameter
d_o	nozzle orifice diameter
$d_{0.5}$	mass or volume median diameter
d_{32}	Sauter mean diameter
f	impact frequency
f_o	function in spray overlap relation
f_1, f_2	spray inclination functions
G	mass flux
g	gravitational acceleration
H	nozzle-to-surface distance
h	heat transfer coefficient
h_{fg}	latent heat of vaporization
k	thermal conductivity
L	surface length; characteristic length
M	radial momentum
$\dot{m}$	mass flow rate of spray
$\dot{m}_e$	mass flow rate of liquid expelled from surface
N	total number of droplets of all sizes in sample
N^+	droplet number density
Nu	Nusselt number
n_i	number of droplets with diameter d_i in sample
P	pressure
ΔP	pressure drop across nozzle
Pr	Prandtl number
P_s	stagnation point pressure
Q	volumetric flow rate
Q''	local volumetric flux
$\overline{Q}''$	mean volumetric flux on surface
q''	surface heat flux
Q''_{sp}	volumetric flux along spherical surface centered at nozzle orifice
q''^*_{CHF}	dimensionless CHF
R	spray cross-sectional radius
r	radius; radial coordinate
R_a	surface roughness
Re	Reynolds number
r_d	bubble departure radius
T	temperature
ΔT_c	critical state temperature difference
ΔT_f	$T_w - T_f$
ΔT_{max}	maximum temperature variation across surface at CHF
ΔT_{sat}	surface superheat, $T_w - T_{sat}$
T^+_{sat}	superheat temperature limit
ΔT_{sub}	liquid subcooling, $T_{sat} - T_f$
u	droplet velocity; characteristic velocity
u_1	liquid velocity upstream of nozzle
u_m	mean droplet velocity
We	Weber number
X	number of droplets crossing unit transverse surface area per unit time
x	x coordinate
x_i	number of droplets with diameter d_i
y	y coordinate
z	distance from nozzle

Greek symbols

α	spray inclination angle
β	angle in spray inclination model
γ	angle in spray inclination model
γ'	angle in spray inclination model
δ	liquid film thickness
ε	expulsion rate
η	evaporation efficiency
θ	spray angle
μ	viscosity
ρ	density
σ	surface tension

Subscripts

a	ambient
atm	atmospheric
CHF	critical heat flux
f	liquid
g	vapor; gas
MIN	minimum heat flux
NB	nucleate boiling
o	nozzle orifice; spray overlap
p	point based
s	spray
sat	saturation
sub	subcooling
w	surface

1. Introduction

1.1. High heat flux cooling solutions

1.1.1. Background and applications

During the past three decades, aggressive micro-miniaturization of electronic components has created an urgent need for innovative cooling schemes to maintain electronic device temperatures safely below limits that are dictated by material and reliability constraints. By the early 1980s, this trend led to rapid escalation in heat dissipation rate, causing a shift from reliance on fan-cooled heat sink attachments to cooling schemes utilizing dielectric liquid coolants using a variety of single-phase cooling schemes, relying entirely on the coolant's sensible heat rise to remove the heat. However, by the mid-1980s, heat dissipation from supercomputer chips approached 100 W/cm^2, exceeding the capabilities of most single-phase liquid cooling schemes [1]. Afterwards, cooling system developers focused their attention on two-phase cooling schemes, to capitalize on the coolant's both sensible and latent heat to reject far greater amounts of heat than that with single-phase schemes, while maintaining lower device temperatures. But heat dissipation concerns were not limited to computer devices. Since the early 1990s, similar heat dissipation challenges were encountered in numerous other applications. As shown in Fig. 1, they include, in addition to computers and data centers, X-ray medical devices, hybrid vehicle power electronics, heat exchangers for hydrogen storage, fusion reactor blankets and particle accelerator targets, magnetohydrodynamic (MHD) electrode walls, rocket nozzles, satellite and spacecraft electronics, laser and microwave directed energy weapons, advanced radars, and air-fuel heat exchangers in high-Mach aircraft engines [2]. These applications can be collectively categorized as *low-temperature*, meaning surface temperatures are maintained safely below the critical heat flux (CHF) limit. On the other, there are other *high-temperature* applications, which are associated mostly with quenching of metal alloy parts from very high temperatures in order to achieve optimum alloy microstructure and superior mechanical properties.

1.1.2. Merits and limitations of two-phase cooling schemes

Several two-phase liquid cooling schemes have been recommended for removal of high heat fluxes from devices used in the above applications. They include pool boiling thermosyphons, channel flow boiling, mini/micro-channel heat sinks, jet-impingement, and spray cooling [3]. Of these schemes, the latter three provide the highest cooling effectiveness and have therefore received the most attention in recent years. Proponents of spray cooling point to several advantages: high flux heat dissipation, low and fairly uniform surface temperature, and ability to cool a relatively large surface area using a single nozzle. For example, studies have shown that spray cooling can dissipate 150–200 W/cm^2 using the dielectric coolant HFE-7100 while maintaining device temperatures below 125 °C [4]. And cooling performance can be enhanced further with micro-structured surfaces, reaching 330–350 W/cm^2 below 125 °C using antifreeze coolant [5,6]. While mini/micro-channel heat sinks and jet-impingement lend themselves better to theoretical and/or semi-empirical modeling, because of its inherent complexity, spray cooling has lagged significantly behind in cooling system implementation.

With single-phase mini/micro-channel cooling, small coolant flow rates produce laminar flow, which, in the absence of phase change, results in a heat transfer coefficient inversely proportional to hydraulic diameter. But achieving very high single-phase heat transfer coefficients with very small diameters can lead to very high pressure drops. Single-phase cooling also compensates for high heat fluxes by large stream-wise increases in both coolant and device temperatures, which can be very detrimental to temperature-sensitive devices such as computer chips [3]. Two-phase mini/micro-channel cooling, on the other hand, permits partial or total consumption of the liquid by evaporation, thus requiring minimal coolant flow rates, and latent heat exchange helps maintain stream-wise temperature uniformity to levels dictated mostly by the coolant's saturation temperature. Yet, the major drawback of two-phase mini/micro-channel cooling is the large pressure drop associated with two-phase friction and acceleration along the channel [7,8].

Jet-impingement cooling involves large concentration of heat removal within the impingement zone, which can produce large surface temperature gradients that are detrimental to temperature-sensitive devices. While surface gradients can be reduced with multiple jets, interference between neighboring jets tends to complicate the flow of expelled coolant and induce flow instabilities in the cooling module. Two-phase jet impingement can be especially problematic because of a tendency of the wall jet emanating from the impingement zone to separate from the surface due to vapor momentum perpendicular to the surface. In fact, CHF in jets is often encountered even with an abundance of liquid in the wall jet [9].

Sprays utilize the momentum of liquid issued from the spray nozzle to induce breakup into fine droplets that impinge individually upon the heated surface. Not only does the breakup increase the surface area to volume ratio of the liquid, but it also helps produce a more uniform spatial distribution of heat removal. Also, vapor can be easily removed from the heated surface, allowing more effective contact of the liquid droplets with the surface. Another important attribute of spray cooling is its ability to greatly reduce or even prevent the wall temperature excursion and subsequent temperature drop associated with incipient boiling. This anomaly is commonplace with most two-phase cooling schemes involving dielectric coolants, and is known to cause thermal shock to electronic devices [10]. Another key attribute of spray cooling is resisting liquid separation from the surface during vigorous boiling. By bombarding the entire surface with droplets, the momentum of individual droplets is better able to resist the opposing vapor momentum perpendicular to the surface than a wall jet. The momentum of droplets allows liquid to penetrate through the vapor barrier created by nucleating bubbles and more effectively replenish the surface; both are highly beneficial to high-flux cooling [11].

However, spray cooling is not without shortcomings. Foremost among those is the high pressure drop sometimes required to break the liquid flow into fine droplets. Another practical drawback is the small size of flow passages within the spray nozzle increasing the likelihood of clogging, which can lead to eventual surface

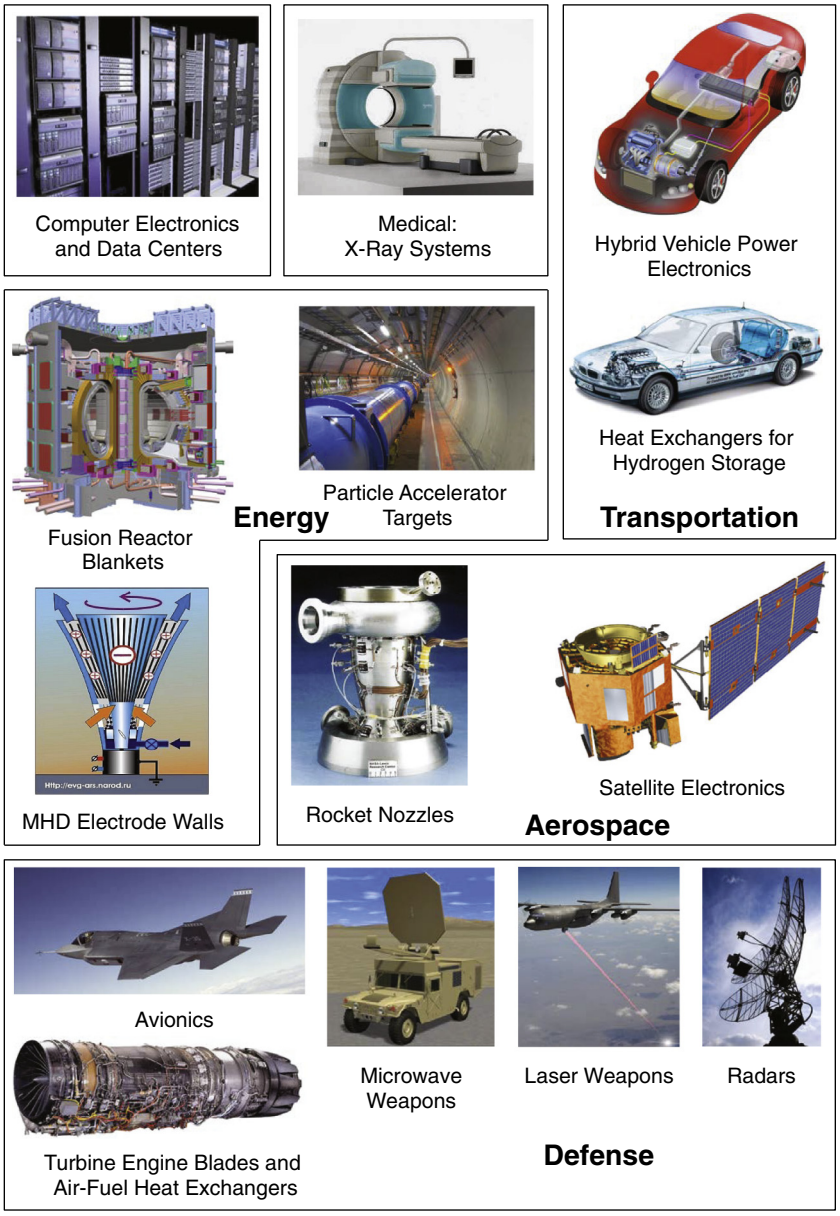

Fig. 1. Examples of applications demanding high heat flux cooling schemes. Adapted from Mudawar [2].

burnout. Furthermore, even minute variations in the fabrication of seemingly identical nozzles can produce profound differences in the spray's impact pattern; careful pre-testing of nozzles is therefore essential to ensuring predictable and repeatable cooling performance [12]. Despite these disadvantages, spray cooling remains quite popular in both low-temperature and high-temperature applications. Noteworthy among low-temperature applications is incorporating spray cooling into refrigeration systems, where a spray chamber serves as refrigeration loop evaporator [13,14].

1.2. Nozzle type and orientation relative to sprayed surface

1.2.1. Nozzle type

Not all types of nozzles are recommended for spray cooling. In general, two types of sprays are commonly used in industry: air-assist (or air-driven) sprays, which are produced by atomizer nozzles, and pressure sprays, which are produced by pressure nozzles [15].

Atomizers are spray nozzles that utilize a secondary gas stream to aid the droplet breakup and produce small droplets. However, for systems used to cool electronic devices, mixing a non-condensable gas into the liquid coolant greatly complicates coolant flow loop operation because of the need to separate the gas from the spent coolant, let alone the detrimental effects of the non-condensable gas on the performance of the flow loop's condenser. Besides, atomizers come in a large variety of designs, making prediction of their cooling performance quite illusive.

Pressure spray nozzles are preferred for spray cooling because of their reliance on momentum of the liquid alone to achieve the droplet breakup. Pressure spray nozzles are classified according to the manner in which they distribute droplets across the surface. Shown in Fig. 2 are three types of pressure nozzles popular in many industries: full cone, hollow cone, and flat. Full cone spray nozzles distribute liquid droplets across the entire impact circle, and are therefore preferred for many spray cooling applications. Hollow cone spray nozzles concentrate most of the droplets near the periphery of the impact circle. On the other hand, flat spray nozzles

produce a narrow oval impact area. With the exception of a few specialized nozzles (*e.g.*, spiral-shaped and acoustically controlled), pressure spray nozzles are generally available in a simple basic design. The present study is focused primarily on pressure sprays.

1.2.2. Nozzle orientation

Aside from normal downward-facing sprays, which are commonplace in many cooling applications, there are other nozzle orientations that are dictated mostly by packaging constraints. Overall, full cone spray orientations/configurations include downward-facing, Fig. 3(a), downward-facing with a small heated surface, Fig. 3(b), upward-facing, Fig. 3(c), horizontal, Fig. 3(d), and inclined, Fig. 3(e). Shown in Fig. 3(a) are key parameters that influence spray cooling. Definitions of these and other parameters will be provided later in Section 2.

For pressure spray nozzles, a minimum nozzle-to-surface distance is required to produce a fully developed spray. This distance allows hydrodynamic instabilities to induce initial breakup of liquid emerging from the nozzle into liquid sheets, followed by tubular ligaments, and ultimately individual droplets. However, stringent volumetric constraints, especially in electronic packages, often preclude the space required to ensure spray breakup. Two techniques that are used to cope with space constraints are (a) tilting the spray from normal orientation relative to the surface, and (b) using micro-sprays that require much shorter breakup distances [16]. Comparing upward-facing and downward-facing sprays over broad ranges of operating conditions and thermophysical properties, Rybicki and Mudawar [17] proved that, because of high droplet velocities, gravity (*i.e.*, orientation) has virtually no effect on spray cooling performance, a conclusion also shared by Qiao and Chandra [18]. On the other hand, Hsieh and Yao [19], Choi and Yao [20], Yoshida et al. [21], and Lin et al. [22] suggested that spray orientation does influence cooling performance.

In cases involving a large heat dissipating surface area or multiple heat dissipating areas, an array of spray nozzles is often used, which can lead to overlap between neighboring sprays. This increases coolant volumetric flux in the overlap regions, but complicates spray behavior and cooling performance.

1.2.3. Practical concerns

There are additional practical concerns in implementing spray cooling, such as corrosion and erosion of the intricate interior of the spray nozzle, single-point failure as a result of nozzle clogging, and lack of repeatability of droplet hydrodynamics and heat transfer performance among seemingly identical nozzles. Estes and Mudawar [23] recommended that only spray nozzles that are made from stainless steel or other corrosion and erosion resistant materials be used. It is also important that an effective filtering system be employed in the cooling loop to prevent clogging.

1.3. Spray boiling curve and quench curve

Heat transfer response of a surface to spray cooling can be quantified with the aid of the *boiling curve* and/or *quench curve* [24]. Shown in Fig. 4(a), the boiling curve depicts the variation of heat flux from the surface to the spray with wall superheat (wall temperature minus liquid saturation temperature). The boiling curve is highly effective for identifying the different heat transfer regimes encountered at different levels of wall superheat. They are comprised of (a) the *single-phase liquid cooling regime* corresponding to low superheats, (b) the *nucleate boiling (NB) regime* consisting of bubble nucleation within the liquid film formed by the impacting droplets and associated with the highest heat transfer coefficients, (c) the *transition boiling (TB) regime* associated with portions of the surface encountering bubble nucleation within the liquid film and other portions blanketed with vapor, and (d) the *film boiling (FB) regime* corresponding to high wall superheats that cause vapor blanketing over the entire surface and resulting in very small heat transfer coefficients. These four regimes are demarcated by three important transition points: (a) *onset of boiling (ONB)* (or *incipient boiling*) corresponding to first bubble formation on the surface, (b) *critical heat flux (CHF),* where bubble nucleation is replaced by localized vapor blankets merging together across the surface, and (c) *minimum heat flux (MIN)* (or *Leidenfrost point*), below which partial breakup of the continuous vapor blanket associated with film boiling begins to take effect. These three transition points clearly have profound influences on cooling effectiveness. For low-temperature applications, optimum cooling is achieved by maintaining conditions above ONB, but safely below CHF. On the other hand, in high-temperature applications, where the surface is gradually cooled (quenched) from a high initial temperature corresponding to the film boiling regime, MIN marks the transition from very slow film boiling to the much faster transition boiling.

Shown in Fig. 4(b), the quench curve provides a better representation of the variations in cooling rate encountered when the surface is cooled from an initial high temperature corresponding to

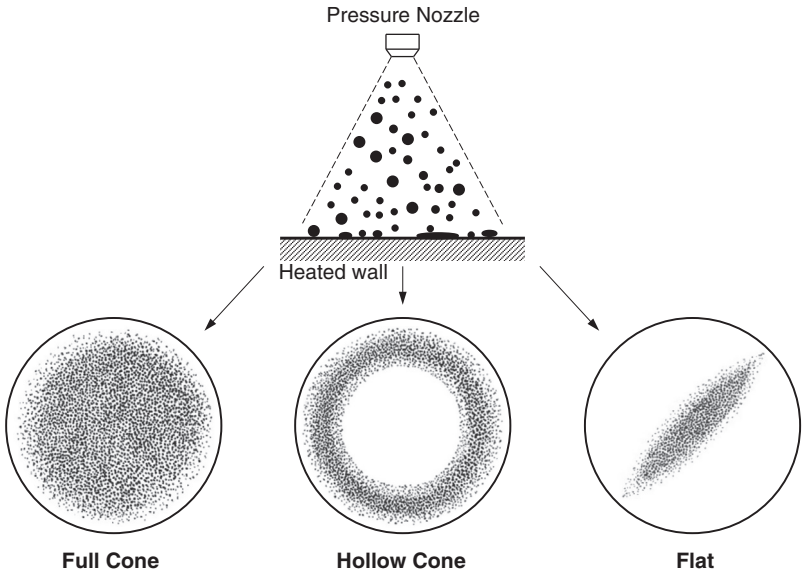

Fig. 2. Droplet impact patterns of pressure nozzles: full cone, hollow cone, and flat.

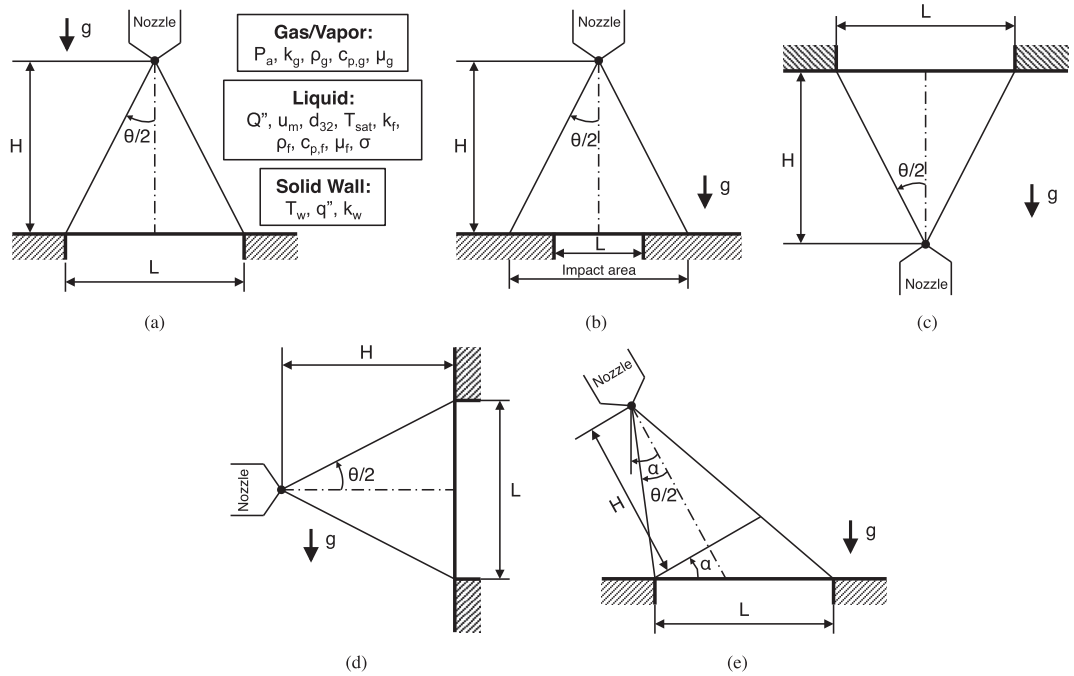

Fig. 3. Schematic representations of (a) downward-facing spray with key nomenclature, (b) downward-facing spray with small surface, (c) upward-facing spray, (d) horizontal spray, and (d) inclined spray with orientation nomenclature.

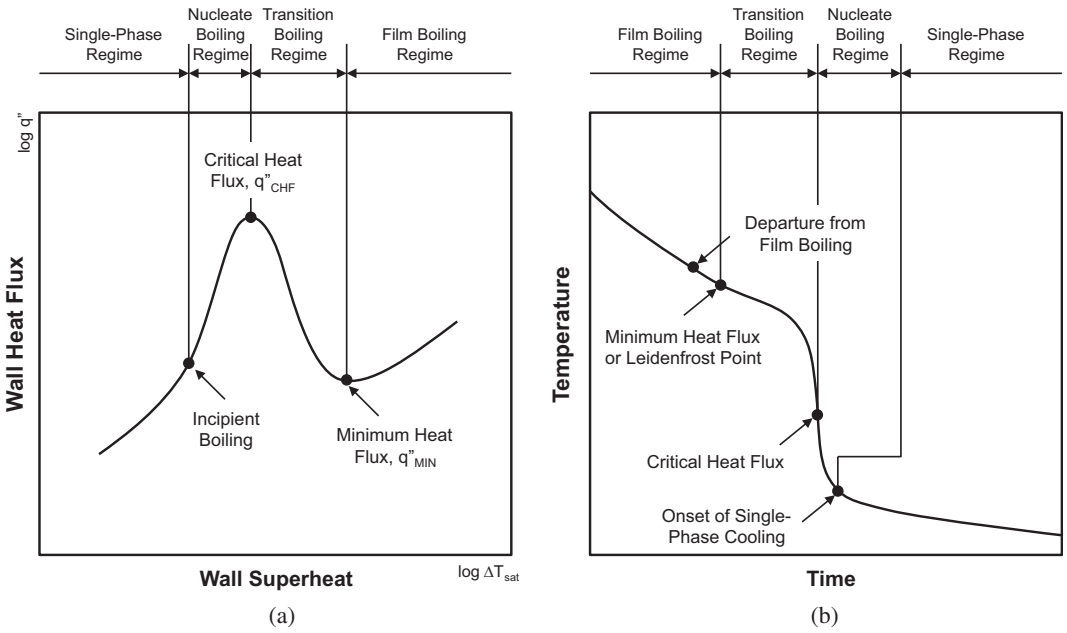

Fig. 4. (a) Boiling curve and (b) quench curve.

film boiling down to a low temperature. Unlike the boiling curve, which is a measure of only surface effects, the quench curve also accounts for thermal mass of the quenched part. The large variations in heat transfer coefficient corresponding to the aforementioned regimes of the boiling curve are associated with significant variations in cooling rate along the quench curve. Fig. 4(b) shows the variations in cooling rate reflected by appreciable slope changes between successive regimes. Quenching is initiated with slow cooling in the film boiling regime down to the Leidenfrost point, below which cooling rate increases in the transition boiling regime, and even more appreciably in the nucleate boiling regime, before subsiding in the single-phase liquid cooling regime. The quench curve emphasizes the importance of the Leidenfrost point, whereupon large changes in cooling rate can have profound influences on the microstructure and mechanical properties of a quenched metal alloy part.

Overall, quantifying spray cooling behavior in both low-temperature and high-temperature applications requires reliable predictive tools for all four boiling regimes as well as the transition points in between. These tools must be presented in terms of measurable spray parameters, which will be discussed in Section 2.

1.4. Prior spray cooling reviews

Several review articles have been published in the past, which either address spray cooling along with other cooling schemes, or are dedicated entirely to spray cooling. Examples of the first category of reviews include an article by Bar-Cohen et al. [25] addressing pool boiling, spray/jet impingement, gas-assisted evaporation, and synthetic jet impingement with dielectric liquids. Ebadian and Lin [26] reviewed high heat flux removal schemes including micro-channel, jet impingement, and spray, as well as wettability effects and piezoelectrically driven droplets. Kandlikar and Bapat [27] reviewed micro-channel, spray, and jet impingement schemes. More recently, Smakulski and Pietrowicz [28] examined porous media, micro-channel, and spray cooling, and concluded that spray cooling is the most promising of all the schemes reviewed.

Examples of reviews dedicated entirely to spray cooling include those by Kim et al. [29], who summarized studies on single-phase and nucleate boiling prior to 2006, and Cheng et al. [30], who focused on spray CHF. Tseng et al. [31] reviewed film boiling heat transfer for high mass flux sprays. Silk et al. [32] reviewed studies on spray cooling in microgravity.

1.5. Objectives of present review

Depending on the spray's volumetric flux (volumetric flow rate per unit area), sprays can be described as dilute, intermediate, or dense. Shown in Fig. 5(a) is a schematic of a dilute spray, where low volumetric flux results in virtually no liquid buildup or interaction among droplets impinging on the surface, along with a depiction of single droplet impact. Fig. 5(b) shows a schematic of an intermediate spray, where interference among impacting droplets can be appreciable but not sufficient to form a continuous liquid film on the surface. On the other hand, Fig. 5(c) depicts a dense spray, where a thin film is formed by accumulation of frequent and successive droplet impacts. Clearly, droplet impact plays a crucial role in all types of spray cooling, but the ensuing heat transfer is also highly sensitive to the spray's volumetric flux. This demonstrates the need to relate, where possible, single droplet impact phenomena (on both dry and wet surfaces) to spray cooling. In fact, this relationship is the key reason behind a series of reviews by the present authors addressing the fluid mechanics of liquid drop impact on a liquid film [33] and on a heated wall [34], culminating in the present two-part spray cooling review.

Unlike prior reviews of spray cooling, the present review will provide a comprehensive assessment of all aspects of spray cooling important to both fundamental understanding of underlying mechanisms and cooling system design, including available models and correlations, as well as recommendations for future research. The review will be presented in two parts. The present part will address determination of dominant hydrodynamic parameters that are used to characterize spray behavior, followed by a detailed review of the *low-temperature cooling regimes*, namely single-phase liquid cooling and nucleate boiling, as well as the CHF limit. The second part [35] will focus on the high-temperature transition and film boiling regimes as well as the Leidenfrost point. Also included in the second part is the use of spray cooling models and/or correlations to predict transient response of metal alloy parts when cooled from high initial temperature. It will also be shown how this response can be combined with metallurgical transformation kinetics to predict detailed spatial distributions of mechanical properties within the cooled part.

2. Hydrodynamic parameters of sprays

2.1. Overall parametric influences

Predicting the cooling performance of sprays is complicated by its dependence on a rather large number of parameters. They include:

(a) Liquid type: water, dielectric fluids (*e.g.*, FC-72, FC-77, FC-87, PF-5060, PF-5052, and HFE-7100), refrigerants (*e.g.*, R-22, R-113, R-600a, R-134a, and ammonia), cryogens (*e.g.,* those used in laser treatment [39,40]), and saline water (used in cooling towers [41]).

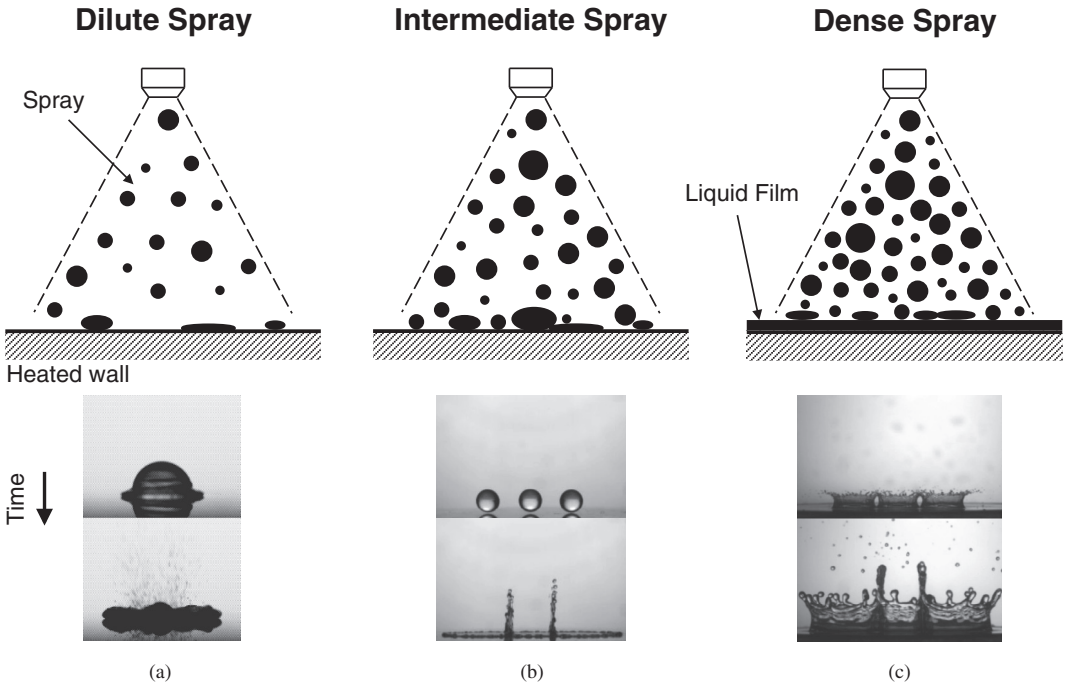

Fig. 5. Schematics of sprays corresponding to different volumetric fluxes, and associated images capturing interactions between droplets and solid surface or liquid film: (a) dilute spray, (b) intermediate spray, and (c) dense spray. Droplet images are adapted from Liang et al. [36], Cossali et al. [37], and Cossali et al. [38].

(b) Liquid saturation temperature, T_{sat}, liquid subcooling, ΔT_{sub}, and thermophysical properties of liquid: density, ρ_f, viscosity, μ_f, thermal conductivity, k_f, specific heat, $c_{p,f}$, surface tension, σ, and latent heat of vaporization, h_{fg}.
(c) Ambient pressure, P_a, and thermophysical properties of surrounding vapor/gas: density, ρ_g, viscosity, μ_g, thermal conductivity, k_g, and specific heat, $c_{p,g}$.
(d) Surface parameters: surface temperature, T_w, surface superheat, ΔT_{sat}, heat flux, q'', and thermal conductivity, k_w.
(e) Flow parameters: flow rate, Q, and pressure drop across the nozzle, ΔP.
(f) Geometrical parameters of spray nozzle: orifice diameter, d_o, spray cone angle, θ, nozzle orientation angle, α, and nozzle-to-surface distance, H.

The influence of the majority of the above parameters is reflected in three spray parameters that play a crucial role in spray cooling: droplet size, d, droplet velocity, u, and volumetric flux, Q''. Also important to cooling performance are the spatial distributions of these three parameters across the sprayed surface.

When multiple droplets impact the surface at a large rate, a continuous liquid film is formed on the surface, the thickness of which can have a significant influence on spray cooling [42]. Surface roughness is another important parameter that can influence droplet impact, liquid film thickness, vapor/gas entrapment, bubble departure pattern and size, and therefore overall heat transfer effectiveness [43]. Thermal conductivity of the surface is yet another parameter that can influence spray cooling [44].

2.2. Mean droplet diameter

As liquid emerges from the nozzle, liquid breakup begins to take effect. Prior to impacting the surface, droplets are formed with different diameters, velocities, and trajectories. When characterizing a spray, it is more convenient to work with a mean droplet diameter instead of the complete distribution of diameters. Use of a mean diameter implies that the actual spray is represented by a spray whose droplets possess the same diameter, while retaining other relevant characteristics of the actual spray [45]. The concept of mean diameter was introduced and its notations were standardized by Mugele and Evans [46]. One of the most popular mean diameters is Sauter mean diameter, d_{32}, defined as the diameter of a droplet whose volume-to-surface area ratio is the same as that for the entire spray sample,

$$d_{32} = \frac{\sum_i n_i d_i^3}{\sum_i n_i d_i^2}, \tag{1}$$

where n_i is the number of droplets with diameter d_i. Another diameter commonly used in commercial spray nozzle catalogs is the mass median diameter, $d_{0.5}$, also referred to as volume median diameter, which is the droplet diameter such that 50% of the total liquid volume is in droplets with smaller diameter.

For full cone sprays, Estes and Mudawar [47] correlated d_{32} for FC-72 and water, liquids with vastly different surface tension values, according to

$$\frac{d_{32}}{d_o} = 3.67\left(We_o^{1/2} Re_o\right)^{-0.259}, \tag{2}$$

where d_o is the nozzle's orifice diameter, having a range of 0.762–1.7 mm, and We_o and Re_o are, respectively, the Weber and Reynolds numbers based on orifice conditions and defined as

$$We_o = \frac{\rho_g (2\Delta P/\rho_f) d_o}{\sigma} \tag{3a}$$

and

$$Re_o = \frac{\rho_f (2\Delta P/\rho_f)^{1/2} d_o}{\mu_f}. \tag{3b}$$

In Eqs. (3a) and (3b), ΔP represents pressure drop across the nozzle, and $(2\Delta P/\rho_f)^{1/2}$ the characteristic liquid velocity. Equation (2) provides a relatively simple and convenient method to determining d_{32} without having to conduct expensive and laborious droplet sizing measurements for individual nozzles.

Ghodbane and Holman [48] suggested the following correlation for $d_{0.5}$ by Bonacina et al. [49], which provides the best agreement with nozzle manufacturers' specifications:

$$\frac{d_{0.5}}{d_o} = \frac{9.5}{\left[\Delta P^{0.37} \sin(\theta/2)\right]}, \tag{4}$$

where θ is the spray's cone angle. Using four full cone pressure spray nozzles, Nasr et al. [50] found that $d_{0.5}$, mean droplet velocity, and mass flux for water decrease with increasing axial distance z downstream from the orifice, and recommended the following correlation for $d_{0.5}$:

$$\frac{d_{0.5}}{d_o} = 0.523 We_o^{-0.659} Re_o^{0.203} (z/d_o)^{-0.361}, \tag{5}$$

which is valid for d_o = 0.61–1.7 mm and volume flow rates of Q = 0.53–5.89 l/min.

Also using full cone pressure spray nozzles, Cheng et al. [51] found that droplet diameter for water changes away from the orifice according to

$$\frac{d_{32}}{d_o} = 13.62 We_o^{-0.12} Re_o^{-0.26} (H/D)^{0.36} (R/D)^{0.39} \exp(-1.07R/D), \tag{6}$$

where H, R, and D are nozzle-to-surface distance, spray cross-sectional radius at a certain spray height, and surface diameter, respectively. The Weber and Reynolds numbers in Eq. (6) are based on the formulations of Ghodbane and Holman [48].

Xie et al. [52] measured droplet size and velocity distributions for water using pressure spray nozzles. They showed that axial distance from the orifice significantly influences droplet size and velocity, and observed two local peaks and one valley of droplet flux within the spray's cross-section. They also identified a critical axial distance below which the spray cone is hollow and droplet diameter decreases with increasing axial distance, and above which the spray cone is fully developed and droplet diameter begins to increase due to coalescence. Droplet velocity was shown to decrease monotonically with the axial distance because of ambient air drag. In another study, Xie et al. [53] examined thermal effects on spray behavior. They observed the spray cone to expand with increasing surface temperature, resulting in dilute volumetric flux in the spray's central region, which influenced the heat transfer coefficient and increased surface temperature non-uniformity. Increasing surface temperature also increased droplet diameter but decreased droplet velocity near the surface.

2.3. Spray volumetric flux

Spray volumetric flux is arguably the most important parameter in spray cooling, evidenced by its dominant influence on heat transfer performance compared to the other hydrodynamic parameters [45]. Two different definitions of volumetric flux are commonly used in the heat transfer literature. The first is local spray volumetric flux, Q'', defined as the volumetric flow rate of liquid impacting an infinitesimal portion of the surface divided by the area of the same portion. The other is mean volumetric flux, $\overline{Q}''$, which can be readily determined by dividing the total volume flow rate of the spray by the portion of the surface directly impacted by the spray - the spray's impact area. Another less accurate definition

of $\overline{Q}''$ used in a few studies is total volume flow rate divided by the total area of the sprayed surface.

Mudawar and Deiters [54] measured the spatial distribution of volumetric flux for water shown in Fig. 6(a), which features peak value at the center of the impact area and gradual decay away from the center. They also observed that, while mean droplet velocity (discussed in the following section) is virtually constant for the entire spray impact area, the heat transfer coefficient peaks at the center and follows essentially the distribution of volumetric flux as shown in Fig. 6(b).

Mudawar and Estes [55] constructed a theoretical model for Q'' based on the geometrical depiction in Fig. 7(a), where volumetric flux Q''_{sp} along any spherical surface centered at the orifice and confined by the spray angle was assumed uniform,

$$Q'' = Q''_{sp}\frac{dA'}{dA} = \frac{1}{2}\left\{\frac{Q}{\pi[H\tan(\theta/2)]^2}\right\}\left[\frac{\tan^2(\theta/2)}{1-\cos(\theta/2)}\right]\left[1+\left(\frac{r}{H}\right)^2\right]^{-3/2}, \tag{7}$$

where r is the radial coordinate. The accuracy of this model was validated using a spray sampler with different sized sampling inserts as shown in Fig. 7(b). For each insert, the volumetric flux distribution given by Eq. (7) was integrated over the sampler's inlet area, and results compared favorably with the flow rate captured in the graduated cylinder of the sampler.

2.4. Mean droplet velocity

Mean droplet velocity, u_m, is commonly used to represent the velocity of spray droplets. Bolle and Moureau [56] suggested a method for calculating u_m for a spray with known droplet size distribution. First, they determined the total number of droplets X crossing a unit transverse surface area per unit time. If the volumetric flux, Q'', for the same unit area is known, then

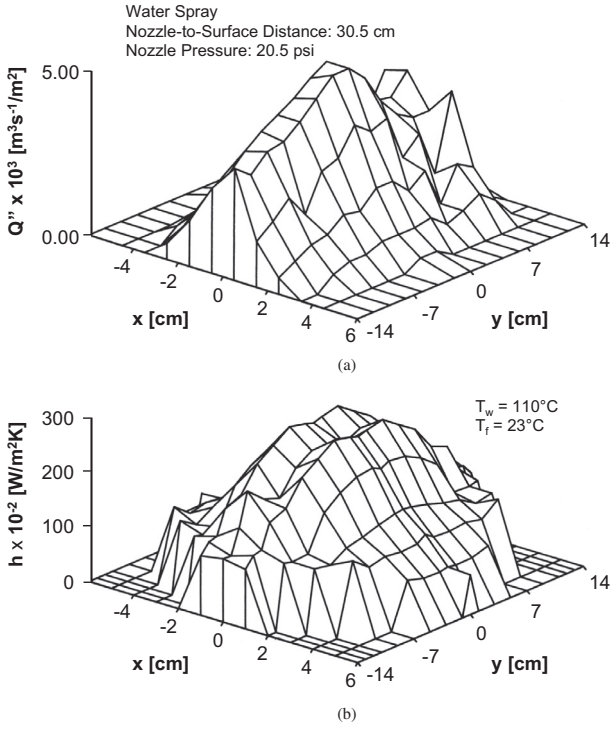

Fig. 6. Variations of (a) volumetric flux, and (b) heat transfer coefficient across the sprayed surface. Adapted from Mudawar and Deiters [24].

$$Q'' = \sum_i x_i(\pi d_i^3/6), \tag{8}$$

where x_i is the total number of droplets with diameter d_i crossing the unit area per unit time, which is proportional to the sample population n_i of droplets with diameter d_i, determined over an adequate measurement period during which the total number of droplets of all sizes is N. Then,

$$\frac{x_i}{X} = \frac{n_i}{N}, \tag{9}$$

where the ratio n_i/N is measured with the aid of a particle analyzer. Therefore, the local mean droplet velocity u_m can be defined as

$$u_m = \frac{\sum_i x_i\rho_f u_i\left(\frac{\pi d_i^3}{6}\right)}{\sum_i x_i\rho_f\left(\frac{\pi d_i^3}{6}\right)} = \frac{\sum_i u_i(n_i/N)\left(\frac{\pi d_i^3}{6}\right)}{\sum_i (n_i/N)\left(\frac{\pi d_i^3}{6}\right)}. \tag{10}$$

In general, u_m can be approximated as droplet velocity exiting the nozzle orifice using an energy balance proposed by Ghodbane and Holman [48], and later modified by Qiao and Chandra [18] to include gravity effects,

$$u_m = \left(u_1^2 + \frac{2\Delta P}{\rho_f} - \frac{12\sigma}{\rho_f d_{0.5}} - 2gH\right)^{1/2}, \tag{11}$$

where u_1 is the flow velocity upstream of the nozzle, and $(2\Delta P/\rho_f)$ is the most dominant term. Notice that droplet diameter in the above equation is represented by $d_{0.5}$ instead of d_{32}, and velocity variations along the axial direction and any droplet-air or droplet-droplet interactions are neglected. In other words, u_m given by Eq. (11) is mean droplet velocity at the exit from the nozzle's orifice. Using full cone pressure nozzles, Ciofalo et al. [57] measured the mean velocity of water droplets close to the spray axis and 5–10 cm away from the orifice, and showed that the measured values are slightly overpredicted by Eq. (11). Later, Ciofalo et al. [58] suggested that u_m can be approximated as

$$u_m = C_q\left(\frac{2\Delta P}{\rho_f}\right)^{1/2}, \tag{12}$$

where C_q is the discharge coefficient ($C_q < 1$), whose value depends on the nozzle's internal structure. In another study involving full cone pressure nozzles, Nasr et al. [50] related u_m for water to axial distance, z, from the orifice,

$$\frac{u_m}{(\Delta P/\rho_f)^{-1/2}} = 0.244We_o^{0.126}Re_o^{0.165}(z/d_o)^{-0.293}. \tag{13}$$

On the other hand, Cheng et al. [51] related u_m at distance H for full cone pressure nozzles to the spray's radius,

$$\frac{u_m}{\left(u_{0.1}^2 + \frac{2\Delta P}{\rho_f} - \frac{12\sigma}{\rho_f d_{32}}\right)^{1/2}} = 17.58We_o^{-0.14}Re_o^{-0.27}\left(\frac{H}{D}\right)^{0.13}\left(\frac{R}{D}\right)^{0.36} \times \exp\left(\frac{-2.13R}{D}\right). \tag{14}$$

Hsieh and Tien [59] used Laser Doppler Velocimetry to measure local u_m for full cone pressure nozzles and its distribution in both the axial and radial directions for R-134a. They showed that radial velocity is highest at the outer edges of the spray and decreases towards the central axis, where axial velocity is maximum.

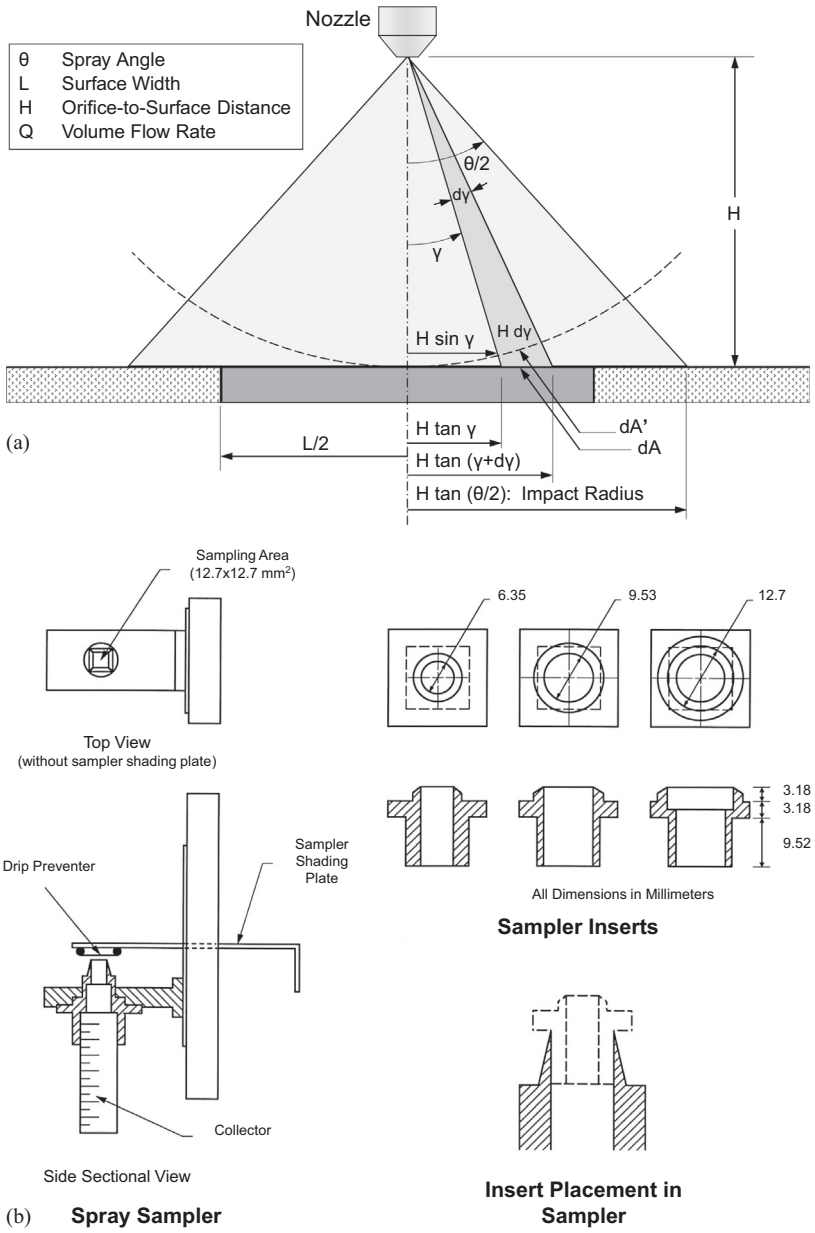

Fig. 7. (a) Geometry used in development of volumetric flux distribution model. (b) Spray sampling technique used to validate the model. Adapted from Mudawar and Estes [55].

3. Single-phase heat transfer

3.1. Heat transfer models and correlations

The single-phase heat transfer regime has received less attention in the heat transfer literature compared to the other spray cooling regimes. This can be attributed to this regime's relatively poor cooling performance, especially when compared to nucleate boiling.

Investigators sought to optimize the spray's nozzle-to-surface distance for square surfaces in order to maximize the single-phase heat transfer coefficient, which is reminiscent of the geometrical approach recommended by Estes and Mudawar [47] to optimize CHF. Guo et al. [60] observed a thin, high velocity film (termed the impellent film) close to but outside the spray impact area, which they deemed important to spray heat transfer. For a square surface, optimum single-phase cooling was achieved when the outer edge of the impellent film just inscribed the square impact surface. However, Zhu et al. [61] reported that the optimal nozzle-to-surface distance for single-phase heat transfer is identical to that recommended by Estes and Mudawar to optimize CHF, *i.e.*, corresponding to a spray impact area just inscribing the square surface, not the surrounding film.

Based on the characteristic length used to correlate single-phase heat transfer data, heat transfer correlations are available in three different forms: (a) Nusselt number correlations based on droplet diameter, (b) Nusselt number correlations based on surface size, and (c) direct heat transfer coefficient correlations.

3.1.1. Nusselt number correlations based on droplet diameter

Mudawar and Valentine [45] correlated the single-phase heat transfer coefficient for full cone pressure nozzles using the conventional Nusselt number, Nu, formulation based on spray Reynolds number, Re_s, and liquid Prandtl number, Pr_f,

$$Nu = 2.512 Re_s^{0.76} Pr_f^{0.56}, \tag{15}$$

where mean volumetric flux and Sauter mean diameter are used as velocity and length scales, respectively. The three dimensionless parameters in Eq. (15) are defined as

$$Nu = \frac{hd_{32}}{k_f}, \tag{16a}$$

$$Re_s = \frac{\rho_f \overline{Q}'' d_{32}}{\mu_f}, \tag{16b}$$

and

$$Pr_f = \frac{c_{p,f}\mu_f}{k_f}, \tag{16c}$$

where h is the heat transfer coefficient, and all liquid properties are evaluated at the mean of surface and liquid temperatures, $(T_w + T_f)/2$.

Mudawar and Valentine also proposed the alternative correlation

$$Nu = 2.569 Re_s^{0.78} Pr_f^{0.56}, \tag{17}$$

where the length scale used in both Nu and Re_s is $d_{0.5}$ instead of d_{32}. Equations (15) and (17) are valid for $\overline{Q}'' = 0.6\times10^{-3}$–$10^{-2}$ m^3 s^{-1}/m^2 and $Pr_f = 2.06$–6.33.

More recently, Rybicki and Mudawar [17] combined their upward-facing PF-5052 spray data along with Mudawar and Valentine's [45] downward-facing water spray data to derive the correlation

$$Nu = 4.70 Re_s^{0.61} Pr_f^{0.32}, \tag{18}$$

which is valid for $\overline{Q}'' = 0.6\times10^{-3}$–$0.186$ m^3 s^{-1}/m^2 and $d_{32} = 0.109$–0.806 mm, as shown in Fig. 8. They also indicated that, because of high droplet velocities, gravity effects are negligible and spray cooling is very weakly dependent on spray orientation.

Cho and Ponzel [62] reported that spray cooling is more effective above saturation temperature during evaporation of the thin liquid film. Although most of their data showed a negligible effect of liquid flow rate on single-phase heat transfer, data for a specific nozzle ($d_o = 0.51$ mm) did show heat transfer improvement with increasing flow rate. They correlated data for water sprays with $Q = 3.7$–8.7 ml/s according to

$$Nu = 2.531 Re_s^{0.667} Pr_f^{0.309}. \tag{19}$$

3.1.2. Nusselt number correlations based on surface size

Several studies have culminated in Nusselt number correlations for the single-phase regime based on surface size instead of droplet diameter,

$$Nu = \frac{hL}{k_f}, \tag{20}$$

where L is the length for square surfaces, which is also replaced by diameter D for circular surfaces.

Using R-134a as working fluid, Hsieh and Tien [59] obtained the following correlation for single-phase heat transfer,

$$Nu = 933\left(\frac{\rho_f u_m^2 d_{32}}{\sigma}\right)^{0.36}\left(\frac{d_{32}}{d_o}\right)^{0.25}\left(\frac{\Delta T_{sub}}{T_w}\right)^{0.027}, \tag{21}$$

which shows dependence on Weber number based on mean droplet velocity, u_m, measured very close to the surface, and defined as

$$We_d = \frac{\rho_f u_m^2 d_{32}}{\sigma}. \tag{22}$$

Eq. (21) is valid for $We_d = 70$–85 and $d_{32} = 28$–50 μm. Notice that the definition of Weber number in Eq. (22) is different from the more popular definition based on mean volumetric flux, $\overline{Q}''$,

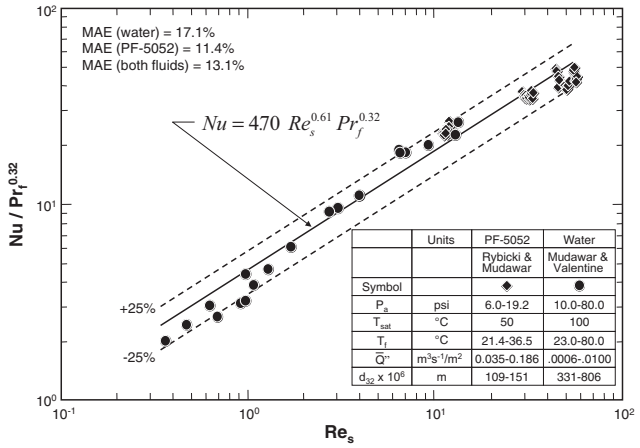

Fig. 8. Single-phase heat transfer correlation for upward-oriented PF-5052 sprays and downward-oriented water sprays. Adapted from Rybicki and Mudawar [17].

$$We_s = \frac{\rho_f \overline{Q}''^2 d_{32}}{\sigma}. \tag{23}$$

Tao et al. [63] investigated water sprays produced by two parallel nozzles impacting a 2-cm^2 surface. They reported significant improvement in cooling performance resulting from increased liquid flow rate or decreased liquid inlet temperature. Heat transfer data For $Q = 2.22$–6.67 ml/s were correlated according to

$$Nu = 0.6751 Re_s^{0.77} Pr_f^{0.84}, \tag{24}$$

where the characteristic velocity in Re_s is volume flow rate divided by surface area rather than impact area. Tao et al. reported that the heat transfer coefficient reaches maximum value at a nozzle-to-surface distance of 1.451 cm. They also observed improvement in the heat transfer coefficient when surfactant was added into the water, and the level of improvement was a function of surfactant concentration.

Jiang and Dhir [64] correlated their water data according to

$$Nu = 9.75 Re_s^{0.7} Pr_f^{1/3}, \tag{25}$$

where $Re_s = 1000$–2000, $Pr_f = 1.76$–6.7, and the definitions of Re_s and Nu are identical to those used by Tao et al. They also achieved much lower heat transfer coefficient values for high concentrations of non-condensable gas in the water.

Karwa et al. [65] correlated data for pressure water spray cooling of a 20-mm diameter surface according to

$$Nu = 20.344 Re_s^{0.659}, \tag{26}$$

which is valid for $G = 2.6$–9.9 kg·s^{-1}/m^2 and $Re_s = 65$–285. They reported that the heat transfer coefficient increases with increasing mass velocity, and, because film thickness increases with increasing mass velocity, the largest fraction of the heat is transferred by single-phase convection rather than by evaporation. Adopting the same correlation form, Oliphant et al. [66] derived the following relation for air-assist atomizer water data:

$$Nu = 32.5 Re_s^{0.51}, \tag{27}$$

which is valid for $Re_s = 100$–1000, where the length scales in Nu and Re_s are the square root of surface area and surface size, respectively.

Cheng et al. [51] correlated water data for full cone pressure nozzles with droplet Weber number and Reynolds number according to

$$Nu = 0.036 Re_d^{1.04} We_d^{0.28} Pr_f^{0.51}\left[3.02 + \left(\frac{T_w - T_f}{T_{sat}}\right)^{1.53}\right], \tag{28}$$

where Pr_f = 2.1–6.8 and Re_d is defined in terms of mean droplet velocity and Sauter mean diameter,

$$Re_d = \frac{\rho_f u_m d_{32}}{\mu_f}. \tag{29}$$

Eq. (28) indicates that heat transfer in the single-phase regime is influenced by surface temperature. Xie et al. [52] arrived at the same conclusion for pressure nozzles and a circular surface, and pointed out the complex influence of orifice-to-surface distance on heat transfer resulting from the spray cone producing different patterns (hollow or full) for different distances. They correlated water data according to

$$Nu = 8.705 Re_o^{0.323} \left(\frac{T_w}{\Delta T_{sub}}\right)^{0.8526} e^{-0.4268 H/D}, \tag{30}$$

where $12{,}600 \le Re_o \le 20{,}250$ and $0.2 \le H/D \le 1.0$, with Re_o based on the nozzle's orifice conditions.

Using a pressure nozzle, Wang et al. [67] found experimentally for water that optimum nozzle-to-surface distance for maximum heat flux is achieved when end points of the major axis of the elliptical spray impact area just inscribe the perimeter of a square surface, and film evaporation plays an important heat transfer role. They noted that strong rotational flow at the impact center creates a recirculating zone that accumulates an unsteady liquid pool at the center, and the extent of the recirculating zone decreases with increasing spray inclination angle. They recommended the following correlation for the single-phase regime:

$$Nu = 7.144 Re_s^{0.438} \left(\frac{T_w}{T_{sat} - T_a}\right)^{0.9016} \tag{31}$$

for both normal and inclined sprays and G = 15.7–24.9 kg·s^{-1}/m^2, where T_a is the ambient temperature and the length scale in Re_s is surface size. They also indicated that heat transfer performance and liquid utilization efficiency are enhanced with increasing spray inclination angle, a conclusion contradicting that of Visaria and Mudawar [68], who reported that inclination angle has little influence on single-phase heat transfer performance. Follow-up work by Wang et al. [69] yielded another correlation for water sprays with relatively high mass fluxes in the range of G = 44–53 kg·s^{-1}/m^2,

$$Nu = 0.1275 Re_s^{0.9322} \left(\frac{T_w}{T_{sat} - T_a}\right)^{2.2485}. \tag{32}$$

Overall, use of surface size as characteristic length in defining Nu is very questionable since different thermal performances are expected depending on whether the test surface is fully or partially impacted by the spray droplets. And even with full surface impact, different impact area coverages of the surface, resulting from different nozzle-to-surface distances, are expected to yield different cooling performances.

3.1.3. Other heat transfer coefficient correlations

Several investigators have opted for direct correlations of heat transfer coefficient, h, rather than ones based on the Nusselt number. Using the assumption that the wall liquid film consists of a turbulent liquid layer flowing over a thin viscous sublayer, Shedd and co-workers [70,71] proposed the following correlation for the single-phase heat transfer coefficient:

$$h = C \rho_f c_{pf} \overline{Q}'' Pr_f^{-1/2}, \tag{33}$$

which was verified for FC-72, FC-74, FC-40, HFE-7000, and HFE-7100. The magnitude of constant C in Eq. (33), which has the unit of m$^{1/2}$ s$^{-1/2}$, is dictated by nozzle configuration: C = 0.149 for a single nozzle and C = 0.129 for a four-nozzle array.

Some et al. [72] reported that the local heat transfer coefficient is related to local pressure, P, in the impinging region. In a related study, Abbasi et al. [73] reported that spray heat transfer depends primarily on kinetic energy of the incoming droplets rather than only the flow rate of liquid through the nozzle. By testing full cone, hollow cone, and flat PF-5060 sprays, they showed that the single-phase heat transfer coefficient has a strong dependence on the local pressure,

$$h = CP^{1/2}, \tag{34}$$

where $C \propto \rho_f^{1/2} c_{pf} Pr_f^n$, and the corresponding values for C are provided in Table 1. They also recommended that this correlation is validated for other fluids, as well as inclined and multiple, overlapping sprays. A follow-up study by Abbasi and Kim [74] involving three different fluids, PF-5060, PAO-2, and PSF-3, culminated in the more general correlation

$$h = 0.042 \rho_f^{1/2} c_{pf} Pr_f^{-0.33} P^{1/2}, \tag{35}$$

which is valid for Pr_f = 12–76 and P < 20 kPa.

Ciofalo et al. [57] measured the single-phase heat transfer coefficient for full cone water sprays corresponding to relatively high mass fluxes in the range of 8–80 kg·s^{-1}/m^2 and a fixed nozzle-to-surface distance of 50 mm. They concluded that the heat transfer coefficient is fairly insensitive to droplet diameter in the range of 0.4–2.2 mm, and correlated their data to mass flux and mean droplet velocity,

$$h = 206 (G u_m)^{0.84}, \tag{36}$$

for u_m = 13–28 m/s. A follow-up study by Ciofalo et al. [58] tested broader ranges of operating conditions and nozzle-to-surface distances from 0.1 to 0.4 m. They found that the heat transfer coefficient in the low mass flux range of G = 0.33–32.7 kg·s^{-1}/m^2 is a function of mass flux alone,

$$h = 2925 G^{0.687}. \tag{37}$$

In many experimental spray studies, the surface constitutes the upper end of a metallic bar that is fitted behind with a cartridge heater, and the surface temperature is extrapolated from an array of thermocouples situated along the axis of the metal bar assuming one-dimensional heat conduction. Therefore, the measured heat transfer coefficient, h, is based on a single surface temperature, which precludes the capture of spatial variations of h across the surface. In reality, h acquires maximum value at the spray axis and decays gradually away from the axis [75]. This points to the need to investigate spatial variations of the heat transfer coefficient more thoroughly, using such techniques as high-resolution thermal infrared imaging or a 3-dimensional matrix of fast-response thermocouples.

3.2. Film thickness measurement

As discussed earlier, spray cooling at high volumetric fluxes produces a very thin liquid film along the surface. The importance of this film to spray cooling has spurred efforts by several investigators to measure its thickness using a variety of techniques.

Table 1
Coefficient C for PF-5060 in Eq. (34) [73].

Spray nozzle	C	P [kPa]
Hollow cone	830	0–5
Full cone	850	0–5
Flat	810	0–5
Flat	710	0–20

Tilton [76] measured the film thickness for water sprays using a needle mounted on a traversing measuring scope. They measured thicknesses in the range of 120–350 μm, assuming uniform film thickness. Using an air-assist nozzle to generate a water spray, Yang et al. [77] measured the time-averaged maximum film thickness by adopting the Fresnel diffraction principle and an interference holographic technique to capture the film's surface topography. For constant air-assist pressure, they reported that film thickness increases with increasing water flow rate. With thickness variations smaller than 1 μm for average thicknesses in the range of 85–235 μm, they concluded that the film is quite flat. Using a non-intrusive optical technique, Mathews et al. [78] measured the instantaneous thickness of a liquid film deposited by an iso-octane atomized spray. The film thickness varied from 20 to 50 μm for droplet size and droplet velocity ranges of 110–350 μm and 10–21 m/s, respectively. It is important to emphasize that all these film thickness measurements were conducted under adiabatic conditions.

Using a non-intrusive total internal reflection technique, Pautsch and Shedd [79] measured the liquid film thickness for FC-72 created both at low flow rates from a single nozzle and high flow rates from a four-nozzle array. They found that film thickness in the spray impact region is virtually identical for adiabatic and diabatic conditions. For example, using a single nozzle with a flow rate of 0.863 ml/s, they measured a film thickness of 18.29 μm under adiabatic conditions, compared to 18.41 μm with a surface heat flux of 15 W/cm^2. Hsieh et al. [80] used an optical method to measured film thicknesses in the range of 1.75–2.75 and 0.02–0.14 mm for water and FC-72 sprays, respectively. Unlike Pautsch and Shedd, they detected a strong dependence of film thickness on heat flux.

Using a high-speed visualization system equipped with a microscope, Martínez-Galván et al. [81,82] found that liquid film thickness for R-134a is weakly dependent on volumetric flow rate or surface roughness within individual boiling curve regimes, but its value is regime dependent. A follow-up study by Martínez-Galván et al. [83] showed that decreasing spray cone angle delays the onset of nucleated boiling, and increases the film thicknesses within the nucleate boiling regime.

Xie et al. [84] constructed a theoretical model for liquid film flow along the surface, which resulted in the following relation for film thickness:

$$\delta(r) = \left\{ \dot{m}(r) \Big/ \left[\frac{\rho_f \pi r}{3\mu_f} \left(\frac{dM(r)}{dr} - \frac{dp}{dr} \right) \right] \right\}^{1/3}, \tag{38}$$

where $\delta(r)$, $\dot{m}(r)$ and $M(r)$ denote, respectively, local film thickness, mass flow rate, and radial momentum, all defined at a radius r from the spray axis. This model showed good agreement with needle conductive measurements by Chen et al. [85]. Based on this model, Xie et al. also developed a model for heat transfer in the single-phase regime. Jia et al. [86] constructed a different model for film thickness by solving continuity, momentum, and energy equations using velocity slip and temperature jump boundary conditions. Their model revealed that the film is thickest under the nozzle orifice and thins out in the radial direction.

Using thermal ink jet atomizers, Sharma et al. [87], Fabris et al. [88], and Escobar-Vargas et al. [89–91] investigated the liquid film produced by monodispersed water sprays with uniform 33-μm droplets. The film thickness was measured using a combination of strobe, microscope, and CCD camera. By calibrating the flow rate to generate a very thin (~5 μm) film, they showed that heat transfer is dominated by conduction across the film, resulting in a very high heat flux of 4000 W/cm^2 and evaporation efficiencies as high as 90%. The film thickness maintained a value of about 8 μm for surface superheats above 2 °C. Additionally, CHF was found to be a function of liquid mass flow rate but weakly dependent on wetted area.

Overall, studies centered on film thickness measurement are quite sparse, and most were conducted under adiabatic conditions; the effects of spray parameters and heat flux under diabatic conditions remain quite illusive. Additionally, there is significant uncertainty concerning the topography, and motion and heat transfer characteristics of the film. These characteristics are complicated by several factors, such as successive impingement of spray droplets, vapor and/or gas entrainment, bubble nucleation, droplet splashing, and coalescence and interference among droplets from neighborhood sprays. Clearly, film thickness warrants further, more in-depth study. Also, employing the relatively new technique of Total Internal Reflection (TIR) in conjunction with high speed imaging, which have both been adopted in drop impact studies, might be capable of capturing detailed behavior of the sprayed film.

3.3. Comparison with jet cooling

As discussed earlier, jet impingement and spray cooling are often deemed as competitors for high heat flux cooling applications. Pereira et al. [92] compared heat transfer performances of square arrays of water sprays and submerged jets. Their results indicated that sprays provide area-averaged heat transfer coefficients comparable to those with jets, but require a smaller coolant flow rate, albeit at the expense of higher pumping power. Sleiti and Kapat [93] arrived at similar conclusions. Karwa et al. [65] and Oliphant et al. [66] also achieved similar results when comparing data for single spray and jet nozzles, but did not address power consumption. They suggested that sprays offer superior cooling performance primarily because of the unsteady boundary layer produced by droplet impact, and secondarily because of evaporative cooling. In contrast to micro-jets, Fabbri et al. [94] found that sprays require a higher ratio of pumping power to heat removal rate. However, sprays provided superior cooling performance compared to micro-jets for a relatively low volumetric flux of 2.87 μl·s^{-1}/mm^2, but performances were comparable for a higher volumetric flux of 4.63 μl·s^{-1}/mm^2.

Several studies also compared cooling performances of sprays and jets in higher temperature regimes. Using R-113 as working fluid, Cho and Wu [95] found that, near CHF, a large fraction of the surface dries out with jet cooling but not spray cooling. And, while CHF values were comparable for both, Cho and Wu concluded that sprays provide superior performance by preventing the large spatial temperature gradients and high surface temperatures resulting from appreciable dryout in jets. They also developed CHF correlations for both cooling schemes, which do not account for droplet size or jet diameter as suggested by the majority of earlier studies.

Estes and Mudawar [23] compared cooling performances of sprays and jets, and showed that increases in liquid flow rate and/or subcooling increase CHF of both schemes. At high subcooling, the two schemes yielded comparable CHF values for equal flow rates. But, at low subcooling, CHF for sprays was much higher than for jets. They attributed this difference to hydrodynamic structure of the liquid film deposited upon the surface. In jet cooling, anchored to the surface only in the central impingement zone, the film (or wall jet) tends to separate from the outer portions of the surface during vigorous boiling due to vapor momentum normal to the surface. While, in spray cooling, individual droplets are quite effective at securing liquid film contact with the surface at low subcoolings, which, for the same flow rate, enhances CHF relative to jet cooling. Labergue et al. [96] compared jet cooling with spray cooling in the film boiling regime and showed that sprays provide superior spatial cooling uniformity. Sprays also

yielded superior cooling efficiency and lower liquid consumption than jets.

4. Nucleate boiling

4.1. Mechanisms

Aside from *homogeneous nucleation* from the surface, two other mechanisms have been proposed for spray phase-change heat transfer [97]. The first is *thin film evaporation and convection* [43], where the spray produces a thin liquid film on the surface through which the heat is conducted. Because saturation temperature is maintained atop the film, a thinner film results in a higher heat transfer rate, which is further enhanced by the droplet impact. The second mechanism is *secondary nucleation* [42,98], where droplets entrain vapor and/or gas into the liquid film, promoting bubble nucleation and vigorous boiling within the film. Additionally, droplets can puncture the rapidly growing bubbles, increasing the bubble nucleation frequency. The bursting bubbles also produce smaller droplets, some of which are re-deposited onto the film and entrain bubbles, producing a chain reaction of secondary nucleation [99]. Visualization experiments have demonstrated that droplet impact can decrease both the life cycle and breakup equivalent diameter of nucleating bubbles [100].

Using air-atomized nozzles rather than pressure nozzles, Pais et al. [43] reported that for surface roughness greater than 1 μm, homogeneous nucleation plays a major heat transfer role. But for a film thickness on the order of 0.1 μm, heat is mostly conducted through the film and evaporated along the interface, yielding very high heat fluxes on the order of 1200 W/cm^2 for water corresponding to low surface superheats. However, Mesler [99] argued that the high heat fluxes reported by Pais et al. are mainly the result of secondary nucleation associated with microlayer evaporation. Rini et al. [98] examined secondary nucleate sites using a high-speed video system fitted with a microscopic lens. They showed that increasing droplet/spray mass flux for a given heat flux increases the number of nucleate sites, which shortens bubble lifetime. However, the fractional contribution of nucleate boiling to the total heat flux remains constant, about 50%, in spite of the increased bubble removal rate. They also suggested that increasing the droplet/spray mass flux can enhance heat transfer by convection and direct evaporation because of enhanced turbulent mixing.

Using the total internal reflection technique, Horacek et al. [97,101] showed that spray heat transfer is primarily dictated by the three-phase contact length rather than the wetted area fraction, implying that it is possible to improve heat transfer by enhancing and/or controlling contact line length on the surface.

Using both heat transfer data and flow visualization techniques, Shedd and Pautsch [102] suggested that spray heat transfer is dominated by three components: a single-phase component in and around the droplet impact region, a two-phase liquid film boiling component away from the impact region, and a single-phase drainage flow component for the case of multi-nozzle sprays. They concluded that phase change is a minor contributor to overall heat transfer rate.

Grissom and Wierum [103] identified three distinct operational modes for spray cooling. The first, which corresponds to conditions yielding total vaporization of impinging droplets, the so-called 'dry-wall' state, was described as *spray evaporative cooling*. They suggested that this mode is highly effective in utilizing the liquid and leads to high heat flux removal from the surface corresponding to small surface superheats [104]; alas this mode is difficult to maintain and control [70]. The second mode, where spray droplets accumulate a thin liquid film on the surface, which serves as a resistance to heat removal, referred to as 'flooded' state, was described as *spray film cooling*. The third, which is produced by high surface temperatures outside the nucleate boiling range, referred to as the 'Leidenfrost' state, was described by impinging droplets being deflected from the surface by a thin vapor film. Grissom and Wierum also developed a conduction-controlled analytical model for droplet evaporation, which showed fairly good agreement with measurements at atmospheric pressure. They reported that, at atmospheric pressure, the spray film cooling mode resembles pool boiling, but, under vacuum conditions, the heat is removed by conduction across the liquid film without nucleation.

Using experimental data, Jia and Qiu [105] suggested that spray heat transfer can be divided into four regions, Fig. 9, using a parameter ε called *expulsion rate*, which is defined as the ratio of local liquid mass flow rate of outgoing liquid, $\dot{m}_e$, to that of incoming liquid, $\dot{m}$,

$$\varepsilon = \frac{\dot{m}_e}{\dot{m}}. \tag{39}$$

In region I, droplets are expelled mainly from splashing between the spray and liquid film. Region II is initiated when surface temperature reaches a few degrees higher than the saturation temperature, and is terminated when the expulsion rate reaches peak value. Expelled droplets in region II are caused by explosion of microbubbles and splashing, causing the liquid film to break into several relatively large portions and its thickness to decrease, and resulting in sharp increases in both heat flux and expulsion rate. Region III is initiated by a subsequent decrease in expulsion rate, where the heat transfer mechanism changes from nucleate boiling within the continuous thin liquid film to droplet evaporative cooling. As heat flux is increased in region III, the liquid film becomes even thinner until it is completely broken into many small droplets and/or disks, which decreases fluid expulsion by micro-bubble explosion and splashing. Region III is terminated at CHF, where expulsion rate reaches a local minimum. In region IV, a vapor layer is generated beneath the droplets, causing them to rebound from the surface and the expulsion rate to increase again. Jia and Qiu characterized these spray heat transfer mechanisms as convective cooling for region I, boiling in the thin liquid film for region II, droplet impact cooling for region III, and film boiling for region IV. They proposed the following simple relation between heat flux and expulsion rate:

$$q'' = G(1-\varepsilon)(h_{fg} + c_{pf}\Delta T_{sub}). \tag{40}$$

They also identified two advantages of adding surfactant to the spray liquid: lower superheat and wider, more stable CHF temperature range. They concluded that surfactant addition can provide added safety against burnout for temperature sensitive devices.

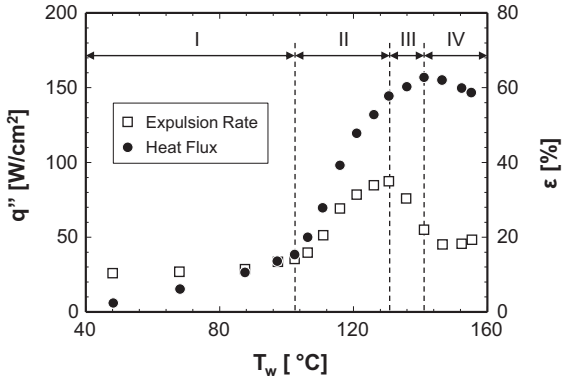

Fig. 9. Heat flux and expulsion rate for water spray cooling with $G = 0.847$ kg·s^{-1}/m^2. Adapted from Jia and Qiu [105].

Webb et al. [106] investigated spray nucleate boiling at low mass fluxes. They suggested that the transition from the single-phase regime to nucleate boiling is related to average concentration of the spray, defined as the ratio of spray mass flux to average droplet velocity. Interestingly, for both pressure nozzles and air-assist nozzles, no clear transition was observed above a critical concentration value of about 0.20 kg/m^3.

Although several nucleate boiling mechanisms have been proposed and verified through experimental measurements and/or flow visualization techniques, modeling work based on these mechanisms is quite sparse. Given that nucleate boiling is the dominant regime for most low temperature spray cooling applications, this regime warrants significant attention in future studies.

4.2. Models and correlations

Mudawar and Valentine [45] found that heat flux in the nucleate boiling regime is insensitive to the spray's hydrodynamic parameters and depends only on surface temperature. They correlated their water data for pressure spray nozzles according to:

$$q''_{NB} = 1.87 \times 10^{-5} \Delta T_f^{5.55}, \tag{41}$$

where q''_{NB} is in W/m^2 and ΔT_f (=$T_w - T_f$) in °C; this correlation is valid for fluid temperatures of 22.5–23.5 °C. Mudawar and Valentine showed that incipient boiling can be correlated with either d_{32} or $d_{0.5}$ using the respective correlations

$$\Delta T_f = 13.43 Re_s^{0.167} Pr_f^{0.123} \left(\frac{k_f}{d_{32}}\right)^{0.220} \tag{42a}$$

and

$$\Delta T_f = 13.50 Re_s^{0.172} Pr_f^{0.123} \left(\frac{k_f}{d_{0.5}}\right)^{0.220}. \tag{42b}$$

For water sprays with 100-ppm surfactant concentration and G = 2.8 kg·s^{-1}/m^2, Qiao and Chandra [18] derived a correlation for nucleate boiling of water sprays similar in form to that of Mudawar and Valentine,

$$q''_{NB} = 0.56 \times 10^{-5} \Delta T_f^6. \tag{43}$$

Dou et al. [107] also adopted a similar form to correlate their water data for flow rates in the range of 30–50 l/min according to

$$q''_{NB} = 1.837 \times 10^4 \Delta T_f^{0.69}. \tag{44}$$

However, Yoshida et al. [21] suggested that heat flux in the nucleate boiling region should be correlated with wall superheat, ΔT_{sat} (=T_w - T_{sat}) instead of ΔT_f. Using this dependence, Pereira et al. [108] correlated their water data for four and five nozzle arrays and ΔT_{sub} = 30–75 °C according to

$$q''_{NB} = 2067 \Delta T_{sat}^{1.57}. \tag{45}$$

In an effort to cover a broad range of fluid properties and subcoolings, Rybicki and Mudawar [17] combined their upward-facing PF-5052 data and downward-facing water data of Mudawar and Valentine [45] to construct the following correlation for the nucleate boiling region, Fig. 10,

$$\frac{q''_{NB} d_{32}}{\mu_f h_{fg}} = 4.79 \times 10^{-3} \left(\frac{\rho_f}{\rho_g}\right)^{2.5} \left(\frac{\rho_f \overline{Q}''^2 d_{32}}{\sigma}\right)^{0.35} \left(\frac{c_{p,f} \Delta T_f}{h_{fg}}\right)^{5.75}. \tag{46}$$

Visaria and Mudawar [109] reported that increasing the liquid subcooling not only delays incipient boiling, but also decreases the slope of the nucleate boiling region of the boiling curve.

When the impact areas of two adjacent sprays overlap, there is an increase in the mean volumetric flux for both impact areas, which can have a significant influence on nucleate boiling heat transfer. Visaria and Mudawar [15] developed a theoretical model for mean volumetric flux of a spray with flow rate Q_1 overlapping with a neighboring spray with flow rate Q_2,

$$\overline{Q}''_1 = \frac{Q_1}{\left(\frac{\pi D^2}{4}\right)} \left\{1 - \frac{Q_1}{\pi[1 - \cos(\theta/2)]} f_o(4 - Q_2/Q_1)\right\}, \tag{47}$$

where f_o is an integral function. To assess the influence of spray overlap on nucleate boiling, the mean volumetric flux in Eq. (46) must be replaced by the mean flux obtained from Eq. (47).

Using R-113 as working fluid, Ghodbane and Holman [48] conducted experiments involving a vertically oriented surface cooled by a horizontal spray. They pointed out that heat flux is independent of surface size when the surface is located in the core of a uniform spray. Increasing the volumetric flux or subcooling delayed both the onset of nucleate boiling and CHF. They also suggested that, because nucleate boiling is highly sensitive to subcooling, the temperature influence on heat flux should be scaled by ΔT_f and not ΔT_{sat}, as reflected in their nucleate boiling correlation

$$\frac{q''_{NB} H}{\mu_f h_{fg}} = 10.55 \left(\frac{\rho_f u_m^2 d_{0.5}}{\sigma}\right)^{0.6} \left(\frac{c_{p,f} \Delta T_f}{h_{fg}}\right)^{1.46}, \tag{48}$$

which is valid for u_m = 5.4–28.5 m/s and $d_{0.5}$ = 0.21–0.98 mm. Later, Holman and Kendall [110] extended these experiments to smaller droplet diameters, and revised their correlation to the form

$$\frac{q''_{NB} H}{\mu_f h_{fg}} = 9.5 \left(\frac{\rho_f u_m^2 d_{0.5}}{\sigma}\right)^{0.6} \left(\frac{c_{p,f} \Delta T_f}{h_{fg}}\right)^{1.5}, \tag{49}$$

which is valid for u_m = 5.4–28.5 m/s and $d_{0.5}$ = 0.096–0.98 mm.

Hsieh et al. [111] correlated nucleate boiling data for water and R-134a, respectively, according to

$$\frac{q''_{NB} H}{\mu_f h_{fg}} = 15.6 \left(\frac{\rho_f u_m^2 d_{32}}{\sigma}\right)^{0.59} \left(\frac{c_{p,f} \Delta T_f}{h_{fg}}\right)^{1.68} \tag{50a}$$

and

$$\frac{q''_{NB} H}{\mu_f h_{fg}} = 2.1 \left(\frac{\rho_f u_m^2 d_{32}}{\sigma}\right)^{0.66} \left(\frac{c_{p,f} \Delta T_f}{h_{fg}}\right)^{1.51}, \tag{50b}$$

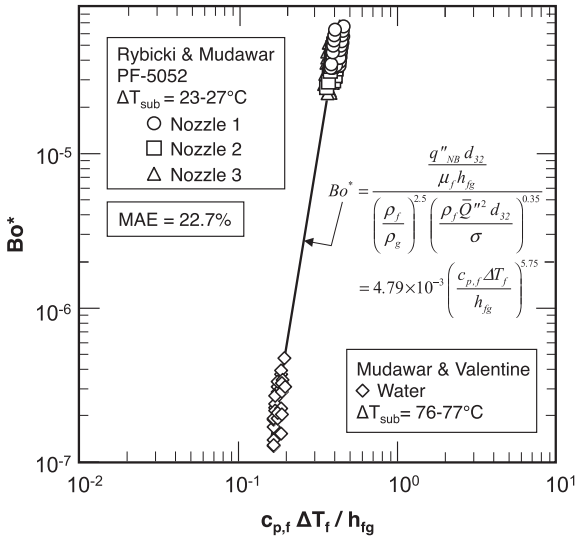

Fig. 10. Nucleate boiling correlation for upward-oriented PF-5052 sprays and downward-oriented water sprays. Adapted from Rybicki and Mudawar [17].

where differences in thermophysical properties between the two fluids are reflected mostly by right-hand-side multipliers. The correlations are valid for We_d = 80–231 and ΔT_{sub} = 55–60 °C for water, and We_d = 50–152, and ΔT_{sub} = 2–4 °C for R-134a. More recently, Hsieh et al. [80] employed a non-intrusive optical technique combining micro-particle image velocimetry and micro-laser-induced fluorescence to investigate water spray cooling with ΔT_{sub} = 77 °C, and correlated their new data according to

$$\frac{q''_{NB}H}{\mu_f h_{fg}} = 12.3\left(\frac{\rho_f u_m^2 d_{32}}{\sigma}\right)^{0.525}\left(\frac{c_{p,f}\Delta T_f}{h_{fg}}\right)^{1.854}\left(\frac{H}{L}\right)^{0.924}. \tag{51}$$

Sehmbey et al. [112,113] investigated liquid nitrogen spray cooling for G = 16.9–88.9 kg·s^{-1}/m^2, d_{32} = 14–29 μm, u_m = 14–30.7 m/s, and heat fluxes as high as 165 W/cm^2. They correlated their nucleate boiling data according to

$$\frac{q''_{NB}c_{p,f}D}{k_f h_{fg}} = 9.4\left(\frac{\rho_f u_m D}{\mu_f}\right)^{0.3}\left(\frac{u_m}{\overline{Q''}}\right)^{0.16}\left(\frac{D}{d_{32}}\right)^{0.24}\left(\frac{c_{p,f}\Delta T_f}{h_{fg}}\right)^{1.12}, \tag{52}$$

where D is hydraulic diameter of the surface.

Ortiz and Gonzalez [114] mathematically correlated data for water sprays with inclination angles in the range of α = 0–90° impacting smooth and rough surfaces, respectively, according to

$$q''_{NB} = 133Q\left(\frac{\Delta T_{sat}}{\Delta T_{sub}}\right)^{0.47} \tag{53a}$$

and

$$q''_{NB} = 120Q\left[1+0.25(\cos\alpha)^{1.75}\right]\left(\frac{\Delta T_{sat}}{\Delta T_{sub}}\right)^{0.30}, \tag{53b}$$

where q''_{NB} is in W/cm^2, and Q in l/h. These correlations are valid for $Q \approx$ 1.5 l/h for the smooth surface and 1.5 < Q < 3 l/h for the rough surface. The smooth surface was achieved by rubbing the surface with 3.0-μm aluminum oxide suspension, followed by 1-μm and 0.25-μm polycrystalline diamond suspensions. The rough surface was achieved by rubbing the surface with silicon carbide abrasive paper with increasing roughness levels of 320, 400, and 600 grit.

Tan et al. [115] investigated spray cooling performance of a six-nozzle array using R-134a as working fluid. They classified their data into two regions: low flux region, 35–120 W/cm^2, where the heat transfer coefficient increases with increasing flow rate, and high flux region, 120–165 W/cm^2, corresponding to deterioration in the heat transfer coefficient. They correlated nucleate boiling data for the low flux region according to

$$\frac{q''_{NB}}{\rho_f \overline{Q''} h_{fg}} = 1.7453\left(\frac{\rho_f u_m^2 d_{32}}{\sigma}\right)^{-0.3514}\left(\frac{c_{p,f}\Delta T_{sat}}{h_{fg}}\right)^{1.5286}\left(\frac{\rho_f \sigma \dot{m}}{\mu_f^3}\right)^{0.1643}\left(\frac{\Delta T_{sub}}{\Delta T_{sat}}\right)^{0.1946}, \tag{54}$$

which is valid for d_{32} = 145–182 μm and u_m = 18.6–19.6 m/s.

Cabrera and Gonzalez [116] fitted their monodispersed water spray data according to

$$\frac{q''_{NB}}{\rho_f u_d h_{fg}} = 0.245\left(\frac{c_{p,f}\Delta T_{sat}}{h_{fg}}\right)^{1.038}\left(\frac{\rho_f \sigma \dot{m}}{\mu_f^3}\right)^{0.133}\left(\frac{\Delta T_{sub}}{\Delta T_{sat}}\right)^{0.491}\left(\frac{R_a}{d_d}\right)^{0.0213}\left(\frac{P_a}{P_{atm}}\right)^{0.291}, \tag{55}$$

where P_a, P_{atm}, and R_a denote ambient pressure, atmospheric pressure, and surface roughness, respectively. This correlation is applicable to mass fluxes of 340–750 kg·s^{-1}/m^2, subcoolings of 25–78 °C, and ambient pressures of 1–1.8 bar, and is fairly effective at predicting data for commercial nozzles by Ortiz and Gonzalez [114].

Liu et al. [117] studied R-134a spray cooling on a copper surface for pressures ranging from 0.2 to 0.4 MPa, and found that both spray efficiency and CHF improve with increasing pressure. They proposed the following nucleate boiling correlation:

$$\frac{q''_{NB}}{\rho_f Q'' h_{fg}} = 0.086\left(\frac{\rho_f Q''^2 d_{32}}{\sigma}\right)^{-1.594}\left(\frac{c_{p,f}\Delta T_{sat}}{h_{fg}}\right)^{1.503} \times \left(\frac{\rho_f \sigma \dot{m}}{\mu_f^3}\right)^{0.517}\left(\frac{\rho_f}{\rho_g}\right)^{0.916}\left[\frac{1}{r_d}\sqrt{\frac{\sigma}{g(\rho_f-\rho_g)}}\right]^{0.418} \tag{56}$$

for flow rates in the range of 0.211–0.356 l/min, where r_d is bubble departure radius.

Chen et al. [118] conducted experiments in which u_m, Q'', and d_{32} were varied independently. For dense water sprays, they showed that excess liquid flows over the surface without being vaporized or significantly heated. Additionally, droplets may be prevented from contacting the surface by the uprising vapor [76]. These findings point to poor performance of dense sprays in terms efficiency of liquid usage, compared to superior efficiency for dilute sprays. Their data showed efficiency varying with $Q''^{-2/3}$, $d_{32}^{-14/5}$, and $u_m^{1/4}$, which implies better efficiency can be realized by increasing droplet velocity and/or decreasing droplet size and number. Chen et al. [119] later compared spray cooling performances for R-134a and R-22. Despite lower CHF for R-134a, mostly because of inferior latent heat of vaporization, R-134a showed superiority to R-22 in the nucleate boiling region below 80 W/cm^2.

Using pressure nozzles, Cheng et al. [120] found that the heat transfer coefficient for water is highest when the surface is not fully impacted by the spray. They also found that the influence of inclination angle on heat transfer depends on both spray angle and nozzle-to-surface distance. Additionally, surface temperature showed appreciable non-uniformity, reaching highest value at the surface center, and lowest value in a nearby location where the liquid film emerges. Their work was continued by Zhao et al. [121], who constructed a model for heat and mass transfer in spray cooling, taking into account droplet-film impact, film formation and flow behavior, bubble formation due to wall nucleation and secondary nucleation, droplet-bubble interaction, bulk air convection, and radiation. They showed that droplet-film impact and film convection play major roles in spray cooling when the surface is not superheated, while bubble nucleation becomes very important for superheated conditions. They also used the same model to explore surface temperature non-uniformity. Cheng et al. [122] investigated this problem further and reported that temperature non-uniformity can be greatly reduced by using a small spray angle, low system pressure, small nozzle-to-surface distance, and/or high nozzle inlet pressure. For vapor-assist nozzles, Yan et al. [123] reported that surface temperature uniformity can be improved by increasing spray flow rate and/or nozzle inlet pressure. Cheng et al. [124] theoretically examined surface temperature non-uniformity in terms of the influences of droplet velocity, Sauter mean diameter (d_{32}), droplet number, and heat input on thickness and velocity of the liquid film. They suggested that using a uniform spray promotes better uniformity in film thickness, which in turn enhances surface temperature uniformity. Overall, surface temperature uniformity was influenced mostly by droplet number, followed by droplet velocity, while d_{32} had only a minor influence.

To simulate spray cooling, Xie et al. [125] recently constructed a numerical model incorporating two sub-models. The first is a spray characteristics sub-model, based on a Monte Carlo algorithm by Kreitzer and Kuhlman [126], which was used to predict droplet diameter, droplet velocity, and spatial distribution of droplet flux. The second is a heat transfer sub-model, which describes spray cooling in terms of liquid film flow boiling with droplet impingement, forced convection, and thin film bubble boiling. However, their model did not account for secondary droplets formed by splashing due to droplet-film interaction, or vapor uprising from the film. Other numerical models of spray cooling include two-

dimensional simulations by Selvam et al. [127,128], and three dimensional simulations by Sarkar and Selvam [129]. These simulations examined growth of micro vapor bubbles due to nucleation in a 40–150 μm liquid film in the presence of droplet impact, using the level set method to capture the interface. The simulations accounted for surface tension, gravity, phase change, and liquid viscosity. They showed that collapse of vapor bubbles, either by liquid droplet impact or merging with vapor atop the thin liquid film, has a significant influence on spray cooling. The simulations identified several mechanisms contributing to spray cooling, including the complicated interactions of thermal conduction from the surface to liquid, liquid convection during droplet impact, vapor bubble breakup, and vapor bubble generation due to nucleation. This numerical approach was later extended to microgravity conditions [130]. Issa and Yao [131,132] simulated single droplet stream impact as well as full cone spray impact from nucleate to film boiling for different ambient pressures. Chen et al. [133] presented numerical simulation results for FC-72 spray cooling, including investigation of the effects of flow rate and nucleation site density on both single-phase and two-phase heat transfer. Their simulations showed that secondary nuclei entrained by the droplets outnumber the surface nuclei. Recently, Hou et al. [134] investigated multi-nozzle spray cooling using a CFD method based on fundamentals of air flow and droplet collision dynamics. Landero and Watkins [135] combined several empirical correlations and models of both spray hydrodynamics and heat transfer to predict spray cooling performance through mathematical and numerical analysis.

Several studies have been dedicated to nucleate boiling heat transfer using air-assist nozzles. For example, using water as working fluid, Yang et al. [42] and Sehmbey et al. [136,137] showed that heat transfer is enhanced by increasing the air flow rate because of a number of factors, including thinning of the liquid film, increasing momentum of water droplets (and therefore local convection), and improving ability to remove the vapor evolving from the liquid film. The latter also reduces partial pressure of vapor near the film's free interface, which in turn reduces phase-change temperature in that region. Yang et al. recommended the following correlation for heat transfer coefficient in the nucleate boiling region [42],

$$Nu = \frac{h\delta}{k_f} = 1.031\left[\overline{Q}''\delta\left(\frac{c_{p,f}\mu_f}{k_f}\right)^{0.5}\frac{\rho_f g^{0.25}}{h_{fg}\sigma^{0.75}\rho_g^{1.25}}\right]^{0.655}, \tag{57}$$

which is based on film thickness, δ, and is valid for droplet diameters and droplet velocities in the ranges of 10–18 μm and 25–58 m/s, respectively. Sehmbey et al. reported that higher contact angles promote nucleation and, hence, improve heat transfer. And despite the benefits of surface roughness to nucleation, a very smooth surface (better than 0.3 μm polish) showed a dramatic increase in cooling performance because of a much thinner liquid film, which promoted liquid evaporation through direct conduction across the film. Yang et al. [77] experimentally determined that the film thickness is fairly uniform. Based on this observation and the assumption of constant volumetric flux, Yang et al. [138] derived the following analytical relation between mean volumetric flux and film thickness for air-assist sprays:

$$\overline{Q}'' = \frac{2}{3}\frac{\rho_g}{\mu_f}C^2\delta^3 + 1.312\sqrt{\frac{C^3\mu_g\rho_g}{\mu_f^2}\delta^2}, \tag{58}$$

where C is an empirical constant.

Despite the large number of published articles addressing the nucleate boiling regime, including experimental data, correlations, and theoretical models, most address single coolants or very limited ranges of operating conditions. Robust and accurate modeling of the nucleate boiling regime, however, remains illusive, and better models are needed that can effectively describe and account for the complex mechanisms associated with spray cooling, including direct thermal conduction, evaporation, convection, surface nucleation, and secondary nucleation.

4.3. Heat transfer in microgravity

As space missions increase in both scope and complexity, there is a commensurate increase in the amounts of heat that need to be rejected from both avionics and astronauts. This has led to a surge in thermal control system concept development for space vehicles that rely on phase change, including spray cooling. Unfortunately, much of the spray cooling knowhow comes from experiments performed in Earth gravity, and whose results may not be equally valid for microgravity.

In general, initial droplet breakup in pressure sprays is only weakly dependent on gravity, but the flow of residual unevaporated liquid can be highly gravity dependent. In microgravity, the liquid acquires strange shapes and flow patterns, such as multiple spherical liquid globs that cannot be easily removed from the surface [139]. This obviously will have a strong bearing on both cooling performance and reliability of the entire thermal control system.

Michalak et al. [140] found that, for accelerations in the range of $0.15\ g < a < 1.80\ g$ and flow rates of 6.18–8.94 ml/s, wall superheat in FC-72 sprays increases with increasing acceleration. This study was conducted in a partially confined spray chamber designed by Baysinger et al. [141] for parabolic flight aboard NASA's KC-135 aircraft. Baysinger et al. also developed a transient analytical model to predict surface temperature and spray heat transfer coefficient. Also adopting a partially confined spray chamber, Yerkes et al. [142] investigated the effects of variable gravity on spray cooling of FC-72 in the single-phase regime. They found that Nu is a function of both the Froude and Galileo numbers. Gambaryan-Roisman et al. [143] investigated a water spray impacting a liquid film under normal and microgravity conditions. They concluded that both the liquid–gas interface and film thickness are influenced by the spray parameters, and cooling performance declines appreciably in microgravity, especially at high flow rates.

Using FC-72 as working fluid, Elston et al. [144,145] investigated the cooling performance of a 16-nozzle array on NASA's C-9 aircraft for flow rates ranging from 13.1 to 21.3 g/s and accelerations of 0.02–2.02g. They found that microgravity can provide better cooling performance compared to terrestrial or elevated gravities, evidenced by lower surface superheats. However, a sudden degradation in performance was encountered at relatively high flow rates of 17.5–21 g/s because of liquid buildup in the spray overlap areas, where liquid film thickness was much greater than that directly under the spray. Also using FC-72, Conrad et al. [146] tested a linear nozzle array in both microgravity and enhanced gravity ($\sim$1.8g) aboard NASA's DC-9B aircraft. They reported that coolant flow rate is the main determinant of the heat transfer coefficient, while gravity bears only a weak influence.

Two major drawbacks of the parabolic flight experiments are high cost and difficulty conducting experiments. To alleviate these problems, Hunnell et al. [147] used a controlled electric field to generate body force, in order to either enhance or balance earth gravity, thereby simulating the effects of variable gravity on spray cooling. They also performed initial tests in terrestrial gravity. To eliminate the influence of gravity perpendicular to the surface, they performed experiments with horizontal sprays, and showed that cooling performance at 9.8×10^{-6} m^3/s with a horizontal spray is better than with a vertical spray. On the other hand, heat transfer was insensitive to orientation for low flow rates. Continuing the work of Hunnell et al., Kreitzer et al. [148] and Kuhlman et al. [149] examined the effects of electrical field on cooling

performance, reporting a 5–15% improvement resulting from the Coulomb force electrode. Further efforts to improve cooling performance were carried out by Kreitzer et al. [150] and Kreitzer and Kuhlman [151] by applying relatively high voltage directly to the nozzle. They observed profound changes in spray pattern, with droplets becoming smaller due to electrostatic atomization when the voltage exceeded 15 kV. Yet, they did not detect any appreciable change in heat transfer performance.

In addition to the above reduced gravity studies, Yoshida et al. [21], Kato et al. [152], and Sone et al. [153] performed experiments to explore the influence of microgravity on CHF. Findings from these studies will be discussed in a later section.

4.4. Heat transfer enhancement

4.4.1. Surface treatment

Pais et al. [43] examined the influence of surface roughness on air-atomized water spray cooling of copper surfaces prepared with polishing pastes having grit sizes in the range of 0.3–22 μm. They found that smoother surfaces (<1 μm), where the heat transfer is dominated by film conduction/evaporation, provide superior cooling performance. Kang and Choi [154] arrived at similar findings for air-assist water sprays and surface roughness values from 0.45 to 4.47 μm. Sehmbey et al. [112,113] investigated the effects of surface roughness with values ranging from 0.05 to 0.15 μm on cooling performance for liquid nitrogen pressure nozzles. Unlike Pais et al. and Kang and Choi, they noted that increasing roughness greatly enhanced heat transfer performance, a conclusion that may be related to differences in thermophysical properties and wetting characteristics between water and liquid nitrogen. Ortiz and Gonzalez [114] also reported that cooling performance for water pressure nozzles is enhanced with increasing surface roughness, but did not provide values for the surface roughness. The same conclusion was shared by Zhang et al. [155] for deionized water pressure sprays impacting a wire-cut grooved surface. Martínez-Galván et al. [156] found that CHF for R-134a increases with increasing flow rate for a surface with R_a = 0.56 μm, but is weakly dependent on flow rate for a smoother surface with R_a = 0.04 μm. The rougher surface was also found to promote earlier onset of nucleate boiling and delay CHF. Fukuda et al. [157] reported that increasing surface roughness improves water spray cooling in the film boiling regime.

Hsieh and Yao [19] investigated evaporative spray cooling of silicon surfaces textured with square micro-studs using very low water mass fluxes. The evaporative mechanism examined in their study was dominated entirely by conduction across the thin liquid film, which is different from that proposed by Grissom and Wierum [103]. Hsieh and Yao suggested four distinct heat transfer regimes: flooded, thin film, partial dryout, and dryout. They concluded that surface micro-texture has a negligible influence on heat transfer in both the flooded regime, where the surface is completely covered with liquid, and the dryout regime, where the surface is covered with vapor. However, the micro-textured surface yielded better heat transfer than a plain surface in the thin film and partial dryout regimes. They suggested that capillary forces between micro-studs not only help retain more water for sustaining the cooling process, but also more effectively spread the liquid into a thinner film, thereby enhancing the evaporative heat transfer. Furthermore, they reported heat transfer dependence on surface material, with aluminum yielding better results than silicon because of better wettability.

Kim et al. [158] compared water spray cooling performances of plain and micro-porous coated flat and cylindrical surfaces. The enhanced surfaces were formed by applying a coating containing micron-sized aluminum particles, which increased both vapor/gas entrapment volume and active nucleation-site density. These increases were attributed to formation of openly connected porous structures with different-sized cavities. Overall, capillary pumping action within the porous coating was observed to enhance evaporative cooling and increase CHF appreciably compared to a plain surface. At low heat fluxes, cooling performance of the coated surface was insensitive to flow rate in the range of 1.25–2.4 ml/min, but, at high heat fluxes, the performance was enhanced with increasing flow rate, and best results were realized with a 100-μm coating. Additionally, the enhancement was better with the micro-porous coating applied to the flat surface than to the cylindrical surface because of inferior wettability and inability to access the portion of the surface opposite to the spray for the latter. Thiagarajan et al. [159] investigated spray cooling of HFE-7100 on a conductive micro-porous copper surface and reported a 300–600% enhancement in the heat transfer coefficient, which is superior to the enhancement achieved with a nano-wire-grown surface [160].

Silk [161] found that a copper surface drilled uniformly with 1.0-mm holes achieves CHF values for PF-5060 as high as 141 W/cm^2, a 75% enhancement compared to a plain surface. Silk et al. [162,163] also compared PF-5060 spray cooling performances for different structured surface geometries: cubic pin fins, pyramids, and straight fins, in addition to a plain surface for both normal and inclined sprays. It should be emphasized that, unlike micro coatings, the characteristic dimensions of these structures are much larger than the liquid film thickness. The sprays were generated by a 2×2 nozzle array at a volumetric flux of 0.016 m^3 s^{-1}/m^2. For normal sprays, they achieved CHF values for the four surfaces of 114, 105, 126, and 80 W/cm^2, respectively, and corresponding evaporation efficiencies of 41%, 38%, 46%, and 29%. They also measured CHF for inclination angles in the range of 0–45° with a constant nozzle-to-surface distance, and the highest CHF value of 140 W/cm^2 was achieved with the straight fin surface and α = 30°. Follow-up work by Coursey et al. [164] extended these findings to surfaces with straight fins with much finer fin width, pitch, and length, to substantially increase the heat transfer area. While long fins showed better cooling performance in the single-phase regime, nucleate boiling showed best performance with 1–3-mm long fins. Hou et al. [165] used an array of eight water spray nozzles to cool micro-structured surfaces, and superior cooling performance in the single-phase and nucleate boiling regimes was achieved with straight fins and cubic pin fins, respectively. The superior single-phase cooling performance of straight fins was also confirmed by Liu et al. [166]. Xie et al. [167] emphasized that, rather than total wetted surface area, fin arrangement on the surface plays a decisive role in heat transfer enhancement, and an improper fin arrangement may offset the benefits of increased wetted area. They also noted that, by providing an abundance of nucleation sites and stronger capillary effects, micro-structured surfaces ensure superior nucleate boiling performance for R-134a. On the other hand, higher CHF was achieved with macro-structured surfaces. Li et al. [168] investigated heat transfer enhancement for R-134a with cubic pin fins, and found that highest heat transfer coefficient is achieved at a flow rate of 1.6 l/min, and maximum CHF of 326 W/cm^2 at 2.15 l/min. Chien et al. [169] showed that, for heat fluxes exceeding 20 W/cm^2, a pin–fin surface yields 10–40% heat transfer enhancement with FC-72 compared to a smooth surface. Similarly, Aamir et al. [170] showed that water sprays impacting an enhanced surface modified with pyramid pins at high temperatures provide better cooling performance compared to a smooth surface. Wang et al. [171] investigated water spray cooling on smooth, drilled, and straight fin surfaces, as well as surfaces with both drilled holes and fins. The drilled surface yielded the highest heat transfer coefficient, while the combined enhancement surface produced the highest cooling efficiency. Zhang and Wang [172] studied water spray cooling on straight-grooved surfaces at

two volumetric fluxes. For the lower volumetric flux of 1.6×10^{-3} - $m^3\ s^{-1}/m^2$, the surface with a groove depth of 0.5 mm and width of 0.4 mm produced the greatest heat flux enhancement in the single-phase regime. On the other hand, a groove depth of 0.5 mm and width of 0.2 mm showed superior performance at the higher volumetric flux of $12.7\times10^{-3}\ m^3\ s^{-1}/m^2$.

Sodtke and Stephan [173] used high-speed infrared imaging to investigate water spray cooling of both smooth and micro-structured surfaces, the latter featuring micro pyramids with different heights. They varied volumetric flux by changing the nozzle-to-surface distance. Overall, their experiments showed great improvement in cooling performance with the micro structured surfaces compared to the smooth surface. The infrared imaging revealed that this enhancement is the result of increasing length of the three-phase contact line, which promotes very efficient thin film evaporation. They also detected high surface temperature gradients commensurate with the rupture of the thin film. Using anhydrous ammonia as working fluid, Bostanci et al. [174,175] examined vapor-assist spray cooling of micro-structured surfaces featuring both indentations and protrusions. For heat fluxes up to 500 W/cm^2, they observed 49% and 112% improvements in the heat transfer coefficient for the micro-indentation and micro-protrusion surfaces, respectively. They attributed these improvements to increases in both number of surface nucleation sites and length of three-phase contact line. Interestingly, they encountered thermal hysteresis with these surfaces, evidenced by lower surface superheats for a given heat flux during surface cool-down compared to heat-up. Follow-up work by Bostanci et al. [176] showed that a multi-scale structured surface, combining the benefits of both micro- and macro-structures, provides a 161% improvement in the heat transfer coefficient compared to a smooth surface. Meanwhile, Bostanci et al. [177] found that enhanced surfaces increase CHF value appreciably through the tendency of capillary forces within the surface structures to better retain liquid and spread the liquid film efficiently, which delays the formation of dry patches. Hsieh et al. [178] studied heat transfer enhancement with a sputtered 50-μm SiC coating, as well as deposited 50-μm diamond and 10-μm carbon nanotube coatings on a copper surface. The most superior enhancement was achieved with the 50-μm diamond coating, which yielded heat fluxes as high as 610 W/cm^2. Zhang et al. [179] suggested that heat transfer enhancement with deionized water spray cooling of micro-structured surfaces with feature sizes in the range of 25–200 μm is minimal in the flooded region but greatly improved in the thin film and partial dryout regions. Follow-up work by Zhang et al. [180,181] with water spray cooling of smooth, micro-structured, nano-structured, and hybrid micro/nano-structured silicon surfaces showed that the nano-structured surface, having the smallest contact angle of the different surfaces tested, produces the highest heat transfer enhancement. Heat transfer enhancement due to impingement of multiple water droplets on a nano-structured surface was also examined by Alvarado and Lin [182].

Yang et al. [183] studied ammonia spray cooling of three different micro-cavity surfaces. Dominated by thermal convection effects, single-phase heat transfer showed no improvement with the micro-cavity surfaces compared to a plain surface. On the other hand, the micro-cavity surfaces produced higher heat transfer coefficients and better surface temperature uniformity in the nucleate boiling regime.

Aside from the above-discussed surface treatments, Souza and Barbosa [184,185] investigated R-134a spray cooling of a surface coated with copper foam, and reported enhancement in the heat transfer coefficient but not CHF. Silk and Bracken [186] and Wang et al. [187] studied performance enhancement with POCO HTC foam and porous copper foam, respectively.

4.4.2. Additives to liquid

Another approach to enhancing heat transfer performance is to use different additives to alter the spray liquid's surface tension, contact angle, and thermal conductivity. Qiao and Chandra [18] reported a 300% enhancement in nucleate boiling resulting from dissolving 100 ppm by weight surfactant in water. They also reported a reduction in surface temperature corresponding to incipient boiling from 118 to 103 °C with the surfactant. They attributed these enhancement effects to promotion of homogeneous bubble nucleation and surfactant foaming.

Cui et al. [188] investigated the effects of NaCl, Na_2SO_4, and $MgSO_4$ soluble salts on the boiling performance of water sprays. All three salts enhanced nucleate boiling heat transfer because of foaming in the liquid film. $MgSO_4$ produced the largest heat transfer enhancement, followed in order by Na_2SO_4 and NaCl. And, with $MgSO_4$, there was an enhancement in cooling performance with increasing concentration up to 0.2 mol/l, above which no further enhancement was achieved. Cheng et al. [189,190] tested two types of additives in water, high-alcohol surfactant (HAS), including 1-octanol and 2-ethyl-hexanol, and dissolved salt additive (DSA), including NaCl and Na_2SO_4. These additives produced opposite effects on surface tension, which decreased with HAS and increased with DSA; the latter was more effective in promoting bubble nucleation. They reported that the heat transfer enhancement depends mainly on the additive concentration, increasing at first with increasing concentration then decreasing for higher concentrations. Wang et al. [171] found that spray heat transfer can be enhanced by adding potassium chloride into water up to a certain concentration, beyond which heat transfer was severely compromised. They also showed that heat transfer performance decreases when adding ethylene glycol in water, regardless of the concentration used.

Recently, spray cooling research was extended to the use of nanofluids, defined as fluids containing solid high thermal conductivity particles with characteristic size below about 100 nm to enhance thermal properties of the liquids. Duursma et al. [191] adopted a needle-type nozzle to investigate spray cooling performances of ethanol and dimethyl sulfoxide (DMSO) based aluminum nanofluids. They detected deterioration in heat transfer with the ethanol-based solutions but slight enhancement with the DMSO nanofluids compared to their respective base-fluid counterparts. Hsieh et al. [192] tested sprays of water-based nanofluids with silver and multi-walled carbon nanotubes (MCNTs) with 0.0025–0.0075% volume fractions. They showed CHF enhancement with the nanofluids by up to 2.4 times that of pure water. As shown in Fig. 11, nucleate boiling heat transfer with silver nanofluids is superior to that for MCNT nanofluids, which was attributed to the tendency of silver particles to disperse more evenly and resist agglomeration. Bansal and Pyrtle [193] reported that the heat transfer performance of water-based alumina nanofluids depends on the range of surface-to-fluid temperature difference. For $\Delta T_f < 45$ °C, they reported enhancement in the cooling performance that was insensitive to mass fraction of the nanoparticle suspension over the range of 0.25–0.5%. But for $45 < \Delta T_f < 140$ °C, the performance of nanofluids deteriorated, and culminated in CHF values below those for pure water. Bellerová et al. [194,195] studied the cooling performance of water-based alumina nanofluids using different types of jet and spray nozzles. The heat transfer coefficient decreased by 45% for jet nozzles and 20% for full-cone spray nozzles as the volume fraction of nanoparticle suspension was increased from 0 to 16.45%. Bellerová et al. [196] also reported that the heat transfer coefficient for water-based titania nanofluids is inferior to that for pure water. Chang et al. [197] further investigated the effects of water-based alumina nanofluids by examining surface composition after the spray cooling with the aid of a scanning electron microscope. They found that a low

nanoparticle volume fraction of 0.001% can yield significant heat transfer enhancement, which they attributed to a mass of nanoparticles bouncing off the surface or being swept away by subsequent droplets. On the other hand, relatively high volume fractions of 0.025–0.05% tend to deposit a thin nanoparticle layer on the surface, which both reduced the number of nucleation sites and hindered convective heat transfer, compromising overall cooling performance. Wu et al. [198] investigated water spray cooling with polymer-encapsulated paraffin nanoparticles, and demonstrated up to 70% enhancement in the heat transfer coefficient. Tseng et al. [199] studied spray cooling of titania nanofluids with mass concentrations ranging from 1 to 40%, and showed that the heat transfer coefficient decreases with increasing nanoparticle concentration. On the other hand, Zhu et al. [61] reported that the heat transfer performance is significantly improved using titania nanofluids with low mass concentrations in the range of 0.1 to 1%. They attributed this enhancement to the nanoparticles destroying the spray boundary layer and intensifying turbulence.

Clearly, the influence of nanofluids on spray cooling is quite complicated, and the findings from different studies are often contradictory. Nanofluids also pose a host of practical problems, especially clogging of the spray nozzle as well as the pump and valves throughout the two-phase cooling loop. Gradual buildup of nanoparticle coatings in these components causes substantial variations in the spray nozzle's pressure drop and flow rate, let alone long-term damage to the same components [200].

4.4.3. Other approaches

Aside from surface modifications and the use of additives to enhance spray cooling performance, investigators have employed other enhancement techniques, such as active flow control using synthetic jet actuators to alter the spray's hydrodynamic structure [201], and pulsed or intermittent sprays [202–214] as proposed by Panão and Moreira [215]. The latter has received significant attention in recent years because of its potential to reduce pumping power consumption and increase efficiency of coolant usage.

Another method consists of mounting an ejector unit upstream of the pump supplying liquid to the spray nozzle [216]. The ejector serves to prevent uncondensed vapor from entering the pump, which enhances pump performance and stabilizes flow circulation in the two-phase flow loop. Using FC-72 and water as coolants, the ejector showed an improvement in nozzle pressure drop by no less than 0.56 bar and resulted in 16% enhancement in CHF. Using flat, straight fin and porous tunnel surfaces, Zhang et al. [217,218] reported that heat transfer can be improved under surface acceleration conditions, but this enhancement is limited. Another enhancement technique is electrospray cooling [219,220], which improves cooling efficiency by preventing droplet rebound on the surface and repelling droplets from each other to generate a fine spray. This is another technique that has attracted appreciable attention because of its ability to reduce overall system weight and energy consumption.

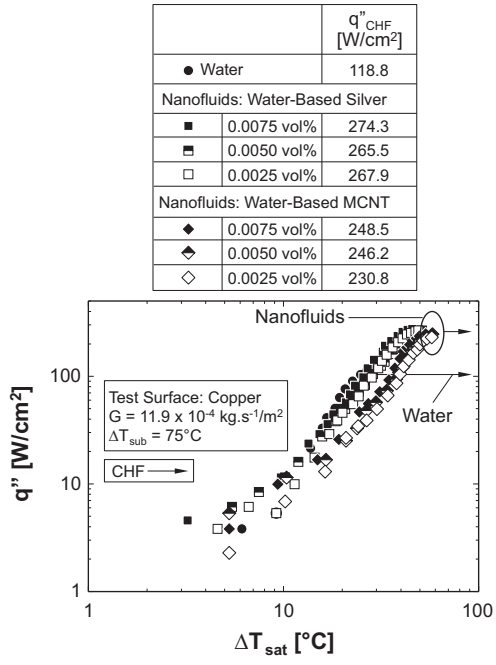

Fig. 11. Comparison of boiling curves for water and nanofluids. Adapted from Hsieh et al. [192].

5. Critical heat flux

5.1. Influencing parameters

Several parameters have been used to correlate CHF data for full-cone sprays. They include thermophysical properties of the working fluid, nozzle flow parameters (flow rate and pressure drop), geometrical parameters (orifice diameter, cone angle, nozzle-to-surface distance, surface size, and spray inclination angle), and spray's hydrodynamic parameters (mean droplet diameter, d_{32}, mean droplet velocity, u_m, local volumetric flux, Q'', and mean volumetric flux, $\overline{Q}''$).

Tilton [76] and Chen et al. [221] reported that volumetric flow rate, Q, has only a minor influence on CHF, while Pais et al. [43], Estes and Mudawar [47], Moreno et al. [222], Chow et al. [223], Hou et al. [224], Toda and Uchida [225] all suggested that CHF increases with increasing flow rate.

Toda [226] reported that CHF for water can be increased by about 50% by increasing droplet diameter from 88 to 120 μm, but Pais et al. [43] and Estes and Mudawar [47] found that CHF benefits from decreasing droplet diameter. On the other hand, Chen et al. [221] showed that CHF is insensitive to droplet diameter.

Toda and Uchida [225–227] showed that CHF for water sprays with 30–60 °C subcooling can reach 250 W/cm^2, and reported that CHF is insensitive to droplet velocity over the range of 2.0–7.0 m/s, contradicting the findings of Monde [228]. Chen et al. [221] found that CHF increases with increasing mean droplet velocity, which is controlled by regulating nozzle inlet pressure. Hou et al. [229] reported that CHF for R-22 sprays first increases then decreases slightly as the nozzle's inlet pressure is increased from 0.6 to 1.0 MPa, and the highest CHF value of 276 W/cm^2 is achieved at an inlet pressure of 0.8 MPa.

Pais et al. [43], Estes and Mudawar [47], Monde [228], Chen et al. [221], and Lin and Ponnappan [230] all demonstrated that CHF increases with increasing volumetric flux. Also, by varying volumetric flux, mean droplet diameter, and mean droplet velocity independently, Chen et al. [221] found that mean droplet velocity has the most dominant influence on water spray heat transfer coefficient and CHF, followed by volumetric flux. They added that, for a given volumetric flux, higher CHF can be achieved by using a dilute spray with higher droplet velocity. In a follow-up study, Chen et al. [118] found that CHF varies with $u_m^{1/4}$ and $\overline{Q}''^{1/6}$, and is independent of d_{32}, and concluded that CHF can be maximized by using nozzles that produce smaller but high velocity droplets. Vorster et al. [231] reported that the spatial distribution of CHF for water sprays is determined by the spatial variations of volumetric flux.

It is important to recognize that spray cooling is a cumulative effect of many droplets impacting the heated surface. Liquid arrives at the surface with a volumetric flux that represents the

volume flow rate striking an infinitesimal portion of the impact area divided by the area of the same portion. And, with units of $m^3\ s^{-1}/m^2$, volumetric flux, Q'', has essentially the same units of m/s as the mean droplet velocity, u_m, but different sprays can possess equal values of u_m but drastically different values of Q''. Failure to account for the cumulative effect of multi-droplet impact is why droplet velocity is generally not recommended for correlating spray CHF data [47] or film boiling heat transfer efficiency data [232].

Kato et al. [152] and Sone et al. [153] found that CHF for water, FC-72, and CFC-113 sprays bears a strong dependence on gravity. A decrement in gravity was shown to decrease CHF for FC-72 and CFC-113 but increase it for water, which they ascribed to differences in liquid film behavior on the surface for different fluids in reduced gravity. In a follow-up study, Yoshida et al. [21], reported the existence of a critical value for volumetric flux. Below this value, they found that droplets impinging on the surface completely vaporize, hardly interacting with one another, and a CHF independent of gravity or surface orientation. But for volumetric fluxes higher than the critical value, they reported the formation of a liquid film on the surface, and a CHF strongly dependent on gravity and orientation. Yoshida et al. reported critical volumetric flux values for water and FC-72 of $7\times10^{-4}\ m^3\ s^{-1}/m^2$ and 4×10^{-4} - $m^3\ s^{-1}/m^2$, respectively.

5.2. Models and correlations

5.2.1. Normal sprays

Katto [233] suggested that the critical heat flux, $q''_{CHF,sat}$, for a generic saturated boiling system can be correlated according to

$$\frac{q''_{CHF,sat}}{\rho_g h_{fg} u} = f\left(\frac{\rho_f}{\rho_g}, \frac{\sigma}{\rho_f u^2 L}\right), \tag{59}$$

where u and L are, respectively, the characteristic velocity and characteristic length associated with the boiling system. To account for subcooling, Ivey and Morris [234] employed a linear relation of the form

$$\frac{q''_{CHF}}{q''_{CHF,sat}} = 1 + C_{sub}\left(\frac{\rho_g}{\rho_f}\right)^{1/4}\left(\frac{\rho_f c_{p,f}\Delta T_{sub}}{\rho_g h_{fg}}\right), \tag{60}$$

where $\rho_f c_{p,f}\Delta T_{sub}/\rho_g h_{fg}$ is the Jacob number, which represents the ratio of sensible heat of a volume of liquid to the latent heat of an equal volume of vapor.

Combining the above two correlation techniques, Mudawar and Valentine [45] correlated their water spray CHF data for T_f = 22.5–80.5 °C according to

$$\frac{q''_{CHF}}{\rho_g h_{fg} Q''} = 122.4\left[1+0.0118\left(\frac{\rho_g}{\rho_f}\right)^{1/4}\left(\frac{\rho_f c_{p,f}\Delta T_{sub}}{\rho_g h_{fg}}\right)\right]\left(\frac{\sigma}{\rho_f Q''^2 d_{32}}\right)^{0.198} \tag{61a}$$

or

$$\frac{q''_{CHF}}{\rho_g h_{fg} Q''} = 134.3\left[1+0.0118\left(\frac{\rho_g}{\rho_f}\right)^{1/4}\left(\frac{\rho_f c_{p,f}\Delta T_{sub}}{\rho_g h_{fg}}\right)\right]\left(\frac{\sigma}{\rho_f Q''^2 d_{0.5}}\right)^{0.192}. \tag{61b}$$

Notably, their CHF data were measured by a circular test surface whose area was much smaller than the spray impact area, as shown in Fig. 3(b), implying the local volumetric flux, Q'', in Eqs. (61a) and (61b) is equal to the mean volumetric flux, $\overline{Q}''$.

Later, using FC-72 and FC-87, Estes and Mudawar [47] tested full-cone sprays with surface areas larger than the spray impact area. They found that surface dryout at CHF commences at the outer edge of the impact area, where volumetric flux is weakest, since this local dryout reduces the fraction of surface area available for cooling and increases heat flux within the shrinking impact area, which causes the dryout to propagate radially inwards in an unstable manner. Therefore, CHF at the edge of the impact area should govern CHF for the entire surface. This hypothesis was confirmed with the aid of visualization techniques by Hsieh et al. [111] for water and R-134a sprays. Pautsch and Shedd [235] reported that CHF commences at the outer edge of the heated surface.

Estes and Mudawar also proved that, to maximize CHF, the nozzle-to-surface distance for a square surface of length L must be configured such that the spray impact area just inscribes the surface, Fig. 12, *i.e.*, when

$$H\tan(\theta/2) = L/2 \tag{62a}$$

and

$$\overline{Q}'' = \frac{Q}{\pi L^2/4}. \tag{62b}$$

A nozzle-to-surface distance that is shorter than required by this criterion was shown to concentrate coolant in a small central portion of the surface, while a larger distance caused a portion of the coolant's flow rate to be wasted outside the surface. For the optimum condition, where the spray impact area just inscribes the surface, CHF at the surface edge can be determined by assuming that all of the heat is transferred through the impact area,

$$q''_{CHF,p} = \frac{q''_{CHF}L^2}{(\pi/4)L^2} = \frac{4}{\pi}q''_{CHF}. \tag{63}$$

Volumetric flux at the outer edge of the impact area can be determined from a spray flux distribution model developed by Estes [236],

$$Q'' = \frac{2Q}{\pi L^2}[1+\cos(\theta/2)]\cos(\theta/2). \tag{64}$$

They developed a new CHF correlation that accurately predicts full-cone spray data for FC-72, FC-87, and water,

$$\frac{q''_{CHF,p}}{\rho_g h_{fg} Q''} = 2.3\left(\frac{\rho_f}{\rho_g}\right)^{0.3}\left(\frac{\rho_f Q''^2 d_{32}}{\sigma}\right)^{-0.35}\left[1+0.0019\left(\frac{\rho_f c_{p,f}\Delta T_{sub}}{\rho_g h_{fg}}\right)\right], \tag{65}$$

which shows CHF dependence on both Q'' and d_{32} for Q'' = 0.6×10^{-3}–$0.216\ m^3\ s^{-1}/m^2$ and d_{32} = 0.11–1.35 mm. This correlation was equally successful at predicting CHF data for upward-facing PF-5052 sprays by Rybicki and Mudawar [17]. Mudawar and Estes [55] combined Eqs. (62b) and (64) to derive a more convenient form of the CHF correlation relating q''_{CHF} to $\overline{Q}''$,

$$\frac{q''_{CHF}}{\rho_g h_{fg}\overline{Q}''} = 1.467\left\{\cos\left(\frac{\theta}{2}\right)\left[1+\cos\left(\frac{\theta}{2}\right)\right]\right\}^{0.3}\left(\frac{\rho_f}{\rho_g}\right)^{0.3} \times\left(\frac{\rho_f\overline{Q}''^2 d_{32}}{\sigma}\right)^{-0.35}\left[1+0.0019\left(\frac{\rho_f c_{p,f}\Delta T_{sub}}{\rho_g h_{fg}}\right)\right]. \tag{66}$$

The form of CHF correlation in Eq. (64) has been widely used by other researchers. Jiang and Dhir [64] adopted the same correlation form, but, to better fit their own water data for $\overline{Q}''$ = 2.9×10^{-3}–$5.1\times10^{-3}\ m^3\ s^{-1}/m^2$, they modified the correlation exponents,

$$\frac{q''_{CHF}}{\rho_g h_{fg}\overline{Q}''} = 2.3\left(\frac{\rho_f}{\rho_g}\right)^{0.5}\left(\frac{\rho_f\overline{Q}''^2 d_o}{\sigma}\right)^{-0.2}\left[1+0.0019\left(\frac{\rho_f c_{p,f}\Delta T_{sub}}{\rho_g h_{fg}}\right)\right], \tag{67}$$

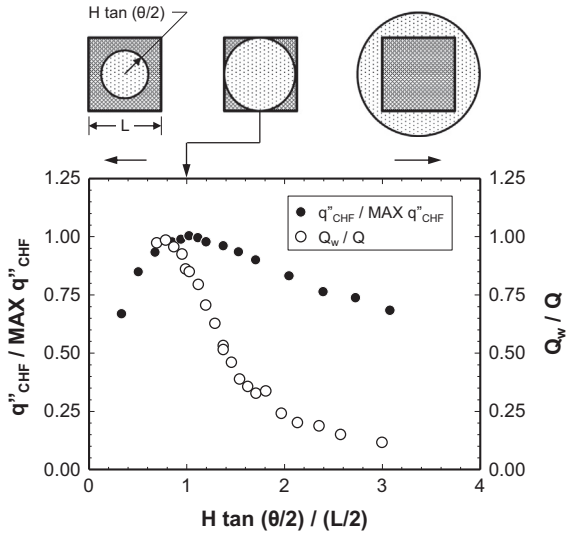

Fig. 12. Optimization of nozzle-to-surface distance for maximum CHF. Adapted from Mudawar and Estes [55].

and used d_o instead of d_{32}. A similar correlation form was also used by Thiagarajan et al. [159], who found that Eq. (64) overestimates their data for HFE-7100 sprays impacting a copper surface, and modified the original correlation into

$$\frac{q''_{CHF}}{\rho_g h_{fg} \overline{Q}''} = 1.449 \left(\frac{\rho_f}{\rho_g}\right)^{0.3} \left(\frac{\rho_f \overline{Q}''^2 d_{32}}{\sigma}\right)^{-0.3371} \left[1 + 0.0058 \left(\frac{\rho_f c_{p,f} \Delta T_{sub}}{\rho_g h_{fg}}\right)\right]. \tag{68}$$

They also verified their correlation using databases by Lin and Ponnappan [237] for FC-87, FC-72, and methanol, Rini et al. [98] for FC-72, Silk [238] for PF-5060, Coursey et al. [239] for PF-5060, Chen et al. [221] for water, and Puterbaugh et al. [240] for FC-72. Thiagarajan et al. also derived the following correlation for micro-porous copper surfaces:

$$\frac{q''_{CHF}}{\rho_g h_{fg} \overline{Q}''} = 2.14 \left(\frac{\rho_f}{\rho_g}\right)^{0.3} \left(\frac{\rho_f \overline{Q}''^2 d_{32}}{\sigma}\right)^{-0.363} \left[1 + 0.0058 \left(\frac{\rho_f c_{p,f} \Delta T_{sub}}{\rho_g h_{fg}}\right)\right], \tag{69}$$

which is also effective at predicting CHF data by Coursey et al. [239] for PF-5060 on copper surfaces with open micro-channels, and by Silk et al. [162] for PF-5060 on surfaces enhanced with cubic pin fins, pyramids, and straight fins. Dou et al. [107] modified the Estes and Mudawar [47] correlation slightly to correlate their water CHF data according to

$$\frac{q''_{CHF}}{\rho_g h_{fg} \overline{Q}''} = 2.52 \times 10^{-3} \left(\frac{\rho_f \overline{Q}''^2 d_{32}}{\sigma}\right)^{-0.4255} \left[1 + 0.013 \left(\frac{\rho_f}{\rho_g}\right)^{-0.25} \left(\frac{\rho_f c_{p,f} \Delta T_{sub}}{\rho_g h_{fg}}\right)\right], \tag{70}$$

which is valid for low rates in the range of 30–50 l/min and a fixed nozzle-to-surface distance of 250 mm.

Visaria and Mudawar [109] examined the influences of subcooling on spray performance and CHF. They were able to achieve high levels of subcooling by using FC-77, which has a relatively high saturation temperature of 97 °C at atmospheric pressure. CHF was enhanced by about 100% when the subcooling was increased from 22 to 70 °C, reaching values as high as 349 W/cm^2. Their experiments also revealed that CHF enhancement is relatively mild at low subcoolings and more appreciable at high subcoolings in excess of 40 °C. On the other hand, Thiagarajan et al. [159] reported that, excepting low flow rates, the heat transfer coefficient and CHF for HFE-7100 acquire higher values for near-saturated than subcooled conditions.

Visaria and Mudawar also combined their CHF data for FC-77 with prior spray CHF data obtained at the Purdue University Boiling and Two-Phase Flow Laboratory (PU-BTPFL) into a broad-based CHF database encompassing different nozzles, fluids, flow rates, spray orientations, and subcoolings. The database they amassed includes (a) normal downward-facing FC-72 sprays by Estes and Mudawar [23,47], (b) normal downward-facing FC-77 sprays by Visaria and Mudawar, (c) normal upward-facing PF-5052 sprays by Rybicki and Mudawar [17], (d) inclined downward-facing PF-5052 sprays by Visaria and Mudawar [16,68], and (e) normal downward-facing water sprays by Mudawar and Valentine [45]. Relying on their new broad subcooling range, Visaria and Mudawar [109] modified the magnitude of the multiplier in the subcooling term of the original Estes and Mudawar [47] correlation developed for relatively low subcoolings, resulting in the following revised 'universal' CHF correlation:

$$\frac{q''_{CHF,p}}{\rho_g h_{fg} Q''} = 2.3 \left(\frac{\rho_f}{\rho_g}\right)^{0.3} \left(\frac{\rho_f Q''^2 d_{32}}{\sigma}\right)^{-0.35} \left[1 + 0.0050 \left(\frac{\rho_f c_{p,f} \Delta T_{sub}}{\rho_g h_{fg}}\right)\right], \tag{71}$$

as shown in Fig. 13a.

An important spray performance parameter that is related to CHF is evaporation efficiency, η. Estes and Mudawar [47] defined η as the percentage of the total heat rate that can be removed by the spray, sensible and latent, that is actually removed at CHF,

$$\eta = \frac{q''_{CHF}}{\rho_f \overline{Q}'' (h_{fg} + c_{p,f} \Delta T_{sub})} \times 100\%. \tag{72}$$

They reported that boiling curves for sprays with high volumetric flux – dense sprays – exhibit an unusually small increase in slope upon transition between the single-phase and nucleate boiling regions because of a suppression of nucleation and reduced evaporation efficiency. Conversely, sprays with low volumetric flux – dilute sprays – display a more pronounced slope increase in the nucleate boiling regime; these sprays feature high evaporation efficiency. Fig. 13b shows that the evaporation efficiency for different fluids decreases monotonically with increasing spray Weber number, We_s, *i.e.*, with increasing mean volumetric flux, $\overline{Q}''$, or droplet diameter, d_{32}, or with decreasing surface tension. However, liquid subcooling does not appear to influence evaporative efficiency.

Sehmbey et al. [112,113] adopted a different approach to correlate CHF data for liquid nitrogen using the theory of macro-layer dryout. Their correlation

$$\frac{q''_{CHF}}{\rho_g h_{fg}} = 0.31 \left(\frac{\rho_f}{\rho_g}\right)^{0.5} \left(\frac{\sigma}{\rho_f} \frac{6\overline{Q}''}{\pi d_{32}}\right)^{1/3} \tag{73}$$

is valid for G = 16.9–88.9 kg·s^{-1}/m^2, d_{32} = 14–29 μm, and u_m = 14–30.7 m/s. They also reported that both the heat transfer coefficient and CHF increase with decreasing diameter of the nozzle's orifice because of an increase in both number and velocity of droplets. Using the same theory, Chow et al. [241] formulated a general correlation for CHF using data for saturated and slightly subcooled liquids from multiple sources [43,76,95,112,136,226,242],

$$\frac{q''_{CHF}}{\rho_f h_{fg} u_m} = 0.38 \left(\frac{\rho_f u_m^2 d_{32}}{\sigma}\right)^{-1/3} \left(\frac{\rho_g}{\rho_f}\right)^{0.5} \left(\frac{P_s}{P_a}\right)^{0.25}, \tag{74}$$

where P_s and P_a are the air flow stagnation pressure and ambient pressure, respectively. They also indicated that this correlation is applicable to both air-assist and pressure nozzles.

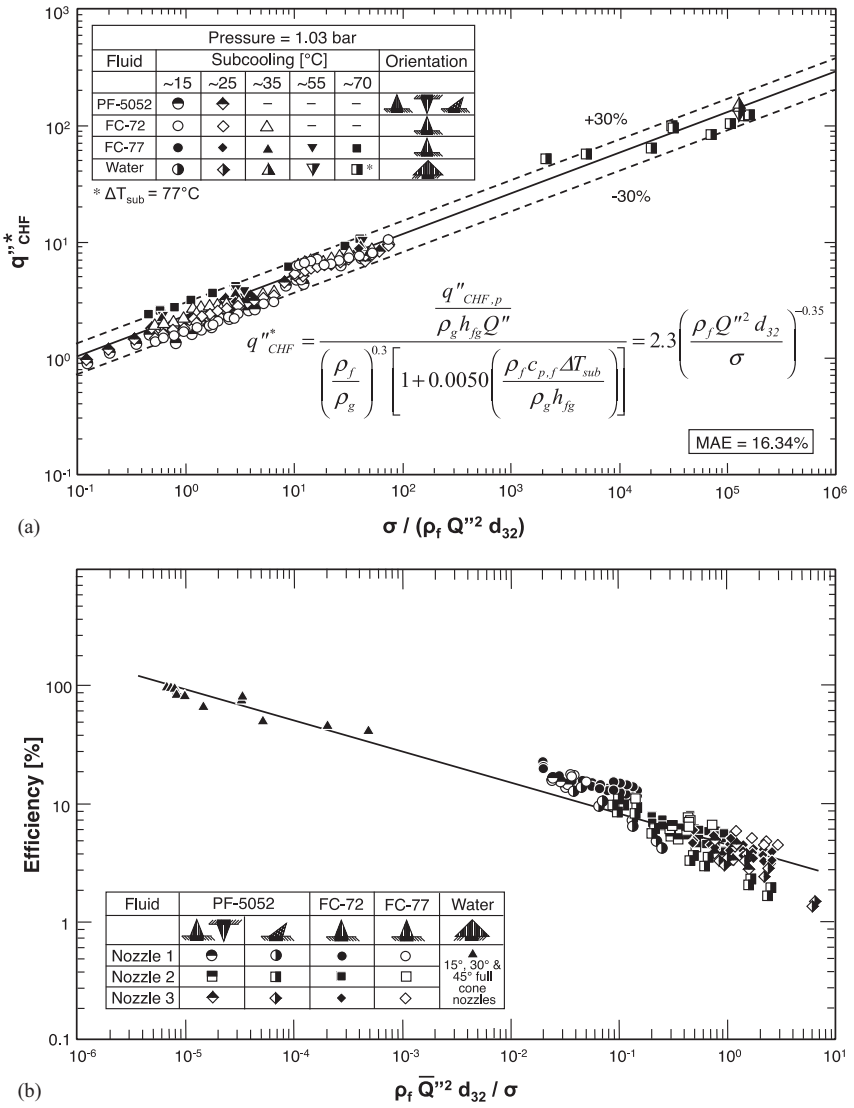

Fig. 13. (a) Correlation of CHF data for different nozzles, fluids, flow rates, subcoolings and orientations. (b) Evaporation efficiency versus We_s based on mean volumetric flux for PF-5052, FC-72, FC-77, and water. Adapted from Visaria and Mudawar [109].

Using forced convection analysis, Silk et al. [243] derived the following CHF correlation using data for PF-5060, FC-72, FC-87, methanol, and water from earlier sources [97,98,221,237,238,244],

$$q''_{CHF} = 5.3 Re_d^{0.55} Pr_f^{0.33} \left[\frac{0.8(c_{p,f}\Delta T_{sub}/h_{fg})+1}{(\rho_f/\rho_g)^{0.4}}\right] \left(\frac{\pi N^+ d_{32}^3}{6}\right)^{0.09} \left(\frac{k_f}{L}\right)\left(\frac{h_{fg}}{c_{p,f}}\right), \quad (75)$$

which is applicable to both gassy and degassed conditions, where N^+ is the droplet number density.

Ciofalo et al. [57] employed full-cone pressure nozzles to produce horizontal water sprays for a fixed nozzle-to-surface distance of 50 mm and relatively high mass fluxes of 8–80 kg·s^{-1}/m^2. Their data revealed that CHF depends on mass flux and mean droplet velocity, but is insensitive to droplet diameter,

$$q''_{CHF} = 0.869 \times 10^6 (Gu_m^2)^{0.245}, \quad (76)$$

where u_m ranges from 13 to 28 m/s. Follow-up work by Ciofalo et al. [58] extended the water mass flux to a lower range of 0.33–32.7 kg·s^{-1}/m^2 and included variations in nozzle-to-surface distance from 0.1 to 0.4 m. They correlated CHF data for $G > 0.5$ kg·s^{-1}/m^2 according to

$$q''_{CHF} = 1.759 \times 10^6 G^{0.567}. \quad (77)$$

Abbasi and Kim [245] determined experimentally that CHF is primarily dependent on local impingement pressure, P, and liquid subcooling. Using both full-cone and hollow cone nozzles, they correlated PF-5060 data according to

$$q''_{CHF} = 9.15 \times 10^4 P^{0.4} \left(1 + 2.42 \frac{c_{p,f}\Delta T_{sub}}{h_{fg}}\right)^{0.52}, \quad (78)$$

where ΔT_{sub} = 11–31 °C.

Cabrera and Gonzalez [116] examined monodispersed water sprays (*i.e.*, consisting of droplets with identical droplet velocities and diameters), accounting for surface roughness effects, and correlated their CHF data as

$$\frac{q''_{CHF}}{Gh_{fg}} = 1.623 \left(\frac{\rho_f u_d^2 d_d}{\sigma}\right)^{-0.315} \left(\frac{R_a}{d_d}\right)^{0.0465}, \quad (79)$$

which is applicable for G = 340–750 kg·s^{-1}/m^2 and R_a = 5–79 μm. Sawyer et al. [246] examined a single stream of monodispersed water droplets, and recommended a CHF correlation that accounts for impact frequency, f,

$$\frac{q''_{CHF}}{\rho_f h_{fg} u_d} = 0.166\left(\frac{\rho_f u_d^2 d_d}{\sigma}\right)^{-0.4138}\left(\frac{f d_d}{u_d}\right)^{0.8906}, \tag{80}$$

where f = 12–42 Hz, u_d = 2.4–4.6 m/s, d_d = 1.5–2.7 mm, and ΔT_{sub} = 75 °C. Healy et al. [247] correlated CHF data for monodispersed water sprays by Halvorson et al. [248] for low Weber numbers, We_d = 55–109, accounting for effects of subcooling and ambient pressure,

$$\frac{q''_{CHF}}{\rho_f u_d[h_{fg} + 0.1(\rho_f/\rho_g)^{3/4} c_{p,f}\Delta T_{sub}]} = 0.146\left(\frac{\rho_f u_d^2 d_d}{\sigma}\right)^{-0.9816}\left(\frac{f d_d}{u_d}\right)^{0.6883}\left(\frac{P_a}{P_{atm}}\right)^{0.6081}, \tag{81}$$

where f = 1–15 Hz, u_d = 1.3 m/s, d_d = 2.3–4.0 mm, P_a = 0.2–2.0 bar, and ΔT_{sub} = 40–101 °C.

5.2.2. Inclined sprays

Visaria and Mudawar [68] used the nozzle positioning system depicted in Fig. 14(a) to accurately set both the nozzle-to-surface distance and inclination angle, α, between the spray axis and normal to the test surface. Using high speed video analysis, they showed that inclined sprays produce an elliptical impact area, where a lateral liquid film flows towards the farthest downstream region of the test surface, Fig. 14(b), providing partial resistance to dryout despite weak volumetric spray flux in the downstream region. Fig. 14(c) shows a schematic of an inclined spray whose nozzle-to-surface distance is adjusted such that the major axis of the impact area just inscribes a square surface in order to maximize CHF. The lowest volumetric flux is encountered along the farthest downstream point of the impact area, but CHF commences along the end points of the minor axis of the impact ellipse rather than the major axis. These are the farthest points from the orifice that do not benefit from the lateral film flow. Results by Visaria and Mudawar showed that α has little influence on heat transfer in both the single-phase and nucleate boiling regimes, but increasing α greatly decreases CHF. They proved that this CHF decrease is the result of a sharp reduction in the fraction of the test surface area that is directly impacted by the spray as shown in Fig. 14(d). Using a theoretical model for the spray's impact area, the previous point-based CHF correlation by Estes and Mudawar [47] for normal sprays was shown to accurately predict the effect of orientation angle on CHF for different nozzles and operating conditions,

$$q''_{CHF} = \frac{A_e q''_{CHF,p}}{L^2} = \left[\frac{\pi}{4}\cos\alpha\sqrt{1-\tan^2\alpha\tan^2(\theta/2)}\right] q''_{CHF,p}. \tag{82}$$

Visaria and Mudawar [16] also proposed a new CHF correlation for inclined PF-5052 sprays based on total surface area and on volumetric flux averaged over the spray impact area,

$$\frac{q''_{CHF}}{\rho_g h_{fg}\overline{Q}''} = 2.3\left(\frac{\rho_f}{\rho_g}\right)^{0.3}\left(\frac{\rho_f \overline{Q}''^2 d_{32}}{\sigma}\right)^{-0.35}\left[1+0.0019\left(\frac{\rho_f c_{p,f}\Delta T_{sub}}{\rho_g h_{fg}}\right)\right]\left(\frac{f_1^{0.30}}{f_2}\right), \tag{83}$$

where

$$f_1 = \frac{Q''}{\overline{Q}''} = \frac{1}{8}\left(\frac{L}{H}\right)^2 \frac{\cos\alpha\sqrt{1-\tan^2\alpha\tan^2(\theta/2)}}{1-\cos(\theta/2)}\frac{dA'}{dA}, \tag{84a}$$

$$f_2 = \frac{q''_{CHF,p}}{q''_{CHF}} = \frac{1}{\left[\frac{\pi}{4}\cos\alpha\sqrt{1-\tan^2\alpha\tan^2(\theta/2)}\right]}, \tag{84b}$$

and

$$\overline{Q}'' = \frac{Q}{\frac{\pi}{4}L^2\cos\alpha\sqrt{1-\tan^2\alpha\tan^2(\theta/2)}}. \tag{84c}$$

They validated this methodology for $Q = 3.5\times10^{-6}$–1.702×10^{-5} m^3/s and α = 0–55°.

Guo et al. [249] proposed that CHF can be maximized by adjusting the nozzle such that four borderlines of the square test surface are tangent to the elliptical spray impact area, rather than only the major axis as proposed by Visaria and Mudawar [68]. This means that the impact area proposed by Guo et al. is larger than by Visaria and Mudawar. Using this modified impact area depiction, Guo et al. modified the CHF model of Visaria and Mudawar [16,68] and found that CHF increases slightly with increasing inclination angle. In a recent theoretical analysis, Zhang and Ruan [250] derived an relation for spray impact area as a function of inclination angle.

Silk et al. [162,251] examined the effects of PF-5060 spray inclination on both plain and enhanced copper surfaces. They tested sprays with α = 0, 30, and 45° while maintaining a constant nozzle-to-surface distance of 17 mm, and their heat flux was based on projected area of the test surface. For both the plain and enhanced surfaces, CHF was highest for α = 30°. Since this maximum was achieved despite the volumetric flux decreasing with increasing α, they suggested that the CHF enhancement is probably the outcome of altered film drainage from the surface due to the nozzle inclination. Ravikumar et al. [252] investigated the influence of inclination angle on CHF for air-assist water nozzles for a constant nozzle-to-surface distance of 60 mm, and found that CHF is highest at α = 30°, while, for water with surfactant, CHF decreases monotonically with increasing α. Yan et al. [253] attributed superior heat transfer performance for inclined sprays to the better liquid drainage on the surface resulting from increased radial droplet momentum. They pointed out, however, that inclined sprays contribute greater surface temperature non-uniformity compared to normal sprays.

Schwarzkopf et al. [254] and Li et al. [255] studied the effects of inclination angle on PF-5060 spray cooling using an upward-facing pressure nozzle. They tested inclination angles in the range of 0–60° while maintaining a fixed nozzle-to-surface distance of 14 mm, and showed that cooling performance is rapidly compromised for α > 40°. Cheng et al. [256] found that CHF for horizontal HFE-7100 and PF-5060 sprays is highest for an inclination angle of 75°, followed by 60° and 45°, and lowest for 90°. Zhang et al. [155] noted that normal water sprays offer the best heat transfer performance. Aguilar et al. [257] used a tubular nozzle to examine the influence of inclination angle on cryogen spray cooling, and found that angles as high as 75° have no appreciable influence on surface temperature, heat flux, or overall heat extraction. Using air-assist water nozzles, Fu et al. [258] found that heat flux increases when α is increased from 0 to 30°, then decreases as α is further increased from 30 to 60°. Using a distilled water pressure spray, Guo et al. [60] obtained a similar trend for inclination angles in the range of 0 to 50° and an optimal angle around 30°.

Although numerous articles have recently been published that address the influence of spray inclination angle on CHF, there are many contradictions concerning mechanisms, data trends, and optimal inclination angle. Additionally, there is overwhelming reliance on empiricism rather than on theoretical modeling. Clearly, more careful experimental work must be conducted in the future using multiple liquids and small increments in inclination angle to more accurately capture CHF.

5.2.3. Multi-nozzle arrays

For relatively large surfaces, a single spray may not provide sufficient surface coverage. Here, multi-nozzle arrays are commonly used and between which spray overlap is quite common. Compared to single spray studies, those addressing multi-nozzle arrays are quite sparse. Table 2 provides a summary of prior multi-nozzle studies. Notice that all these studies employed pressure nozzles excepting Yan et al. [123,253], who used air-assist nozzles.

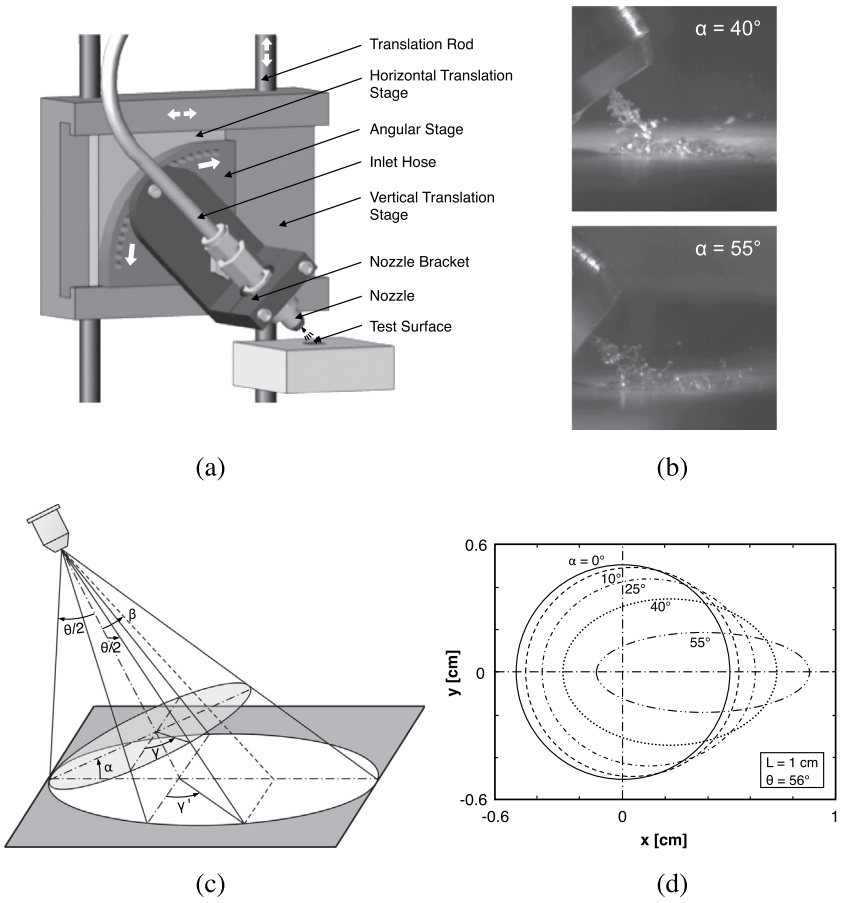

Fig. 14. (a) Nozzle inclination system. (b) Images of spray impact patterns for different inclination angles. (c) Model of inclined spray impacting a square surface. (d) Predicted variations of spray impact area with inclination angle. Adapted from Visaria and Mudawar [68].

Using an array of 8 miniature nozzles in a multi-nozzle plate, Lin and Ponnappan [237] studied spray cooling of a 1×2-cm^2 surface using FC-87, FC-72, and methanol. Their heat transfer trends were similar to those for a single nozzle, and multi-nozzle CHF data were correlated according to [259]

$$\frac{q''_{CHF}}{\rho_g h_{fg} \overline{Q}''} = 0.386 \left(\frac{\rho_f}{\rho_g}\right)^{0.549} \left(\frac{\rho_f \overline{Q}''^2 d_{32}}{\sigma}\right)^{-1/3}, \tag{86}$$

which is valid for $\overline{Q}''$ = 0.0144–0.0363 m^3 s^{-1}/m^2, d_{32} = 36–80 μm, and subcoolings below 12 °C. In a follow-up study, Lin et al. [22] used 48 miniature nozzles to cool a larger 2.54×7.60 cm^2 surface. Compared with earlier results for the 1×2-cm^2 surface, the maximum heat transfer coefficient and CHF for the large surface were lower by approximately 30% and 34%, respectively. These reductions were attributed to differences in the interaction between spray droplets and the counter-current vapor flow as illustrated in Fig. 15(a) and (b). This counter-current vapor flow was likened to that of a buoyant jet as described by Gonzalez and Black [262]. Lin et al. hypothesized that interaction in the central region of the surface is much weaker for a smaller than a larger surface.

Visaria and Mudawar [15] reported that, with proper layout of multi-nozzle arrays, overlap between adjacent spray impact areas may not affect CHF since CHF is dictated by the location and magnitude of the weakest volumetric flux. Pautsch and Shedd [235] found that the geometrical layout of nozzle arrays has little influence on overall heat transfer performance. And Horacek et al. [101] determined experimentally that the average heat flux within the spray impact region is about the same for a single nozzle and two nozzles with the same nozzle-to-surface distance. However, overlap between the two sprays is minimal because of the dilute nature of the sprays used.

Other studies indicated that, unlike single sprays, where CHF commences along the outer edge of the surface, CHF for multiple sprays often occurs in the central region of the surface because of flow interactions and blockage between neighboring sprays [47,235]. Additionally, multi-nozzle arrays were found to achieve higher CHF than single nozzles, but do so with lower fluid usage efficiency. Using their three-component heat transfer hypothesis, and assuming homogeneous nucleation within the thin liquid film, Shedd and Pautsch [102] proposed the following CHF relation for nitrogen-saturated single nozzle and four-nozzle sprays:

$$q''_{CHF} = h\left[(T_{sat} + \Delta T_c) - \left(T_f + \frac{\Delta T_{max}}{2}\right)\right], \tag{87}$$

where h is the heat transfer coefficient, which, for a single spray with Q = 0.38–1.13 ml/s, and four sprays with Q = 2.13–4.83 ml/s, is given, respectively, by

$$h = 0.4627 \rho_f c_{p,f} \overline{Q}'' + 0.01612 \overline{Q}'' \Delta T_{sat} \tag{87a}$$

and

$$h = 0.2284 + 0.2141 \rho_f c_{p,f} \overline{Q}'' + 0.003812 \overline{Q}'' \Delta T_{sat}. \tag{87b}$$

Parameters ΔT_{max} and ΔT_c in the above equations signify the maximum temperature variation across the surface at CHF, and the critical state temperature difference, respectively; the latter is calculated from [263],

Table 2
Summary of prior multi-nozzle spray cooling studies.

Authors	Nozzle array	Test fluid(s)	Surface material	Surface size
Lin and Ponnappan [237,259]	2 × 4	FC-87, FC-72, methanol, water	Copper	1 × 2 cm^2
Lin et al. [22,216]	4 × 12	FC-72	Copper	2.54 × 7.60 cm^2
Pautsch and Shedd [75,102,235]	Designed by Parker Hannifin Co.	FC-72	Multi-chip module built by IBM Co.	7 × 7 cm^2
Pereira et al. [92,108,260]	Four or five nozzles	Water	Copper	10 × 10 cm^2
Horacek et al. [101]	1 × 2	FC-72	Platinum sputtered onto titanium	0.7 × 0.7 cm^2
Yan et al. [123,253]	2 × 2	R-134a	Copper	15.1 × 13.5 cm^2
Tan et al. [115] and Xie et al. [167]	2 × 3	R-134a	Copper	1 × 2 cm^2
Xie et al. [261]	9 × 6	R-134a	Copper	23.3 × 16 cm^2
Tao et al. [63]	1 × 2	Water	Copper	2 cm^2
Hou et al. [165]	2 × 4	Water	Copper	3.2 × 1.6 cm^2
Some et al. [72]	1 × 2 and 2 × 2	PF-5060	Platinum sputtered onto titanium	0.7 × 0.7 cm^2
Bostanci et al. [5,6]	1 × 2	Antifreeze	Copper	1 × 2 cm^2
Hou et al. [134]	1 × 3	Water	(Simulation)	2 × 4 cm^2
Elston et al. [144,145]	4 × 4	FC-72	Glass	2.54 × 2.54 cm^2
Silk et al. [162]	2 × 2	PF-5060	Copper	2 cm^2
Wang et al. [187]	1 × 2	Water	Copper	1 × 2 cm^2
Escobar-Vargas et al. [90]	2 × 24	Water	Copper	3 × 5 mm^2, 1.3 × 2 mm^2

$$\Delta T_c = 0.83(T_{sat}^{+} - T_{sat}), \tag{88}$$

where T_{sat}^{+} is the superheat temperature limit.

A potential problem with multi-nozzle spray cooling is liquid accumulation or flooding, which results in a thick and uneven liquid film on the surface. Such accumulation not only reduces coolant usage efficiency, but also compromises both surface temperature uniformity and cooling performance. In extreme cases, heat transfer, especially in the central region of the surface, may shift from spray cooling to highly ineffective pool boiling. To prevent the liquid accumulation, excess liquid may be removed by gravity using inclined, horizontal or upward-facing spray orientations [22,190,253]. Glassman et al. [264] devised a different method to resolve the liquid accumulation problem, by using an array of suction tubes to drain liquid from the flooding zones, which resulted in remarkable improvement in cooling performance. Xie et al. [261] recommended yet another method to manage the liquid accumulation, which consisted of employing horizontal and vertical bridges between neighboring sprays to drain excess liquid by gravity.

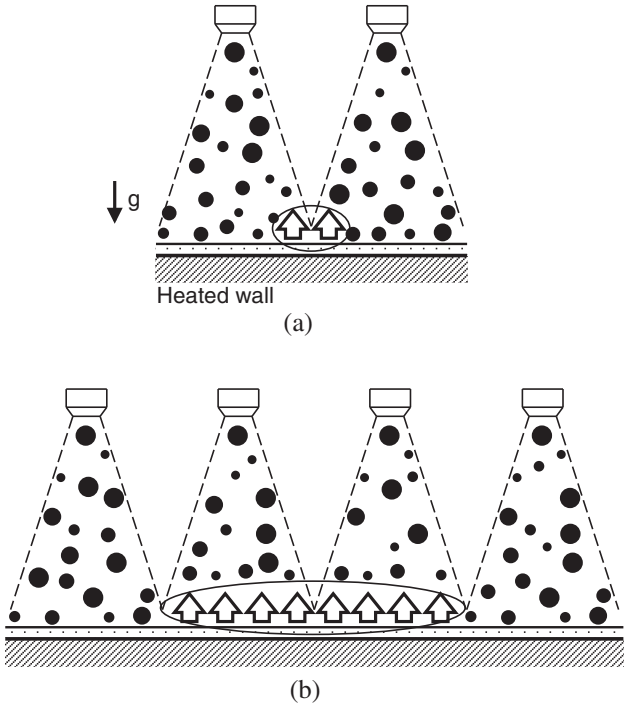

Fig. 15. Schematic of interaction between spray droplets and vapor upflow: (a) small area spray cooling and (b) large area spray cooling. Adapted from Lin et al. [22].

5.3. Gas effects

Tilton et al. [265] noted that non-condensable gases in the spray liquid increase surface temperature and degrade the performance of the condenser in the two-phase cooling loop. Lin and Ponnappan [237] measured spray CHF values with FC-72 and FC-87 as high as 90 W/cm^2, compared to up to 490 W/cm^2 for methanol and 500 W/cm^2 for water. They reported that the presence of air not only increases surface temperature, by increasing the saturation temperature, but also increases overall thermal resistance of the cooling loop. They determined that a cooling system without air provides better performance for q'' < 70 W/cm^2, while, for q'' > 70 W/cm^2, dissolved air provides better performance because of secondary nucleation created by the air bubbles. Experiments by Milke and Tinker [266] showed that spray cooling performance of non-degassed water is superior to that of degassed water.

Later, Horacek et al. [97,267] investigated spray heat transfer mechanisms with variable amounts of dissolved gas, which were carefully controlled and measured. They identified two types of subcooling: thermally subcooled, associated with decreasing liquid temperature alone, and gas subcooled, resulting from increased saturation temperature because of the dissolved gas. They reported that the presence of gas increases effective subcooling of the liquid, shifting the spray boiling curve to higher surface temperatures, but increases CHF, a trend observed in prior studies. Aside from increasing the subcooling, they suggested that the gas may cause bubbles to nucleate within the droplets or the surface liquid film, spreading liquid over a larger heated area and increasing the liquid–solid contact area, which improves cooling performance. Interestingly, they also reported that their CHF data with dissolved gas were well predicted by the correlation of Mudawar and Estes [55], Eq. (65). Using air-assist spray nozzles, Yang et al. [11] reported the existence of an optimum liquid flow rate to achieve maximum CHF for a given air flow rate.

Puterbaugh et al. [240] studied spray cooling performance of FC-72 with dissolved air volume concentrations in the range of 5–18%, and with spray chamber pressures ranging from 69 to

82.7 kPa. Unlike findings by other investigators, they reported that heat transfer is insensitive to the air dissolved in the spray system, and hypothesized that the influence of dissolved gas on CHF reported by others is the result of varying saturation pressure in response to variations in the system pressure. Jiang and Dhir [64] also reported that spray heat flux is not affected by partial pressure of non-condensable gas, but depends on total system pressure. Using a 16-nozzle array, Elston et al. [144] found that dissolved air volume concentrations of 10.1–16.8% in FC-72 do not significantly influence cooling performance.

In should be emphasized that non-condensable gases are prevalent mostly in spray cooling systems utilizing air-assist nozzles. Despite the reported benefits of non-condensable gases to spray cooling, mostly due to secondary nucleation effects, use of air-assist nozzles for cooling purposes is quite limited compared to pressure nozzles. Not only are pressure nozzles easier to characterize, but, unlike air-assist nozzles, they also have minimal influence on the performance of a closed cooling loop.

6. Concluding remarks

This study is the first part of a two-part review of spray cooling, focusing mainly on the relatively low-temperature single-phase liquid cooling and nucleate boiling regimes, as well as critical heat flux (CHF). These phenomena are important to many applications involving high-heat-flux removal from temperature sensitive devices. This review provides detailed identification of dominant mechanisms, data trends, correlations, and predictive models. Key observations from this review can be summarized as follows.

(1) Pressure spray nozzles are favored over air-assist nozzles because of better predictability and minimal impact on cooling loop. However, even for pressure nozzles, future work must take into consideration several practical concerns, including corrosion and erosion within the spray nozzle, nozzle clogging, and lack of repeatability for poorly fabricated nozzles.
(2) For both the single-phase liquid cooling and nucleate boiling regimes, different spray parameters have been identified as having dominant influences on heat transfer performance. They include mostly volumetric flux, mean droplet diameter, and mean droplet velocity. But contradictory findings among investigators, caused by incorrect use of characteristic length in defining the Nusselt number, and the lack of assessment of surface temperature spatial gradients and complex mechanisms of spray impact, all point to a need for future experiments that must be conducted very carefully and systematically, especially in regards to nozzle-to-surface distance, using many fluids with vastly different thermophysical properties, and broad ranges of operating conditions.
(3) Many investigations have pointed to the behavior of the liquid film deposited upon the sprayed surface as influencing all aspects of spray cooling in both the single-phase liquid and nucleate boiling regimes. This behavior is complicated by several phenomena, including vapor entrapment, bubble nucleation, and droplet impact and splashing. Further experimental work and theoretical modeling are needed to better quantify film thickness as well as its temporal and spatial variations.
(4) Despite the sizable body of literature addressing the dominant heat transfer mechanisms in nucleate boiling, including thin film evaporation, convection, surface homogenous nucleation, and secondary nucleation, these mechanisms have been mostly postulated rather than experimentally verified. Also lacking in most spray nucleate boiling literature are the non-uniformities in surface temperature, heat transfer coefficient, and heat flux. This is especially the case for large surfaces that are cooled by multiple nozzles. Here, more rigorous testing methods must be adopted to ensure that multi-nozzle arrays are configured to reduce the surface temperature gradients.
(5) Critical heat flux (CHF) has been the focus of many recent studies that showed that this important heat flux limit is dictated mostly by volumetric flux and mean droplet diameter, but not droplet velocity. A CHF correlation form by Estes and Mudawar has been widely validated by several investigators in fitting their own data for different fluids and other operating conditions. CHF issues that warrant further study include the effects of dissolved gas, spray inclination angle, and interaction between neighboring sprays when using multi-nozzle arrays to cool large surfaces.
(6) More recently, attention in spray cooling research has shifted to heat transfer enhancement methods. They include micro and macro modifications to the surface itself, additives to the liquid, and use of nanofluids. Unfortunately, findings from these studies often contradict one another, and, for those involving modification to the liquid itself, lack rigorous assessment of several potentially important practical problems, such as erosion, corrosion, and eventual clogging of the spray nozzle as well as several other flow loop components.

Conflict of interest

The authors declare that there is no conflict of interest.

Acknowledgements

Support of the National Natural Science Foundation of China under Grant No. 51506023, the China Postdoctoral Science Foundation under Grant No. 2016T90220, and the Fundamental Research Funds for Central Universities of Ministry of Education of China are gratefully acknowledged.

References

[1] T.M. Anderson, I. Mudawar, Microelectronic cooling by enhanced pool boiling of a dielectric fluorocarbon liquid, J. Heat Transf. – Trans. ASME 111 (1989) 752–759.
[2] I. Mudawar, Recent advances in high-flux, two-phase thermal management, J. Therm. Sci. Eng. Appl. 5 (2013) 021012.
[3] I. Mudawar, Assessment of high-heat-flux thermal management schemes, IEEE Trans. Compon. Packag. Technol. 24 (2001) 122–141.
[4] I. Mudawar, D. Bharathan, K. Kelly, S. Narumanchi, Two-phase spray cooling of hybrid vehicle electronics, IEEE Trans. Compon. Packag. Technol. 32 (2009) 501–512.
[5] H. Bostanci, D. Van Ee, B.A. Saarloos, D.P. Rini, L.C. Chow, Spray cooling of power electronics using high temperature coolant and enhanced surface, in: IEEE Vehicle Power and Propulsion Conference, IEEE, Dearborn, USA, 2009, pp. 609–613.
[6] H. Bostanci, D. Van Ee, B.A. Saarloos, D.P. Rini, L.C. Chow, Thermal management of power inverter modules at high fluxes via two-phase spray cooling, IEEE Trans. Compon. Packag. Manuf. Technol. 2 (2012) 1480–1485.
[7] M.B. Bowers, I. Mudawar, Two-phase electronic cooling using mini-channel and micro-channel heat sinks: part 2-flow rate and pressure drop constraints, J. Electron. Packag. – Trans. ASME 116 (1994) 298–305.
[8] W. Qu, I. Mudawar, Measurement and prediction of pressure drop in two-phase micro-channel heat sinks, Int. J. Heat Mass Transf. 46 (2003) 2737–2753.
[9] M. Monde, H. Kusuda, H. Uehara, Burnout heat flux in saturated forced convection boiling with two or more impinging jets, Trans. JSME 46 (1980) 1834–1843.
[10] C.H. Amon, S.-C. Yao, C.-F. Wu, C.-C. Hsieh, Microelectromechanical system-based evaporative thermal management of high heat flux electronics, J. Heat Transfer – Trans. ASME 127 (2005) 66–75.
[11] J. Yang, M.R. Pais, L.C. Chow, Critical heat flux limits in secondary gas atomized liquid spray cooling, Exp. Heat Transf. 6 (1993) 55–67.

[12] D.D. Hall, I. Mudawar, Experimental and numerical study of quenching complex-shaped metallic alloys with multiple, overlapping sprays, Int. J. Heat Mass Transf. 38 (1995) 1201–1216.
[13] C. Si, S. Shao, C. Tian, H. Xu, Development and experimental investigation of a novel spray cooling system integrated in refrigeration circuit, Appl. Therm. Eng. 33 (2012) 246–252.
[14] H. Xu, C. Si, S. Shao, C. Tian, Experimental investigation on heat transfer of spray cooling with isobutane (R600a), Int. J. Therm. Sci. 86 (2014) 21–27.
[15] M. Visaria, I. Mudawar, Application of two-phase spray cooling for thermal management of electronic devices, IEEE Trans. Compon. Packag. Technol. 32 (2009) 784–793.
[16] M. Visaria, I. Mudawar, A systematic approach to predicting critical heat flux for inclined sprays, J. Electron. Packag. – Trans. ASME 129 (2007) 452–459.
[17] J.R. Rybicki, I. Mudawar, Single-phase and two-phase cooling characteristics of upward-facing and downward-facing sprays, Int. J. Heat Mass Transf. 49 (2006) 5–16.
[18] Y.M. Qiao, S. Chandra, Spray cooling enhancement by addition of a surfactant, J. Heat Transfer – Trans. ASME 120 (1998) 92–98.
[19] C.-C. Hsieh, S.-C. Yao, Evaporative heat transfer characteristics of a water spray on micro-structured silicon surfaces, Int. J. Heat Mass Transf. 49 (2006) 962–974.
[20] K.J. Choi, S.C. Yao, Mechanisms of film boiling heat transfer of normally impacting spray, Int. J. Heat Mass Transf. 30 (1987) 311–318.
[21] K.-I. Yoshida, Y. Abe, T. Oka, Y. Mori, A. Nagashima, Spray cooling under reduced gravity condition, J. Heat Transfer – Trans. ASME 123 (2001) 309–318.
[22] L. Lin, R. Ponnappan, K. Yerkes, B. Hager, Large area spray cooling, in: 42nd AIAA Aerospace Sciences Meeting and Exhibit, AIAA, Reno, USA, 2004.
[23] K.A. Estes, I. Mudawar, Comparison of two-phase electronic cooling using free jets and sprays, J. Electron. Packag. – Trans. ASME 117 (1995) 323–332.
[24] N. Mascarenhas, I. Mudawar, Analytical and computational methodology for modeling spray quenching of solid alloy cylinders, Int. J. Heat Mass Transf. 53 (2010) 5871–5883.
[25] A. Bar-Cohen, M. Arik, M. Ohadi, Direct liquid cooling of high flux micro and nano electronic components, Proc. IEEE 94 (2006) 1549–1570.
[26] M.A. Ebadian, C.X. Lin, A review of high-heat-flux heat removal technologies, J. Heat Transf. – Trans. ASME 133 (2011) 110801.
[27] S.G. Kandlikar, A.V. Bapat, Evaluation of jet impingement, spray and microchannel chip cooling options for high heat flux removal, Heat Transf. Eng. 28 (2007) 911–923.
[28] P. Smakulski, S. Pietrowicz, A review of the capabilities of high heat flux removal by porous materials, microchannels and spray cooling techniques, Appl. Therm. Eng. 104 (2016) 636–646.
[29] J. Kim, Spray cooling heat transfer: the state of the art, Int. J. Heat Fluid Flow 28 (2007) 753–767.
[30] W.-L. Cheng, W.-W. Zhang, H. Chen, L. Hu, Spray cooling and flash evaporation cooling: the current development and application, Renew. Sustain. Energy Rev. 55 (2016) 614–628.
[31] A.A. Tseng, M. Raudensky, T.-W. Lee, Liquid sprays for heat transfer enhancements: a review, Heat Transf. Eng. 37 (2016) 1401–1417.
[32] E.A. Silk, E.L. Golliher, R.P. Selvam, Spray cooling heat transfer: technology overview and assessment of future challenges for micro-gravity application, Energy Convers. Manage. 49 (2008) 453–468.
[33] G. Liang, I. Mudawar, Review of mass and momentum interactions during drop impact on a liquid film, Int. J. Heat Mass Transf. 101 (2016) 577–599.
[34] G. Liang, I. Mudawar, Review of drop impact on heated walls, Int. J. Heat Mass Transf. 106 (2017) 103–126.
[35] G. Liang, I. Mudawar, Review of spray cooling-Part 2: High temperature boiling regimes and quenching applications, Int. J. Heat Mass Transf. 115 (2017) 1206–1222.
[36] G. Liang, S. Shen, Y. Guo, J. Zhang, Boiling from liquid drops impact on a heated wall, Int. J. Heat Mass Transf. 100 (2016) 48–57.
[37] G.E. Cossali, M. Marengo, M. Santini, Multiple drop impact on heated surface, in: Proceedings of the 9th ICLASS, Sorrento, Italy, 2003.
[38] G.E. Cossali, M. Marengo, M. Santini, Impact of single and multiple drop array on a liquid film, in: Proc. 19th ILASS-Eurpope, Nottingham, UK, 2004.
[39] G. Aguilar, B. Majaron, W. Verkruysse, Y. Zhou, J.S. Nelson, E.J. Lavernia, Theoretical and experimental analysis of droplet diameter, temperature, and evaporation rate evolution in cryogenic sprays, Int. J. Heat Mass Transf. 44 (2001) 3201–3211.
[40] D. Li, B. Chen, W.J. Wu, G.-X. Wang, Y.L. He, Multi-scale modeling of tissue freezing during cryogen spray cooling with R134a, R407c and R404a, Appl. Therm. Eng. 73 (2014) 1489–1500.
[41] M.H. Sadafi, S.G. Ruiz, M.R. Vetrano, I. Jahn, J. van Beeck, J.M. Buchlin, K. Hooman, An investigation on spray cooling using saline water with experimental verification, Energy Convers. Manage. 108 (2016) 336–347.
[42] J. Yang, L.C. Chow, M.R. Pais, Nucleate boiling heat transfer in spray cooling, J. Heat Transf. 118 (1996) 668–671.
[43] M.R. Pais, L.C. Chow, E.T. Mahefkey, Surface roughness and its effects on the heat transfer mechanism in spray cooling, J. Heat Transf. – Trans. ASME 114 (1992) 211–219.
[44] A. Cebo-Rudnicka, Z. Malinowski, A. Buczek, The influence of selected parameters of spray cooling and thermal conductivity on heat transfer coefficient, Int. J. Therm. Sci. 110 (2016) 52–64.
[45] I. Mudawar, W.S. Valentine, Determination of the local quench curve for spray-cooled metallic surfaces, J. Heat. Treat. 7 (1989) 107–121.
[46] R.A. Mugele, H.D. Evans, Droplet size distribution in sprays, Ind. Eng. Chem. 43 (1951) 1317–1324.
[47] K.A. Estes, I. Mudawar, Correlation of Sauter mean diameter and critical heat flux for spray cooling of small surfaces, Int. J. Heat Mass Transf. 38 (1995) 2985–2996.
[48] M. Ghodbane, J.P. Holman, Experimental study of spray cooling with Freon-113, Int. J. Heat Mass Transf. 34 (1991) 1163–1174.
[49] C. Bonacina, S. Del Giudice, G. Comini, Dropwise evaporation, J. Heat Transf. – Trans. ASME 101 (1979) 441–446.
[50] G.G. Nasr, R. Sharief, D.D. James, J.R. Jeong, I.R. Widger, A.J. Yule, Studies of high pressure water sprays from full cone atomizers, in: ILASS-Europe, Toulouse, France, 1999.
[51] W.-L. Cheng, F.-Y. Han, Q.-N. Liu, H.-L. Fan, Spray characteristics and spray cooling heat transfer in the non-boiling regime, Energy 36 (2011) 3399–3405.
[52] J.L. Xie, Z.W. Gan, F. Duan, T.N. Wong, S.C.M. Yu, R. Zhao, Characterization of spray atomization and heat transfer of pressure swirl nozzles, Int. J. Therm. Sci. 68 (2013) 94–102.
[53] J.L. Xie, Z.W. Gan, T.N. Wong, F. Duan, S.C.M. Yu, Y.H. Wu, Thermal effects on a pressure swirl nozzle in spray cooling, Int. J. Heat Mass Transf. 73 (2014) 130–140.
[54] I. Mudawar, T.A. Deiters, A universal approach to predicting temperature response of metallic parts to spray quenching, Int. J. Heat Mass Transf. 37 (1994) 347–362.
[55] I. Mudawar, K.A. Estes, Optimizing and predicting CHF in spray cooling of a square surface, J. Heat Transf. – Trans. ASME 118 (1996) 672–679.
[56] G.F. Hewitt, J.M. Delhaye, N. Zuber, Multiphase Science and Technology, Hemisphere, New York, 1973, pp. 1–93.
[57] M. Ciofalo, I. Di Piazza, V. Brucato, Investigation of the cooling of hot walls by liquid water sprays, Int. J. Heat Mass Transf. 42 (1999) 1157–1175.
[58] M. Ciofalo, A. Caronia, M. Di Liberto, S. Puleo, The Nukiyama curve in water spray cooling: its derivation from temperature-time histories and its dependence on the quantities that characterize drop impact, Int. J. Heat Mass Transf. 50 (2007) 4948–4966.
[59] S.-S. Hsieh, C.-H. Tien, R-134a spray dynamics and impingement cooling in the non-boiling regime, Int. J. Heat Mass Transf. 50 (2007) 502–512.
[60] Y.-X. Guo, Z.-F. Zhou, J.-Y. Jia, S.-R. Zhou, Optimal heat transfer criterion and inclination angle effects on non-boiling regime spray cooling, in: 25th Annual IEEE SEMI-THERM, IEEE, San Jose, USA, 2009, pp. 193–200.
[61] D.S. Zhu, J.Y. Sun, S.D. Tu, Z.D. Wang, Experimental study of non-boiling heat transfer by high flow rate nanofluids spray, in: The 6th International Symposium on Multiphase Flow, Heat Mass Transfer and Energy Conversion, AIP, Xi'an, China, 2010, pp. 476–482.
[62] C. Cho, R. Ponzel, Experimental study on the spray cooling of a heated solid surface, in: Proc. 1997 ASME International Mechanical Engineering Congress and Exposition, ASME, Dallas, USA, 1997, pp. 265–272.
[63] Y. Tao, X. Huai, L. Wang, Z. Guo, Experimental characterization of heat transfer in non-boiling spray cooling with two nozzles, Appl. Therm. Eng. 31 (2011) 1790–1797.
[64] S. Jiang, V.K. Dhir, Spray cooling in a closed system with different fractions of non-condensibles in the environment, Int. J. Heat Mass Transf. 47 (2004) 5391–5406.
[65] N. Karwa, S.R. Kale, P.M.V. Subbarao, Experimental study of non-boiling heat transfer from a horizontal surface by water sprays, Exp. Therm. Fluid Sci. 32 (2007) 571–579.
[66] K. Oliphant, B.W. Webb, M.Q. McQuay, An experimental comparison of liquid jet array and spray impingement cooling in the non-boiling regime, Exp. Therm. Fluid Sci. 18 (1998) 1–10.
[67] Y. Wang, M. Liu, D. Liu, K. Xu, Y. Chen, Experimental study on the effects of spray inclination on water spray cooling performance in non-boiling regime, Exp. Therm. Fluid Sci. 34 (2010) 933–942.
[68] M. Visaria, I. Mudawar, Theoretical and experimental study of the effects of spray inclination on two-phase spray cooling and critical heat flux, Int. J. Heat Mass Transf. 51 (2008) 2398–2410.
[69] Y. Wang, M. Liu, D. Liu, K. Xu, Heat flux correlation for spray cooling in the nonboiling regime, Heat Transf. Eng. 32 (2011) 1075–1081.
[70] T.A. Shedd, Next generation spray cooling: high heat flux management in compact spaces, Heat Transf. Eng. 28 (2007) 87–92.
[71] A.C. Ashwood, T.A. Shedd, Spray cooling with mixtures of dielectric fluids, in: 23rd Annual IEEE SEMI-THERM, IEEE, San Jose, USA, 2007, pp. 144–148.
[72] T. Some, E. Lehmann, H. Sakamoto, J. Kim, J.T. Chung, E. Steinthorssen, Pressure based prediction of spray cooling heat transfer coefficients, in: ASME 2007 International Mechanical Engineering Congress and Exposition, ASME, Seattle, USA, 2007, pp. 1131–1138.
[73] B. Abbasi, J. Kim, A. Marshall, Dynamic pressure based prediction of spray cooling heat transfer coefficients, Int. J. Multiph. Flow 36 (2010) 491–502.
[74] B. Abbasi, J. Kim, Development of a general dynamic pressure based single-phase spray cooling heat transfer correlation, J. Heat Transf. 133 (2011) 052201.
[75] S. Freund, A.G. Pautsch, T.A. Shedd, S. Kabelac, Local heat transfer coefficients in spray cooling systems measured with temperature oscillation IR thermography, Int. J. Heat Mass Transf. 50 (2007) 1953–1962.
[76] D.E. Tilton, Spray cooling PhD Dissertation, University of Kentucky, Lexington, USA, 1989.
[77] J. Yang, L.C. Chow, M.R. Pais, A. Ito, Liquid film thickness and topography determination using Fresnel diffraction and holography, Exp. Heat Transf. 5 (1992) 239–252.

[78] W.S. Mathews, C.F. Lee, J.E. Peters, Experimental investigations of spray/wall impingement, Atomiz. Sprays 13 (2003) 223–242.
[79] A.G. Pautsch, T.A. Shedd, Adiabatic and diabatic measurements of the liquid film thickness during spray cooling with FC-72, Int. J. Heat Mass Transf. 49 (2006) 2610–2618.
[80] S.-S. Hsieh, G.-W. Chen, Y.-F. Yeh, Optical flow and thermal measurements for spray cooling, Int. J. Heat Mass Transf. 87 (2015) 248–253.
[81] E. Martínez-Galván, J.C. Ramos, R. Antón, R. Khodabandeh, Influence of surface roughness on a spray cooling system with R134a. Part II: Film thickness measurements, Exp. Therm. Fluid Sci. 48 (2013) 73–80.
[82] E. Martínez-Galván, J.C. Ramos, R. Antón, R. Khodabandeh, Film thickness and heat transfer measurements in a spray cooling system with R134a, J. Electron. Packag. – Trans. ASME 133 (2011) 011002.
[83] E. Martínez-Galván, R. Antón, J.C. Ramos, R. Khodabandeh, Effect of the spray cone angle in the spray cooling with R134a, Exp. Therm. Fluid Sci. 50 (2013) 127–138.
[84] J.L. Xie, R. Zhao, F. Duan, T.N. Wong, Thin liquid film flow and heat transfer under spray impingement, Appl. Therm. Eng. 48 (2012) 342–348.
[85] X.-Q. Chen, L.C. Chow, M.S. Sehmbey, Thickness of film produced by pressure atomizing nozzles, in: 30th AIAA Thermophysics Conference, AIAA, San Diego, USA, 1995.
[86] J.-Y. Jia, Y.-X. Guo, W.-D. Wang, S.-R. Zhou, Modeling and experimental research on spray cooling, in: 24th Annual IEEE SEMI-THERM, IEEE, San Jose, USA, 2008, pp. 118–123.
[87] R.K. Sharma, C.E. Bash, C.D. Patel, Experimental investigation of heat transfer characteristics of inkjet assisted spray cooling, in: ASME 2004 Heat Transfer/Fluids Engineering Summer Conference, ASME, Charlotte, USA, 2004, pp. 479–486.
[88] D. Fabris, S. Escobar-Vargas, J.E. Gonzalez, R. Sharma, C. Bash, Monodisperse spray cooling of small surface areas at high heat flux, Heat Transf. Eng. 33 (2012) 1161–1169.
[89] S. Escobar-Vargas, J.E. Gonzalez, O. Ruiz, C. Bash, R. Sharma, D. Fabris, Near critical heat flux from small substrates under controlled spray cooling, in: ASME 2009 Heat Transfer Summer Conference, ASME, San Francisco, USA, 2009, pp. 877–883.
[90] S. Escobar-Vargas, J.E. Gonzalez, D. Fabris, R. Sharma, C. Bash, High heat flux with small scale monodisperse sprays, J. Heat Transf. – Trans. ASME 134 (2012) 122202.
[91] S. Escobar, R. Sharma, D. Fabris, J.E. Gonzalez, C. Bash, High power density dissipations by spray cooling, in: ASME/JSME 2007 Thermal Engineering Heat Transfer Summer Conference, ASME, Vancouver, Canada, 2007, pp. 791–795.
[92] R.H. Pereira, S.L. Braga, J.A.R. Parise, Comparing single phase heat transfer to arrays of impinging jets and sprays, in: ASME 2002 International Mechanical Engineering Congress and Exposition, ASME, New Orleans, USA, 2002, pp. 351–358.
[93] A.K. Sleiti, J.S. Kapat, An experimental investigation of liquid jet impingement and single-phase spray cooling using polyalphaolefin, Exp. Heat Transf. 19 (2006) 149–163.
[94] M. Fabbri, S. Jiang, V.K. Dhir, A comparative study of cooling of high power density electronics using sprays and microjets, J. Heat Transf. – Trans. ASME 127 (2005) 38–48.
[95] C. Cho, K. Wu, Comparison of burnout characteristics in jet impingement cooling and spray cooling, in: ASME Proceedings of the National Heat Transfer Conference, ASME, Houston, USA, 1988, pp. 561–567.
[96] A. Labergue, M. Gradeck, F. Lemoine, Comparative study of the cooling of a hot temperature surface using sprays and liquid jets, Int. J. Heat Mass Transf. 81 (2015) 889–900.
[97] B. Horacek, K.T. Kiger, J. Kim, Single nozzle spray cooling heat transfer mechanisms, Int. J. Heat Mass Transf. 48 (2005) 1425–1438.
[98] D.P. Rini, R.-H. Chen, L.C. Chow, Bubble behavior and nucleate boiling heat transfer in saturated FC-72 spray cooling, J. Heat Transf. – Trans. ASME 124 (2002) 63–72.
[99] R. Mesler, Discussion: "Surface roughness and its effects on the heat transfer mechanism of spray cooling" (Pais, M.R., Chow, L.C., and Mahefkey, E.T., 1992, ASME J. Heat Transfer, 114, pp. 211-219), J. Heat Transf. – Trans. ASME 115 (1993), 1083-1083.
[100] N. Xie, X. Hu, D. Tang, Visualization of microbubble dynamics behavior in rectangular capillary microgrooves under spray cooling condition, Heat Transf. Eng. 32 (2011) 1019–1025.
[101] B. Horacek, J. Kim, K.T. Kiger, Spray cooling using multiple nozzles: visualization and wall heat transfer measurements, IEEE Trans. Device Mater. Reliab. 4 (2004) 614–625.
[102] T.A. Shedd, A.G. Pautsch, Spray impingement cooling with single-and multiple-nozzle arrays. Part II: Visualization and empirical models, Int. J. Heat Mass Transf. 48 (2005) 3176–3184.
[103] W.M. Grissom, F.A. Wierum, Liquid spray cooling of a heated surface, Int. J. Heat Mass Transf. 24 (1981) 261–271.
[104] C. Bonacina, G. Comini, S. Del Giudice, Evaporation of atomized liquid on hot surfaces, Lett. Heat Mass Transf. 2 (1975) 401–406.
[105] W. Jia, H.-H. Qiu, Experimental investigation of droplet dynamics and heat transfer in spray cooling, Exp. Therm. Fluid Sci. 27 (2003) 829–838.
[106] B.W. Webb, M. Qpeiroz, K.N. Oliphant, M.P. Bonin, Onset of dry-wall heat transfer in low-mass-flux spray cooling, Exp. Heat Transf. 5 (1992) 33–50.
[107] R. Dou, Z. Wen, G. Zhou, Heat transfer characteristics of water spray impinging on high temperature stainless steel plate with finite thickness, Int. J. Heat Mass Transf. 90 (2015) 376–387.
[108] R.H. Pereira, E.P.B. Filho, S.L. Braga, J.A.R. Parise, Nucleate boiling in large arrays of impinging water sprays, Heat Transf. Eng. 34 (2013) 479–491.
[109] M. Visaria, I. Mudawar, Effects of high subcooling on two-phase spray cooling and critical heat flux, Int. J. Heat Mass Transf. 51 (2008) 5269–5278.
[110] J.P. Holman, C.M. Kendall, Extended studies of spray cooling with Freon-113, Int. J. Heat Mass Transf. 36 (1993) 2239–2241.
[111] S.-S. Hsieh, T.-C. Fan, H.-H. Tsai, Spray cooling characteristics of water and R-134a. Part I: nucleate boiling, Int. J. Heat Mass Transf. 47 (2004) 5703–5712.
[112] M.S. Sehmbey, L.C. Chow, O.J. Hahn, M.R. Pais, Effect of spray characteristics on spray cooling with liquid nitrogen, J. Thermophys. Heat Transf. 9 (1995) 757–765.
[113] M.S. Sehmbey, L.C. Chow, O.J. Hahn, M.R. Pais, Spray cooling of power electronics at cryogenic temperatures, J. Thermophys. Heat Transf. 9 (1995) 123–128.
[114] L. Ortiz, J.E. Gonzalez, Experiments on steady-state high heat fluxes using spray cooling, Exp. Heat Transf. 12 (1999) 215–233.
[115] Y.B. Tan, J.L. Xie, F. Duan, T.N. Wong, K.C. Toh, K.F. Choo, P.K. Chan, Y.S. Chua, Multi-nozzle spray cooling for high heat flux applications in a closed loop system, Appl. Therm. Eng. 54 (2013) 372–379.
[116] E. Cabrera, J.E. Gonzalez, Heat flux correlation for spray cooling in the nucleate boiling regime, Exp. Heat Transf. 16 (2003) 19–44.
[117] J. Liu, R. Xue, L. Chen, X. Liu, Y. Hou, Influence of chamber pressure on heat transfer characteristics of a closed loop R134-a spray cooling, Exp. Therm. Fluid Sci. 75 (2016) 89–95.
[118] R.-H. Chen, L.C. Chow, J.E. Navedo, Optimal spray characteristics in water spray cooling, Int. J. Heat Mass Transf. 47 (2004) 5095–5099.
[119] S. Chen, J. Liu, X. Liu, Y. Hou, An experimental comparison of heat transfer characteristic between R134-a and R22 in spray cooling, Exp. Therm. Fluid Sci. 66 (2015) 206–212.
[120] W.-L. Cheng, Q.-N. Liu, R. Zhao, H.-L. Fan, Experimental investigation of parameters effect on heat transfer of spray cooling, Heat Mass Transf. 46 (2010) 911–921.
[121] R. Zhao, W.-L. Cheng, Q.-N. Liu, H.-L. Fan, Study on heat transfer performance of spray cooling: model and analysis, Heat Mass Transf. 46 (2010) 821–829.
[122] W.-L. Cheng, F.-Y. Han, Q.-N. Liu, R. Zhao, H.-L. Fan, Experimental and theoretical investigation of surface temperature non-uniformity of spray cooling, Energy 36 (2011) 249–257.
[123] Z.B. Yan, K.C. Toh, F. Duan, T.N. Wong, K.F. Choo, P.K. Chan, Y.S. Chua, Experimental study of impingement spray cooling for high power devices, Appl. Therm. Eng. 30 (2010) 1225–1230.
[124] W.-L. Cheng, F.-Y. Han, Q.-N. Liu, R. Zhao, Theoretical investigation on the mechanism of surface temperature non-uniformity formation in spray cooling, Int. J. Heat Mass Transf. 55 (2012) 5357–5366.
[125] J. Xie, T.N. Wong, F. Duan, Modelling on the dynamics of droplet impingement and bubble boiling in spray cooling, Int. J. Therm. Sci. 104 (2016) 469–479.
[126] P.J. Kreitzer, J.M. Kuhlman, Spray cooling droplet impingement model, in: 10th AIAA/ASME Joint Thermophysics and Heat Transfer Conference, AIAA, Chicago, USA, 2010.
[127] R.P. Selvam, L. Lin, R. Ponnappan, Direct simulation of spray cooling: effect of vapor bubble growth and liquid droplet impact on heat transfer, Int. J. Heat Mass Transf. 49 (2006) 4265–4278.
[128] R.P. Selvam, S. Bhaskara, J.C. Balda, F. Barlow, A. Elshabini, Computer modeling of liquid droplet impact on Heat transfer during spray cooling, in: ASME 2005 Summer Heat Transfer Conference, ASME, San Francisco, USA, 2005, pp. 179–188.
[129] S. Sarkar, R.P. Selvam, Direct numerical simulation of heat transfer in spray cooling through 3D multiphase flow modeling using parallel computing, J. Heat Transf. – Trans. ASME 131 (2009) 121007.
[130] B.L. Rowden, R.P. Selvam, E.A. Silk, Spray cooling development effort for microgravity environments, in: Space Technology and Applications International Forum, AIP, Albuquerque, USA, 2006, pp. 134–144.
[131] R.J. Issa, S.C. Yao, A numerical model for the mist dynamics and heat transfer at various ambient pressures, J. Fluids Eng. 127 (2005) 631–639.
[132] R.J. Issa, S.-C. Yao, Numerical model for spray-wall impaction and heat transfer at atmospheric conditions, J. Thermophys. Heat Transf. 19 (2005) 441–447.
[133] R.-H. Chen, D.S. Tan, K.-C. Lin, L.C. Chow, A.R. Griffin, D.P. Rini, Droplet and bubble dynamics in saturated FC-72 spray cooling on a smooth surface, J. Heat Transf. – Trans. ASME 130 (2008) 101501.
[134] Y. Hou, Y. Tao, X. Huai, Z. Guo, Numerical characterization of multi-nozzle spray cooling, Appl. Therm. Eng. 39 (2012) 163–170.
[135] J.C. Landero, A.P. Watkins, Modeling of steady-state heat transfer in a water spray impingement onto a heated wall, Atomiz. Sprays 18 (2008) 1–47.
[136] M.S. Sehmbey, M.R. Pais, L.C. Chow, Effect of surface material properties and surface characteristics inevaporative spray cooling, J. Thermophys. Heat Transf. 6 (1992) 505–512.
[137] M.S. Sehmbey, M.R. Pais, L.C. Chow, A study of diamond laminated surfaces in evaporative spray cooling, Thin Solid Films 212 (1992) 25–29.
[138] J. Yang, L.C. Chow, M.R. Pais, An analytical method to determine the liquid film thickness produced by gas atomized sprays, J. Heat Transf. – Trans. ASME 118 (1996) 255–258.
[139] E.L. Golliher, C.P. Zivich, S.C. Yao, Exploration of unsteady spray cooling for high power electronics at microgravity using NASA Glenn's drop tower, in: ASME 2005 Summer Heat Transfer Conference, ASME, San Francisco, USA, 2005, pp. 609–612.

[140] T.E. Michalak, K.L. Yerkes, S.K. Thomas, J.B. McQuillen, Acceleration effects on the cooling performance of a partially confined FC-72 spray, J. Thermophys. Heat Transf. 24 (2010) 463–479.
[141] K.M. Baysinger, K.L. Yerkes, T.E. Michalak, R.J. Harris, J. McQuillen, Design of a microgravity spray cooling experiment, in: 42nd AIAA Aerospace Sciences Meeting and Exhibit, AIAA, Reno, USA, 2004.
[142] K.L. Yerkes, T.E. Michalak, K.M. Baysinger, R. Puterbaugh, S.K. Thomas, J. McQuillen, Variable-gravity effects on a single-phase partially-confined spray cooling system, J. Thermophys. Heat Transf. 20 (2006) 361–370.
[143] T. Gambaryan-Roisman, O. Kyriopoulos, I. Roisman, P. Stephan, C. Tropea, Gravity effect on spray impact and spray cooling, Microgr. Sci. Technol. 19 (2007) 151–154.
[144] L.J. Elston, K.L. Yerkes, S.K. Thomas, J. McQuillen, The effect of variable gravity on the cooling performance of a 16-nozzle spray array, in: 47th AIAA Aerospace Sciences Meeting Including the New Horizons Forum and Aerospace Exposition, AIAA, Orlando, USA, 2009.
[145] L.J. Elston, K.L. Yerkes, S.K. Thomas, J. McQuillen, Cooling performance of a 16-nozzle array in variable gravity, J. Thermophys. Heat Transf. 23 (2009) 571–581.
[146] B.L. Conrad, J.C. Springmann, L.A. McGill, T.A. Shedd, Effectiveness of linear spray cooling in microgravity, in: Space, Propulsion, and Energy Sciences International Forum, AIP, Melville, USA, 2009, pp. 67–72.
[147] C.A. Hunnell, J.M. Kuhlman, D.D. Gray, Spray cooling in terrestrial and simulated reduced gravity, in: Space Technology and Applications International Forum, AIP, Albuquerque, USA, 2006, pp. 126–133.
[148] P.J. Kreitzer, S.L. Glaspell, J.M. Kuhlman, D. Mehra, D.D. Gray, Electrical force effects on spray cooling, in: SAE Power Systems Conference, SAE, New Orleans, USA, 2006.
[149] J.M. Kuhlman, P.J. Kreitzer, D. Mehra, D.D. Gray, K.L. Yerkes, Influence of the Coulomb force on spray cooling, in: Space Technology and Applications International Forum, AIP, Albuquerque, USA, 2007, pp. 100–109.
[150] P.J. Kreitzer, J.M. Kuhlman, D. Mehra, D. Gray, K.L. Yerkes, Effects of contact charging on spray impingement heat transfer performance and spray behavior, in: 39th AIAA Thermophysics Conference, AIAA, Miami, USA, 2007.
[151] P.J. Kreitzer, J.M. Kuhlman, Visualization of electrohydrodynamic effects and time scale analysis for impinging spray droplets of HFE-7000, in: Space Technology and Applications International Forum, AIP, Albuquerque, USA, 2008, pp. 86–93.
[152] M. Kato, Y. Abe, Y. Mori, A. Nagashima, Spray cooling characteristics under reduced gravity, J. Thermophys. Heat Transf. 9 (1995) 378–381.
[153] K. Sone, K. Yoshida, T. Oka, Y. Abe, Y. Mori, A. Nagashima, Spray cooling characteristics of water and FC-72 under reduced and elevated gravity for space application, in: Proceedings of the 31st IECEC, IEEE, Washington D.C., USA, 1996, pp. 1500–1505.
[154] B.-S. Kang, K.-J. Choi, Cooling of a heated surface with an impinging water spray, KSME Int. J. 12 (1998) 734–740.
[155] Z. Zhang, J. Li, P.-X. Jiang, Experimental investigation of spray cooling on flat and enhanced surfaces, Appl. Therm. Eng. 51 (2013) 102–111.
[156] E. Martínez-Galván, R. Antón, J.C. Ramos, R. Khodabandeh, Influence of surface roughness on a spray cooling system with R134a. Part I: Heat transfer measurements, Exp. Therm. Fluid Sci. 46 (2013) 183–190.
[157] H. Fukuda, N. Nakata, H. Kijima, T. Kuroki, A. Fujibayashi, Y. Takata, S. Hidaka, Effects of surface conditions on spray cooling characteristics, ISIJ Int. 56 (2016) 628–636.
[158] J.H. Kim, S.M. You, S.U.S. Choi, Evaporative spray cooling of plain and microporous coated surfaces, Int. J. Heat Mass Transf. 47 (2004) 3307–3315.
[159] S.J. Thiagarajan, S. Narumanchi, R. Yang, Effect of flow rate and subcooling on spray heat transfer on microporous copper surfaces, Int. J. Heat Mass Transf. 69 (2014) 493–505.
[160] S.J. Thiagarajan, S. Narumanchi, C. King, W. Wang, R. Yang, Enhancement of heat transfer with pool and spray impingement boiling on microporous and nanowire surface coatings, in: 14th International Heat Transfer Conference, ASME, Washington, DC, USA, 2010, pp. 819–828.
[161] E.A. Silk, Investigation of pore size effect on spray cooling heat transfer with porous tunnels, in: Space Technology and Applications International Forum, AIP, Albuquerque, USA, 2008, pp. 112–122.
[162] E.A. Silk, J. Kim, K. Kiger, Spray cooling of enhanced surfaces: impact of structured surface geometry and spray axis inclination, Int. J. Heat Mass Transf. 49 (2006) 4910–4920.
[163] E.A. Silk, J. Kim, K. Kiger, Investigation of enhanced surface spray cooling, in: ASME 2004 International Mechanical Engineering Congress and Exposition, ASME, Anaheim, USA, 2004, pp. 685–690.
[164] J.S. Coursey, J. Kim, K.T. Kiger, Spray cooling of small-pitched, straight-finned, copper heat sinks, in: ASME 2005 International Mechanical Engineering Congress and Exposition, ASME, Orlando, USA, 2005, pp. 271–277.
[165] Y. Hou, Y. Tao, X. Huai, The effects of micro-structured surfaces on multi-nozzle spray cooling, Appl. Therm. Eng. 62 (2014) 613–621.
[166] M. Liu, Y. Wang, D. Liu, K. Xu, Y. Chen, Experimental study of the effects of structured surface geometry on water spray cooling performance in non-boiling regime, Front. Energy 5 (2011) 75–82.
[167] J.L. Xie, Y.B. Tan, F. Duan, K. Ranjith, T.N. Wong, K.C. Toh, K.F. Choo, P.K. Chan, Study of heat transfer enhancement for structured surfaces in spray cooling, Appl. Therm. Eng. 59 (2013) 464–472.
[168] Q. Li, P. Tie, Y. Xuan, Investigation on heat transfer characteristics of R134a spray cooling, Exp. Therm. Fluid Sci. 60 (2015) 182–187.
[169] L.-H. Chien, T.-L. Wu, S.-C. Lee, A study of spray-impingement cooling on smooth and pin-finned surfaces using FC-72, J. Enhanc. Heat Transf. 18 (2011) 375–387.
[170] M. Aamir, Q. Liao, W. Hong, Z. Xun, S. Song, M. Sajid, Transient heat transfer behavior of water spray evaporative cooling on a stainless steel cylinder with structured surface for safety design application in high temperature scenario, Heat Mass Transf. (2016), http://dx.doi.org/10.1007/s00231-016-1830-5.
[171] Y. Wang, N. Zhou, Z. Yang, Y. Jiang, Experimental investigation of aircraft spray cooling system with different heating surfaces and different additives, Appl. Therm. Eng. 103 (2016) 510–521.
[172] W. Zhang, Z. Wang, Heat transfer enhancement of spray cooling in straight-grooved surfaces in the non-boiling regime, Exp. Therm. Fluid Sci. 69 (2015) 38–44.
[173] C. Sodtke, P. Stephan, Spray cooling on micro structured surfaces, Int. J. Heat Mass Transf. 50 (2007) 4089–4097.
[174] H. Bostanci, D.P. Rini, J.P. Kizito, L.C. Chow, Spray cooling with ammonia on microstructured surfaces: performance enhancement and hysteresis effect, J. Heat Transf. – Trans. ASME 131 (2009) 071401.
[175] H. Bostanci, High heat flux spray cooling with ammonia on enhanced surfaces PhD Dissertation, University of Central Florida, Orlando, USA, 2010.
[176] H. Bostanci, D.P. Rini, J.P. Kizito, V. Singh, S. Seal, L.C. Chow, High heat flux spray cooling with ammonia: Investigation of enhanced surfaces for HTC, Int. J. Heat Mass Transf. 75 (2014) 718–725.
[177] H. Bostanci, D.P. Rini, J.P. Kizito, V. Singh, S. Seal, L.C. Chow, High heat flux spray cooling with ammonia: Investigation of enhanced surfaces for CHF, Int. J. Heat Mass Transf. 55 (2012) 3849–3856.
[178] S.-S. Hsieh, S.-Y. Luo, R.-Y. Lee, H.-H. Liu, Spray cooling heat transfer on microstructured thin film enhanced surfaces, Exp. Therm. Fluid Sci. 68 (2015) 123–134.
[179] Z. Zhang, P.-X. Jiang, X.-L. Ouyang, J.-N. Chen, D.M. Christopher, Experimental investigation of spray cooling on smooth and micro-structured surfaces, Int. J. Heat Mass Transf. 76 (2014) 366–375.
[180] Z. Zhang, P.-X. Jiang, D.M. Christopher, X.-G. Liang, Experimental investigation of spray cooling on micro-, nano-and hybrid-structured surfaces, Int. J. Heat Mass Transf. 80 (2015) 26–37.
[181] Z. Zhang, P.-X. Jiang, X.-L. Ouyang, J.-N. Chen, D.M. Christopher, K.-L. Jiang, Experimental investigation of spray cooling on nano-and hybrid-structured surfaces, in: ASME 2013 4th International Conference on Micro/Nanoscale Heat and Mass Transfer, ASME, Hong Kong, China, 2013.
[182] J.L. Alvarado, Y.-P. Lin, Multiple droplet impingements on nanostructured surfaces for enhanced spray cooling, in: ASME/JSME 2011 8th Thermal Engineering Joint Conference, ASME, Honolulu, USA, 2011.
[183] B.H. Yang, H. Wang, X. Zhu, Q. Liao, Y.D. Ding, R. Chen, Heat transfer enhancement of spray cooling with ammonia by microcavity surfaces, Appl. Therm. Eng. 50 (2013) 245–250.
[184] A.G.U. de Souza, J.R. Barbosa, Spray cooling of plain and copper-foam enhanced surfaces, Exp. Therm. Fluid Sci. 39 (2012) 198–206.
[185] A.G.U. de Souza, J.R. Barbosa, Experimental evaluation of spray cooling of R-134a on plain and enhanced surfaces, Int. J. Refrig. 36 (2013) 527–533.
[186] E.A. Silk, P. Bracken, Spray cooling heat flux performance using POCO HTC foam, J. Thermophys. Heat Transf. 24 (2010) 157–164.
[187] J.-X. Wang, Y.-Z. Li, H.-S. Zhang, S.-N. Wang, Y.-F. Mao, Y.-N. Zhang, Y.-H. Liang, Investigation of a spray cooling system with two nozzles for space application, Appl. Therm. Eng. 89 (2015) 115–124.
[188] Q. Cui, S. Chandra, S. McCahan, The effect of dissolving salts in water sprays used for quenching a hot surface: Part 2-Spray cooling, J. Heat Transf. – Trans. ASME 125 (2003) 333–338.
[189] W. Cheng, B. Xie, F. Han, H. Chen, An experimental investigation of heat transfer enhancement by addition of high-alcohol surfactant (HAS) and dissolving salt additive (DSA) in spray cooling, Exp. Therm. Fluid Sci. 45 (2013) 198–202.
[190] W.-L. Cheng, W.-W. Zhang, L.-J. Jiang, S.-L. Yang, L. Hu, H. Chen, Experimental investigation of large area spray cooling with compact chamber in the non-boiling regime, Appl. Therm. Eng. 80 (2015) 160–167.
[191] G. Duursma, K. Sefiane, A. Kennedy, Experimental studies of nanofluid droplets in spray cooling, Heat Transf. Eng. 30 (2009) 1108–1120.
[192] S.-S. Hsieh, H.-Y. Leu, H.-H. Liu, Spray cooling characteristics of nanofluids for electronic power devices, Nanoscale Res. Lett. 10 (2015) 139.
[193] A. Bansal, F. Pyrtle, Alumina nanofluid for spray cooling enhancement, in: ASME/JSME 2007 Thermal Engineering Heat Transfer Summer Conference, ASME, Vancouver, Canada, 2007, pp. 797–803.
[194] H. Bellerová, A.A. Tseng, M. Pohanka, M. Raudensky, Heat transfer of spray cooling using alumina/water nanofluids with full cone nozzles, Heat Mass Transf. 48 (2012) 1971–1983.
[195] H. Bellerová, A.A. Tseng, M. Pohanka, M. Raudensky, Spray cooling by solid jet nozzles using alumina/water nanofluids, Int. J. Therm. Sci. 62 (2012) 127–137.
[196] H. Bellerová, M. Pohanka, M. Raudensky, A.A. Tseng, Spray cooling by Al_2O_3 and TiO_2 nanoparticles in water, in: 12th IEEE Intersociety Conference on Thermal and Thermomechanical Phenomena in Electronic Systems, IEEE, Las Vegas, USA, 2010, pp. 1–5.
[197] T.-B. Chang, S.-C. Syu, Y.-K. Yang, Effects of particle volume fraction on spray heat transfer performance of Al_2O_3-water nanofluid, Int. J. Heat Mass Transf. 55 (2012) 1014–1021.
[198] W. Wu, H. Bostanci, L.C. Chow, S.J. Ding, Y. Hong, M. Su, J.P. Kizito, L. Gschwender, C.E. Snyder, Jet impingement and spray cooling using slurry of

nanoencapsulated phase change materials, Int. J. Heat Mass Transf. 54 (2011) 2715–2723.
[199] A.A. Tseng, H. Bellerová, M. Pohanka, M. Raudensky, Effects of titania nanoparticles on heat transfer performance of spray cooling with full cone nozzle, Appl. Therm. Eng. 62 (2014) 20–27.
[200] J. Lee, I. Mudawar, Assessment of the effectiveness of nanofluids for single-phase and two-phase heat transfer in micro-channels, Int. J. Heat Mass Transf. 50 (2007) 452–463.
[201] A.A. Pavlova, K. Otani, M. Amitay, Active performance enhancement of spray cooling, Int. J. Heat Fluid Flow 29 (2008) 985–1000.
[202] M.R.O. Panão, A.L.N. Moreira, Thermo-and fluid dynamics characterization of spray cooling with pulsed sprays, Exp. Therm. Fluid Sci. 30 (2005) 79–96.
[203] S. Somasundaram, A.A.O. Tay, An experimental study of closed loop intermittent spray cooling of ICs, Appl. Therm. Eng. 31 (2011) 2321–2331.
[204] A.L.N. Moreira, J. Carvalho, M.R.O. Panao, An experimental methodology to quantify the spray cooling event at intermittent spray impact, Int. J. Heat Fluid Flow 28 (2007) 191–202.
[205] A.L.N. Moreira, M.R.O. Panao, Heat transfer at multiple-intermittent impacts of a hollow cone spray, Int. J. Heat Mass Transf. 49 (2006) 4132–4151.
[206] M.R.O. Panão, A.L.N. Moreira, D.F.G. Durão, Thermal-fluid assessment of multijet atomization for spray cooling applications, Energy 36 (2011) 2302–2311.
[207] S. Somasundaram, A.A.O. Tay, Comparative study of intermittent spray cooling in single and two phase regimes, Int. J. Therm. Sci. 74 (2013) 174–182.
[208] S. Somasundaram, A.A.O. Tay, A study of intermittent spray cooling process through application of a sequential function specification method, Inverse Prob. Sci. Eng. 20 (2012) 553–569.
[209] Z. Zhou, B. Chen, Y. Wang, L. Guo, G. Wang, An experimental study on pulsed spray cooling with refrigerant R-404a in laser surgery, Appl. Therm. Eng. 39 (2012) 29–36.
[210] Z. Zhang, P.-X. Jiang, Y.-T. Hu, J. Li, Experimental investigation of continual-and intermittent-spray cooling, Exp. Heat Transf. 26 (2013) 453–469.
[211] Z.-F. Zhou, R. Wang, B. Chen, T. Yang, G.-X. Wang, Heat transfer characteristics during pulsed spray cooling with R404A at different spray distances and back pressures, Appl. Therm. Eng. 102 (2016) 813–821.
[212] M.R.O. Panão, A.M. Correia, A.L.N. Moreira, High-power electronics thermal management with intermittent multijet sprays, Appl. Therm. Eng. 37 (2012) 293–301.
[213] S. Somasundaram, A.A. Tay, Intermittent spray cooling-solution to optimize spray cooling, in: IEEE 14th Electronics Packaging Technology Conference, IEEE, Singapore, 2012, pp. 588–593.
[214] M.R.O. Panão, J.P.P.V. Guerreiro, A.L.N. Moreira, Microprocessor cooling based on an intermittent multijet spray system, Int. J. Heat Mass Transf. 55 (2012) 2854–2863.
[215] M.R.O. Panão, A.L.N. Moreira, Intermittent spray cooling: a new technology for controlling surface temperature, Int. J. Heat Fluid Flow 30 (2009) 117–130.
[216] L. Lin, R. Ponnappan, K. Yerkes, Actively pumped two-phase loop for spray cooling, J. Thermophys. Heat Transf. 20 (2006) 107–110.
[217] Y. Zhang, L.P. Pang, Y.Q. Xie, S.C. Jin, M. Liu, Y.B. Ji, Experimental investigation of spray cooling heat transfer on straight fin surface under acceleration conditions, Exp. Heat Transf. 28 (2015) 564–579.
[218] Y. Zhang, L. Pang, M. Liu, Y. Xie, Investigation of spray cooling: Effect of different heater surfaces under acceleration, Int. Commun. Heat Mass Transf. 75 (2016) 223–231.
[219] W. Deng, A. Gomez, Electrospray cooling for microelectronics, Int. J. Heat Mass Transf. 54 (2011) 2270–2275.
[220] H.-C. Wang, A.V. Mamishev, Heat transfer correlation models for electrospray evaporative cooling chambers of different geometry types, Appl. Therm. Eng. 40 (2012) 91–101.
[221] R.-H. Chen, L.C. Chow, J.E. Navedo, Effects of spray characteristics on critical heat flux in subcooled water spray cooling, Int. J. Heat Mass Transf. 45 (2002) 4033–4043.
[222] G. Moreno, S.M. You, E. Steinthorsson, Spray cooling performance of single and multi-jet spray nozzles using subcooled FC-72, in: ASME/JSME 2007 Thermal Engineering Heat Transfer Summer Conference, ASME, Vancouver, Canada, 2007, pp. 783–790.
[223] L.C. Chow, M.S. Sehmbey, M.R. Pais, High heat flux spray cooling, Annu. Rev. Heat Transf. 8 (1997) 291–318.
[224] Y. Hou, J. Liu, X. Su, Y. Qian, L. Liu, X. Liu, Experimental study on the characteristics of a closed loop R134-a spray cooling, Exp. Therm. Fluid Sci. 61 (2015) 194–200.
[225] S. Toda, H. Uchida, Study of liquid film cooling with evaporation and boiling, Heat Transf.-Jap. Res. 2 (1973) 44–62.
[226] S. Toda, A study of mist cooling (1st report: investigation of mist cooling), Heat Transf.-Jap. Res. 1 (1972) 39–50.
[227] S. Toda, A study of mist cooling (2nd report: theory of mist cooling and its fundamental experiments), Heat Transf.-Jap. Res. 3 (1974) 1–44.
[228] M. Monde, Critical heat flux in the saturated forced convection boiling on a heated disk with impinging droplets, Trans. JSME 45 (1980) 849–858.
[229] Y. Hou, X. Liu, J. Liu, M. Li, L. Pu, Experimental study on phase change spray cooling, Exp. Therm. Fluid Sci. 46 (2013) 84–88.
[230] L. Lin, R. Ponnappan, Critical heat flux of multi-nozzle spray cooling, J. Heat Transf. – Trans. ASME 126 (2004) 482–485.
[231] W.J.J. Vorster, S.A. Schwindt, J. Schupp, A.M. Korsunsky, Analysis of the spray field development on a vertical surface during water spray-quenching using a flat spray nozzle, Appl. Therm. Eng. 29 (2009) 1406–1416.
[232] S.C. Yao, T.L. Cox, A general heat transfer correlation for impacting water sprays on high-temperature surfaces, Exp. Heat Transf. 15 (2002) 207–219.
[233] Y. Katto, Critical heat flux in forced convective flow, in: Proc. ASME/JSME Thermal Engineering Joint Conference, Honolulu, USA, 1983, pp. 1–10.
[234] H.J. Ivey, D.J. Morris, On the relevance of vapor liquid exchange mechanism for subcooled boiling heat transfer at higher pressure, in: U.K. Report AEEW-R-137, AEEWR, Winfrith, England, 1962.
[235] A.G. Pautsch, T.A. Shedd, Spray impingement cooling with single-and multiple-nozzle arrays. Part I: Heat transfer data using FC-72, Int. J. Heat Mass Transf. 48 (2005) 3167–3175.
[236] K.A. Estes, Critical heat flux in spray cooling and jet impingement cooling of small targets Masters Thesis, Purdue University, West Lafayette, 1994.
[237] L. Lin, R. Ponnappan, Heat transfer characteristics of spray cooling in a closed loop, Int. J. Heat Mass Transf. 46 (2003) 3737–3746.
[238] E.A. Silk, Investigation into enhanced surface spray cooling PhD Dissertation, University of Maryland, College Park, USA, 2006.
[239] J.S. Coursey, J. Kim, K.T. Kiger, Spray cooling of high aspect ratio open microchannels, J. Heat Transf. – Trans. ASME 129 (2007) 1052–1059.
[240] R.L. Puterbaugh, K.L. Yerkes, S.K. Thomas, Partially confined FC-72 spray-cooling performance: effect of dissolved air, J. Thermophys. Heat Transf. 23 (2009) 582–591.
[241] L.C. Chow, M.S. Sehmbey, M.R. Pais, Critical heat flux in spray cooling, in: AIAA 33rd Aerospace Sciences Meeting and Exhibit, AIAA, Reno, USA, 1996.
[242] J. Yang, Spray cooling with an air atomizing nozzle PhD Dissertation, University of Kentucky, Lexington, USA, 1993.
[243] E.A. Silk, J. Kim, K. Kiger, Energy conservation based spray cooling CHF correlation for flat surface small area heaters, in: ASME/JSME 2007 Thermal Engineering Heat Transfer Summer Conference, ASME, Vancouver, Canada, 2007, pp. 805–813.
[244] R.L. Puterbaugh, K.L. Yerkes, T.E. Michalak, S.K. Thomas, Cooling performance of a partially-confined FC-72 spray: the effect of dissolved air, in: 45th AIAA Aerospace Sciences Meeting and Exhibit, Reno, USA, 2007.
[245] B. Abbasi, J. Kim, Prediction of PF-5060 spray cooling heat transfer and critical heat flux, J. Heat Transf. – Trans. ASME 133 (2011) 101504.
[246] M.L. Sawyer, S.M. Jeter, S.I. Abdel-Khalik, A critical heat flux correlation for droplet impact cooling, Int. J. Heat Mass Transf. 40 (1997) 2123–2131.
[247] W.M. Healy, P.J. Halvorson, J.G. Hartley, S.I. Abdel-Khalik, A critical heat flux correlation for droplet impact cooling at low Weber numbers and various ambient pressures, Int. J. Heat Mass Transf. 41 (1998) 975–978.
[248] P.J. Halvorson, R.J. Carson, S.M. Jeter, S.I. Abdel-Khalik, Critical heat flux limits for a heated surface impacted by a stream of liquid droplets, J. Heat Transf. – Trans. ASME 116 (1994) 679–685.
[249] Y. Guo, J. Jia, W. Wang, S. Zhou, Nozzle track and C HF prediction of spray cooling for inclined sprays, in: ASME 2008 Heat Transfer Summer Conference, ASME, Jacksonville, USA, 2008, pp. 727–733.
[250] P. Zhang, L. Ruan, Theoretical study of the effect of spray inclination on spray cooling for large-scale electronic equipment, IERI Procedia 4 (2013) 118–125.
[251] E.A. Silk, J. Kim, K. Kiger, Effect of spray cooling trajectory on heat flux for a straight finned enhanced surface, in: Proc. National Heat Transfer Summer Conference, San Francisco, USA, 2005.
[252] S.V. Ravikumar, J.M. Jha, S.S. Mohapatra, A. Sinha, S.K. Pal, S. Chakraborty, Experimental study of the effect of spray inclination on ultrafast cooling of a hot steel plate, Heat Mass Transf. 49 (2013) 1509–1522.
[253] Z.B. Yan, F. Duan, T.N. Wong, K.C. Toh, K.F. Choo, P.K. Chan, Y.S. Chua, L.W. Lee, Large area impingement spray cooling from multiple normal and inclined spray nozzles, Heat Mass Transf. 49 (2013) 985–990.
[254] J. Schwarzkopf, T. Cader, K. Okamoto, B.Q. Li, B. Ramaprian, Effect of spray angle in spray cooling thermal management of electronics, in: ASME 2004 Heat Transfer/Fluids Engineering Summer Conference, ASME, Charlotte, USA, 2004, pp. 423–431.
[255] B.Q. Li, T. Cader, J. Schwarzkopf, K. Okamoto, B. Ramaprian, Spray angle effect during spray cooling of microelectronics: experimental measurements and comparison with inverse calculations, Appl. Therm. Eng. 26 (2006) 1788–1795.
[256] W.-L. Cheng, W.-W. Zhang, S.-D. Shao, L.-J. Jiang, D.-L. Hong, Effects of inclination angle on plug-chip spray cooling in integrated enclosure, Appl. Therm. Eng. 91 (2015) 202–209.
[257] G. Aguilar, H. Vu, J.S. Nelson, Influence of angle between the nozzle and skin surface on the heat flux and overall heat extraction during cryogen spray cooling, Phys. Med. Biol. 49 (2004) 147–153.
[258] T.L. Fu, Z.D. Wang, X.T. Deng, G.H. Liu, G.D. Wang, The influence of spray inclination angle on the ultra fast cooling of steel plate in spray cooling condition, Appl. Therm. Eng. 78 (2015) 500–506.
[259] L. Lin, R. Ponnappan, Critical heat flux of multinozzle spray cooling in a closed loop, in: 37th Intersociety Energy Conversion Engineering Conference, IEEE, Washington D.C., USA, 2002, pp. 341–346.
[260] R.H. Pereira, S.L. Braga, J.A.R. Parise, Single phase cooling of large surfaces with square arrays of impinging water sprays, Appl. Therm. Eng. 36 (2012) 161–170.
[261] J.L. Xie, Y.B. Tan, T.N. Wong, F. Duan, K.C. Toh, K.F. Choo, P.K. Chan, Y.S. Chua, Multi-nozzle array spray cooling for large area high power devices in a closed loop system, Int. J. Heat Mass Transf. 78 (2014) 1177–1186.

[262] J.E. Gonzalez, W.Z. Black, Study of droplet sprays prior to impact on a heated horizontal surface, J. Heat Transf. – Trans. ASME 119 (1997) 279–287.
[263] I.A. Kopchikov, G.I. Voronin, T.A. Kolach, D.A. Labuntsov, P.D. Lebedev, Liquid boiling in a thin film, Int. J. Heat Mass Transf. 12 (1969) 791–796.
[264] B. Glassman, S. Kuravi, J. Du, Y.-R. Lin, G. Zhao, L. Chow, A fluid management system for a multiple nozzle array spray cooler, in: 37th AIAA Thermophysics Conference, AIAA, Portland, USA, 2004.
[265] D.E. Tilton, C.L. Tilton, M.R. Pais, M.J. Morgan, High-flux spray cooling in a simulated multichip module, in: Proc. ASME Heat Transfer Conference, ASME, 1992, pp. 73–79.
[266] J.A. Milke, S.C. Tinker, Effect of dissolved gases on spray evaporative cooling with water, Fire Technol. 33 (1997) 99–114.
[267] B. Horacek, J. Kim, K.T. Kiger, Effects of noncondensable gas and subcooling on the spray cooling of an isothermal surface, in: ASME 2003 International Mechanical Engineering Congress and Exposition, ASME, Washington D.C., USA, 2003, pp. 69–77.